SPALLATION OF MEDIUM WEIGHT ELEMENTS

BY

GÖSTA RUDSTAM

UPPSALA 1956

SPALLATION OF MEDIUM WEIGHT ELEMENTS

INAUGURAL DISSERTATION

BY

GÖSTA RUDSTAM

Fil. lic., V.-D.

By due permission of the Mathematics-Natural Science Faculty of the University of Uppsala, to be publicly discussed in the lecture hall of the Institute of Chemistry, January 19, 1957, at 10 a. m., for the degree of Doctor of Philosophy.

UPPSALA 1956
APPELBERGS BOKTRYCKERI AB

4672/56

SPALLATION OF MEDIUM WEIGHT ELEMENTS

BY

GÖSTA RUDSTAM

UPPSALA 1956

UPPSALA 1956
APPELBERGS BOKTRYCKERI AB

Contents

Preface 7

Introduction 8

Chapter I. Experimental Methods 11

A. Bombardments 11

1. Energy Spectrum of the Beam 11
2. Targets 12
3. Bombardments 12

B. Cross Sections 14

1. Calculation of Cross Sections 14
2. The Effect of Parent Nuclides 15
3. Monitors 18

C. Counting Equipment 22

1. Lead Housing 22
2. Geiger-Müller Tubes 22
3. Sample Changer 24

D. Chemical Separations in General 24

1. Common Technique 24
2. Chemical Separation with Small Amounts of Carriers 25
3. Isotopic Exchange 26
4. Chemical Yield 27
5. Samples for Particle Counting 28
6. Cases where the Amount of Carrier cannot be Small 31

E. Special Chemical Methods 31

1. General Remarks 31
2. Separation of Spallation Products from Arsenic 32
3. Separation and Purification Methods 34
4. Methods of Analysis 41

F. Determination of Disintegration Rates 43

1. Conversion of Counting Rates to Disintegration Rates 43

2. Correction Factors for β-Particles .. 45
a. The Disintegration Scheme 45
b. Absorption in Air and Window .. 45
c. Air- and House-Scattering 49
d. Self-Scattering and Self-Absorption 50
e. Backscattering 53
f. The Efficiency of the GM-Tube .. 57
g. The F-Values for β-Particles 57
3. Correction Factors for Conversion Electrons 57
4. Correction Factors for γ-Rays 59
5. Correction Factors for X-Rays 60

G. Identification of Nuclides 63
1. Half-life 63
2. β-Energy 63

H. Estimation of the Error (Standard Deviation) of the Cross Section Determinations 64

Chapter II. Experimental Results 66

A. Decay Data of the Investigated Nuclides 66

B. Experimental Cross Sections 76
1. Independent Cross Sections 76
2. Irradiation of Arsenic with 170 Mev Protons 76
3. Irradiation of Arsenic with 103 Mev Protons 79
4. Irradiation of Arsenic with 49 Mev Protons 82
5. Irradiation of Cobalt with 170 Mev Protons 84
6. Irradiation of Manganese with 170 Mev Protons 85
7. Irradiation of Vanadium with 170 Mev Protons 87

Chapter III. Cross Section Distributions 90
A. The Cross Section Formula 90
B. Evaluation of the Parameters of the Cross Section Formula 90
C. Results of the Calculations 92
1. General Conclusions about the Cross Section Distributions 92
2. Comparison between Experimental and Calculated Cross Sections 95
3. Independent Cross Sections 99
D. Comparison between Different Spallation Groups 101
1. Introductory Remarks 101
2. The Parameter P 101
3. The Parameter R 103
4. The Parameter S 104
E. Estimation of Relative Cross Sections.. 106

Chapter IV. The Cascade Process 108
A. Introduction 108
B. The Cascade Model 109
1. The Cascade Model *versus* the Compound Nucleus Model 109
2. The Momentum Distribution in the Nucleus 109
3. The Depth of the Potential Well .. 110
4. The Two-Dimensional Geometry .. 111
5. The Mean Free Path in the Nucleus 113
6. The Cascade Calculation 115
a. The Energy of the Incident Proton 116
b. The Penetration Point 117
c. The Collision Point 117
d. The Collision Partner 117
e. The Momentum of the Collision Partner 118
f. The Scattering Angle 119

g. Construction of Angles and Energies 120
h. Example of a Nucleon Cascade .. 121
C. Results of the Cascade Calculation 122
1. The Inelastic Cross Section 122
2. The Excitation Energy of the Residual Nucleus 124
3. Distribution in Energy and Angle of the Cascade Particles 126

Chapter V. The Evaporation Process 131
A. Introduction 131
B. Monte Carlo Calculation for High Excitation Energies 131
1. The Emission Probabilities 131
2. Separation Energy and Coulomb Barrier 135
3. The Energy Distribution of the Evaporated Particles 136
4. The Evaporation Calculation 137
5. Some Results of the Evaporation Calculation 140
C. Low Excitation Energy 143

Chapter VI. Comparison between Experimental and Calculated Cross Sections 145
A. The Spallation Products 145
1. Cross Sections of the Spallation Products 145
2. Fine Structure of the Yields 151
B. The Evaporated Particles 152
C. Cross Sections of Isomers 154

Summary 158

References 160

Preface

The present investigation was carried out at the Gustaf Werner Institute for Nuclear Chemistry during the years 1952–1956.

To the Head of the Institute, Professor The Svedberg, I wish to express my sincere gratitude for his great interest in my work and for his never-failing support.

I am much indebted to Dr. Wladislaw J. Swiatecki for his useful suggestions concerning the theoretical calculations and for his revision of the English text. I also want to thank Dr. Alexis C. Pappas for many interesting discussions on various parts of the work.

Thanks are due to Mr. Åke Svanheden and the cyclotron staff for carrying out the irradiations.

The determination of the cross sections of certain gallium and chlorine isotopes has been rendered possible thanks to collaboration with Mr. Göran Andersson and Mr. Edvin Arbman, which is gratefully acknowledged.

Finally, I should like to thank my colleagues at the Institute for stimulating discussions and helpful advice. I also want to express my appreciation to the members of the staff of the Institute for their very valuable assistance.

The investigation has been supported by grants from the Swedish Atomic Energy Commission and from the Nobel Committee for Chemistry of the Royal Swedish Academy of Sciences.

Uppsala, November 1956.

Gösta Rudstam

Introduction

A reaction in which an energetic particle (or photon) hits a nucleus and knocks out one or more nucleons or clusters of nucleons is called a spallation reaction. The part of the nucleus which remains after the emission of nucleons is known as the spallation product. Evidently a spallation reaction, initiated by a proton, can be written as follows:

$$Z^A + p = Z_1^{A_1} + \nu_1\, p + \nu_2\, n + \nu_3\, d + \nu_4\, \mathrm{H}^3 + \nu_5\, \mathrm{He}^3 + \nu_6\, a + \\ + \text{heavier fragments.} \qquad (1)$$

A nucleus with the atomic number Z and the mass number A is hit by a proton, and ν_1 protons, ν_2 neutrons, etc., are emitted in the reaction leaving the nucleus $Z_1^{A_1}$ as the spallation product.

High energy particles can give rise to a great many different spallation reactions in a target. It is often suitable to use a notation for all spallation reactions associated with the bombardment of a given element (Z) with particles of a given kind (a) and energy (E). This whole group of spallation reactions, or spallation group, is denoted by the symbol: $G(Z;\, a;\, E)$.

Experiments have shown that neutrons, protons, deuterons, tritons, helium-3, and alpha-particles are really emitted from irradiated targets (1–4). There are also indications that heavier fragments are emitted (1, 2, 5–7).

One way to study the spallation reactions is to investigate the particles emitted and measure their angular and energy distributions. This has been done by many investigators (8–19). A complementary experiment is to measure the yield, or cross section, of the spallation products. The yield determination can be easily done if the spallation product is radioactive and has a suitable half-life and decay scheme. The experimental investigations described in the present work deal exclusively with the determination of the formation cross section of the spallation products formed by the irradiation of different targets (vanadium, manganese, cobalt, and arsenic) with high energy

protons. The experimental methods are described in Chapter I, and the results of the cross section determinations are given in Chapter II.

Many spallation investigations with medium weight targets have been reported in the literature (20–53). Protons, neutrons, deuterons, tritons, alpha-particles, heavy particles such as nitrogen-14, and x-rays have been used to initiate the reactions.

It has been shown (44, 54) that the formation cross sections vary fairly regularly with the atomic number and mass number of the spallation products. The author has found an empirical formula which describes the whole cross section distribution with a fair degree of accuracy. This formula provides a useful tool for comparisons between different spallation groups, which is shown in Chapter III.

Already the earliest spallation investigations with high energy particles gave as a surprising result that spallation reactions with only few nucleons emitted are favoured. Thus it was recognized (36, 41) that a compound nucleus in the Bohr sense (55) is not formed. Serber (56) pointed out that fast particles would have a mean free path in the nucleus comparable with the nuclear radius. Thus a particle might pass through a nucleus making only few collisions with the nucleons, or even without any collision at all, and retain a large part of its initial energy. In the case of a collision, the collision partner may also have a large mean free path and might eventually leave the nucleus after some further collisions. In this way a cascade is developed in the nucleus, which results in a number of prompt particles (from now on called "cascade" particles) and a residual nucleus, usually in an excited state.

Serber's theory was treated quantitatively by Goldberger (57) who used a "Monte Carlo" technique (58) to follow the cascade. Such a calculation, among other things, yields information about the excitation energy of the residual nucleus, and it was therefore used in the present work to follow the nucleon cascades developed in arsenic by high energy protons. The calculation is described in Chapter IV.

The nucleus remaining at the end of the cascade will be de-excited by evaporation of neutrons, protons, deuterons, alpha-

particles, etc. This evaporation process has been treated analytically by Le Couteur (59), who gives a method of estimating the average behaviour during the de-excitation. In the present work a Monte Carlo method was applied also to the evaporation calculation. This method allows one to retain the individual properties of the different nuclides throughout the calculation. It yields the distribution of spallation products from excited nuclei and also the energy distribution of the evaporated particles. The evaporation calculation is described in Chapter V.

The absolute cross section of the spallation products can now be obtained by a combination of the results of the cascade calculation and the evaporation calculation. The cross sections calculated in this way are compared with the experimental cross sections in Chapter VI.

CHAPTER I

Experimental Methods

A. *Bombardments*

1. ENERGY SPECTRUM OF THE BEAM

All bombardments were carried out in the circulating beam of the synchrocyclotron of the Gustaf Werner Institute for Nuclear Chemistry. The targets were irradiated at a radius corresponding to 187, 120, or 60 Mev. The energy spectrum of the protons in the target has been measured by Svanheden (60) using a technique similar to that of Bloembergen and van Heerden (61). The energy distribution of the protons is shown in Figs. 1 and 2 (target thickness: 0.1–0.2 g/cm^2). The energy distribution given in Fig. 1 is representative for higher irradiation energies (maximum energy 120 or 187 Mev), whereas the distribution in Fig. 2 is valid for the maximum energy 60 Mev.

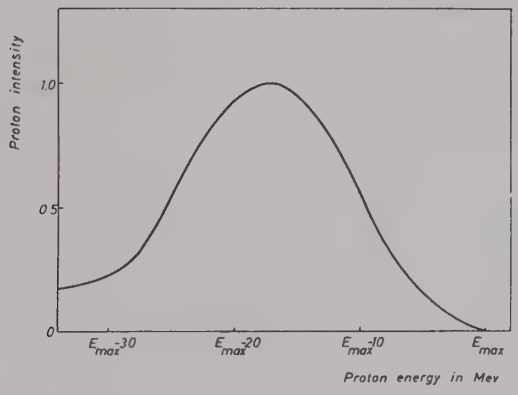

Fig. 1. Energy distribution of the protons in the circulating beam. Maximum energy: 120 or 187 Mev.

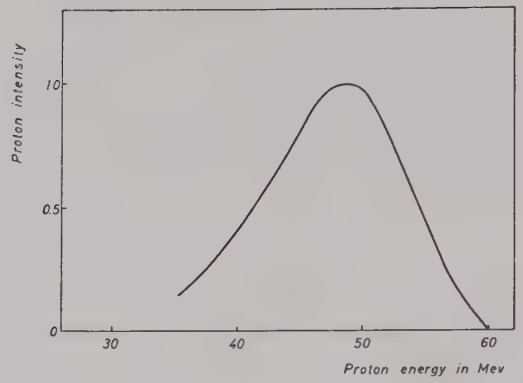

Fig. 2. Energy distribution of the protons in the circulating beam. Maximum energy: 60 Mev.

The most probable proton energy (170, 103, or 49 Mev) is used to characterize the different bombardments in the present work.

2. TARGETS

It is important that very pure chemicals are used as targets since small impurities might cause large errors in the cross section determinations. Most of the chemicals (arsenic, cobalt, manganese) were "Specpure" chemicals obtained from Johnson, Matthey and Co., London. The vanadium foil was obtained from Carbon and Carbide Co., New York.

Some data for the target materials used are listed in Table 1.

The impurities in the target materials are not likely to interfere with the measurements.

3. BOMBARDMENTS

The different bombardments carried out are tabulated in Table 2.

Table 1

Target materials

Target material	Physical form	Impurities	
		Element	Amount
arsenic	metal powder	Cu	0.0002 %
		Mg	0.0001 %
		Ag	0.0001 %
		Si	< 0.0001 %
cobalt	metal powder	Al	0.0002 %
		Mg	< 0.0001 %
		Si	0.0001 %
		Fe	< 0.0005 %
		Cu	< 0.0001 %
manganese	metal pieces	Cu	< 0.0001 %
		Mg	< 0.0001 %
manganous-manganic oxide	powder	Fe	0.05 %
		Ca	0.07 %
		PO_4	0.005 %
		SO_4	0.02 %
vanadium	metal foil	Al	0.05 %
		Ca	0.001 %
		Cr	0.01 %
		Cu	0.001 %
		Fe	0.01 %
		Mg	0.0001 %
		Na	< 0.005 %
		Ni	0.01 %
		Pb	0.001 %
		Se	< 0.001 %
		Si	0.001 %
		Ti	< 0.0001 %
		K	< 0.01 %
aluminium	metal powder	Cu	0.007 %
		Fe	0.04 %
		Cr	< 0.002 %
magnesium	metal powder	Ga	< 0.02 %
		Ge	0.006 %
		Zn	0.03 %
		Ni	0.04 %

Table 2

Bombardments

Target element	Average energy	Number of bombardments
arsenic	170 Mev	22
„	103 „	9
„	49 „	6
cobalt	170 „	5
manganese	170 „	10
vanadium	170 „	13

The length of the bombardments was usually between fifteen minutes and one hour. Occasionally long bombardments (up to three hours) were used.

B. *Cross Sections*

1. CALCULATION OF CROSS SECTIONS

The formation of a certain nuclide as a spallation product is governed by the following equation (thin target):

$$\frac{dN}{dt} = I n \sigma - \lambda N, \qquad (2)$$

with the symbols:

N = number of nuclei of the nuclide in question;
σ = formation cross section for this nuclide;
n = number of target nuclei per unit area at right angles to the beam;
I = ion current = number of incident particles per unit time;
λ = decay constant of the nuclide;
t = time.

Eq. (2) is immediately soluble, if the ion current is constant during the irradiation time T. In many bombardments, however, the ion current was not constant. In such cases the following procedure to solve (2) was adopted. The ion current

in the cyclotron was recorded as a function of time. This ion current-time diagram was then divided into a suitable number of time intervals such that the ion current could be considered to vary linearly in each time interval. One of the time intervals i is now chosen, and the number of nuclei of a certain nuclide is calculated from (2) as follows. The ion current is assumed to vary according to the formula

$$I = I_i (1 + K_i t) \tag{3}$$

in the interval. The end of the interval is t_i and the length of the interval T_i. The equation to be solved is now

$$\frac{dN_i}{dt} = I_i (1 + K_i t) n \sigma - \lambda N_i. \tag{4}$$

The equation is easily solved, and the number of nuclei formed in the actual time interval and remaining at the time t is

$$N_i (t) = \frac{I_i n \sigma}{\lambda} \left[\left(1 - \frac{K_i}{\lambda} \right) (1 - e^{-\lambda T_i}) + K_i T_i \right] e^{-\lambda (t - t_i)}. \tag{5}$$

The total number of nuclei formed directly in the bombardment is then obtained by summing over all time intervals.

$$N (t) = \Sigma_i N_i (t) = \frac{I_0 n \sigma Q (t)}{\lambda}, \tag{6}$$

with

$$Q (t) = \Sigma_i \frac{I_i}{I_0} \left[\left(1 - \frac{K_i}{\lambda} \right) (1 - e^{-\lambda T_i}) + K_i T_i \right] e^{-\lambda (t - t_i)}. \tag{7}$$

2. THE EFFECT OF PARENT NUCLIDES

The formula (6) gives the independent yield of a nuclide of the cross section σ, *i.e.* the number of nuclei formed directly in the spallation reactions and remaining at the time t. This is not the only contribution to the total number of nuclei $N(t)$ of the nuclide in question, however. Part of the nuclei are formed by the disintegration of parent nuclides. For the spalla-

tion groups which are considered in this work, the charge distribution curves have their maxima close to the stability line, and the cross sections fall rapidly on both sides. This means that any nuclide, as a rule, has a much lower cross section than its daughter. For this reason the cross sections calculated from equation (6) by inserting the experimental values of $N(t)$ are generally a good approximation to the independent cross sections. Anyway, if a correction for the contribution from parent nuclides is to be applied, it is quite sufficient to consider only the nearest parent. This correction can then be made as follows. The parent nuclide is assumed to have the cross section σ_p. The cross section σ of its daughter nuclide is to be determined from the measured number of nuclei. This can be considered as composed of three parts:

$$N = N^{(1)} + N^{(2)} + N^{(3)}, \tag{8}$$

with

$N^{(1)}$ = number of independently formed nuclei;

$N^{(2)}$ = number of nuclei formed by the decay of the parent nuclide during the bombardment;

$N^{(3)}$ = number of nuclei formed by the decay of the parent nuclide after the end of the bombardment.

$N^{(1)}$ is given by (6). Thus

$$N^{(1)}(t) = \frac{I_0 n \sigma Q(t)}{\lambda}. \tag{9}$$

In order to calculate $N^{(2)}$ consider a time interval i where the ion current varies according to (3). The following system of equations is obtained:

$$\begin{cases} \dfrac{d N_i^p}{d t} = I_i (1 + K_i t) n \sigma_p - \lambda_p N_i^p ; \\ \dfrac{d N_i^{(2)}}{d t} = \lambda_p N_i^p - \lambda N_i^{(2)}. \end{cases} \tag{10}$$

N_i^p, σ_p, and λ_p refer to the parent nuclide.

The solution is:

$$N_i^{(2)}(t) = \frac{I_i n \sigma_p}{\lambda}\left[\frac{\lambda e^{-\lambda_p T_i}(1-K_i/\lambda_p) - \lambda_p e^{-\lambda T_i}(1-K_i/\lambda)}{\lambda_p - \lambda} + \right.$$

$$\left. + K_i\left(T_i - \frac{1}{\lambda_p} - \frac{1}{\lambda}\right) + 1\right] e^{-\lambda(t-t_i)};$$

$$N^{(2)}(t) = \Sigma_i N_i^{(2)}(t). \qquad (11)$$

For the calculation of $N^{(3)}$ the time t_0 when the parent nuclide is first separated from the daughter nuclide must be known. The following system of equations has to be solved:

$$\begin{cases} \dfrac{dN_i^p}{dt} = -\lambda_p N_i^p; \quad N_i^p(t_i) = \dfrac{I_i n \sigma_p}{\lambda_p}\left[\left(1 - \dfrac{K_i}{\lambda_p}\right)(1 - e^{-\lambda_p T_i}) + K_i T_i\right]; \\ \dfrac{dN_i^{(3)}}{dt} = \lambda_p N_i^p - \lambda N_i^{(3)}. \end{cases} \qquad (12)$$

The result is:

$$N_i^{(3)}(t) = \frac{\lambda_p N_i^p(t_i)}{\lambda_p - \lambda}\left(e^{-\lambda(t_0 - t_i)} - e^{-\lambda_p(t_0 - t_i)}\right) e^{-\lambda(t-t_0)};$$

$$N^{(3)}(t) = \Sigma_i N_i^{(3)}(t). \qquad (13)$$

Thus if σ_p is known, $N^{(2)}$ and $N^{(3)}$ can be calculated from (11) and (13). $N^{(1)}$ is then obtained from (8), and σ can be calculated from (9).

It often happens that σ_p cannot be determined because the half-life of the parent nuclide is very short. In that case Eqs. (11) and (13) simplify. The result is:

$$\begin{cases} N^{(2)} = \dfrac{I_0 n \sigma_p Q(t)}{\lambda}; \\ N^{(3)} = 0. \end{cases} \qquad (14)$$

Thus

$$N(t) = \frac{I_0 n (\sigma_p + \sigma) Q(t)}{\lambda}. \qquad (15)$$

If the experimental value of $N(t)$ is inserted into (15), the sum of the cross sections of the parent and the daughter nuclides is now obtained. If the cross section of the parent nuclide is unknown, it is not possible to calculate the independent cross section of the daughter nuclide. The cross section of the parent nuclide can be estimated, however, using "spallation systematics" as will be shown in Chapter III, and the independent cross section can then be obtained from Eq. (15).

3. MONITORS

If the disintegration rate (corrected for parent effect) is denoted by $D(t)$ $(= \lambda N(t))$, the independent cross section is obtained from (9).

$$\sigma = \frac{D(t)}{In\,Q(t)}. \tag{16}$$

The relative cross sections of two nuclides, a and b, formed in the same bombardment from the same target isotope, are then

$$\frac{\sigma_a}{\sigma_b} = \frac{D_a(t)}{D_b(t)} \frac{Q_b(t)}{Q_a(t)}. \tag{17}$$

The factors n and I do not appear here, and an absolute determination of the ion current is not necessary. It is therefore advantageous to use one of the spallation products as an internal monitor and to determine all cross sections relative to this one using Eq. (17). It is not necessary to know the absolute disintegration rate $D(t)$, if only quantities which are proportional to the disintegration rates are known.

In order to convert the relative cross sections to absolute ones, one must determine the absolute cross section of the internal monitor. This can be done by a comparison with another reaction where the absolute cross section is known. As an absolute monitor the formation of the nuclide Na^{24} from aluminium (or magnesium) was used. The comparison with the reaction $Al^{27}(p, 3pn)Na^{24}$ was carried out in two

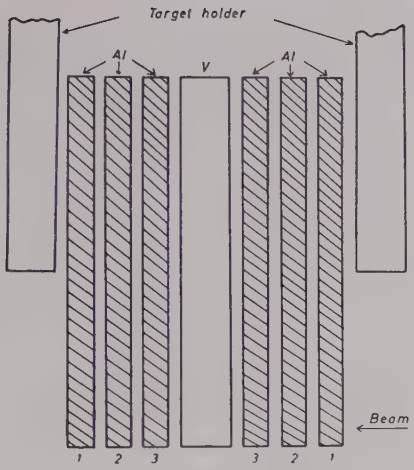

Fig. 3. Target assembly in the vanadium bombardments.

different ways depending on the form of the target material. Since the vanadium was obtained in thin foils, the technique described in the reference (44) could be used. The vanadium foil (0.2 mm) was sandwiched between aluminium foils (0.01 mm), three on each side, and all foils were carefully aligned so as to ensure that the same ion current passes through all foils. The arrangement is shown in Fig. 3.

The second aluminium foil is the monitor foil. The third foil is a guard foil which prevents recoils from the target to reach the second foil. Fung and Perlman (62) have shown that a significant number of Na^{24}-nuclei are lost from a thin aluminium foil by recoils. They measured a loss of eighteen per cent of the total number of Na^{24}-nuclei from a 0.25 mil aluminium foil at bombardments with 180 Mev protons. The first and the third foils will correct for this effect since the second foil should gain about as much Na^{24} as it loses.

The second aluminium foil on each side of the vanadium foil was counted, and the average count was used for the cross section determinations. The difference between the activity of these foils was usually within five per cent.

The method described above has the advantage that the aluminium foils can be counted directly and no chemical separation of sodium is necessary. This is because Na^{24} (apart from a small amount of Na^{22} and Be^{7}) gives the only detectable activity a few hours after the bombardment. The method is not suitable, however, when the target is in powder form. Therefore a new method was used for arsenic, manganese, and cobalt. The finely powdered target element was intimately mixed with a known amount of aluminium powder. The mixture, the composition of which must be known, was bombarded in a small container of platinum (not aluminium because Na^{24} from the container might recoil into the target mixture). The ion current can be assumed to be the same for both constituents of the mixture. After the irradiation, sodium was chemically separated, and the activity of Na^{24} was measured. A correction should be made for the amount of Na^{24} formed from the proper target element.

For both methods one obtains, using (16):

$$\frac{\sigma_a}{\sigma_b} = \frac{D_a(t)}{D_b(t)} \frac{n_b Q_b(t)}{n_a Q_a(t)}. \tag{18}$$

D_b and Q_b now refer to Na^{24} and D_a and Q_a to the internal monitor. n_b is the number of aluminium (magnesium) nuclei and n_a the number of arsenic (cobalt, manganese, vanadium) nuclei subject to the beam. Note that for the powder method it is only necessary to know the percentage composition of the mixture.

The cross section for formation of Na^{24} from aluminium has been measured by Hintz and Ramsey (63), by Chackett, Chackett, Reasbeck, Symonds, and Warren (64), and by Hicks, Stevenson, and Nervik (65). For the present work the data of Hicks *et al.* were used.

The excitation function of the reaction $Al^{27}(p, 3pn)Na^{24}$ falls steeply below 50 Mev. Thus this reaction was not suitable to monitor the irradiations carried out at 49 Mev. Here magnesium powder was used instead of aluminium powder. The excitation functions of the reactions $Mg^{25}(p, 2p)Na^{24}$ and

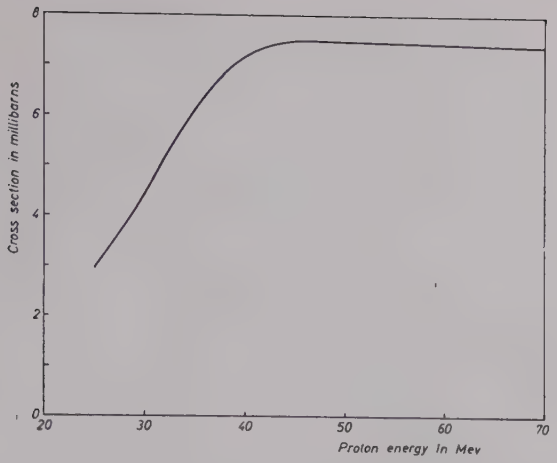

Fig. 4. Excitation function for formation of Na^{24} from natural magnesium.

$Mg^{26}(p, 2pn)Na^{24}$ have been determined by Meadows and Holt (66). They measured the cross sections relative to the cross section of the reaction $C^{12}(p, pn)C^{11}$. For this reaction they used the cross section determinations by Aamodt, Peterson, and Phillips (67). More recent determinations by Crandall, Millburn, Pyle, and Birnbaum (68) and by Burcham, Symonds, and Young (69) indicate, however, that the absolute cross sections given by Aamodt *et al.* are too high. Crandall *et al.* therefore normalized Aamodt's data to the cross section 36.0 millibarns at 350 Mev, and they give the whole excitation curve in their paper. The excitation function for formation of Na^{24} from natural magnesium, shown in Fig. 4, was obtained using the relative cross sections given by Meadows and Holt and the absolute $C^{12}(p, pn)C^{11}$-excitation curve given by Crandall *et al.*

In the actual bombardments the following formation cross sections of Na^{24} were used:

Proton energy:	49 Mev	103 Mev	170 Mev
Target:	Mg	Al	Al
Cross section:	7.5 mb	10.7 mb	8.9 mb

A standard deviation of about fifteen per cent was assumed.

C. *Counting Equipment*

1. LEAD HOUSING

The determination of disintegration rates was carried out with an end window Geiger-Müller tube. In order to reduce the background, the tube was placed in a lead housing with walls 40 mm thick. The inner surfaces were covered with 5 mm aluminium to reduce scattering effects. The samples were placed in a holder which could be inserted in a shelf arrangement (of aluminium) at four different distances from the tube window. This arrangement allowed all samples to be counted in the same position relative to the GM-tube. As a rule, the samples were counted at the second shelf from the window. The counting arrangement described here was chosen because Zumwalt (70) has thoroughly investigated an almost identical arrangement. Thus Zumwalt's results regarding scattering of β-particles from the walls of the lead housing and in the air between the sample and the counter tube could be used. A more extensive description of the lead housing is given by Pappas (71). The lead housing and the sample holder are shown in Figs. 5 and 6.

The scaler, timing unit, and power supply used in the counting arrangement were all standard.

2. GEIGER-MÜLLER TUBES

The GM-tubes were of the organic quench type. Several makes were used, namely Siemens, Victoreen, and Tracerlab. All tubes had thin mica windows. These GM-tubes have a high sensitivity, close to a hundred per cent, for those β-particles which have reached the sensitive volume of the tube (72).

Pappas (71) recommends coating the window with a very thin layer of aqua dag in order to avoid hysteresis in the response of the tubes to changes in intensity. That was done for the Victoreen tube. The Tracerlab tube was aqua dag coated at the delivery.

In order to obtain a more stable dead time a quench circuit was used. The dead time was measured with an oscillograph.

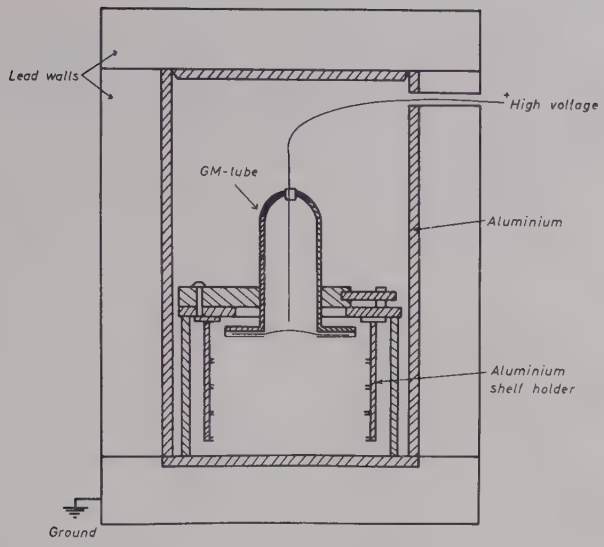

Fig. 5. Counting arrangement (reprinted from the reference (71)).

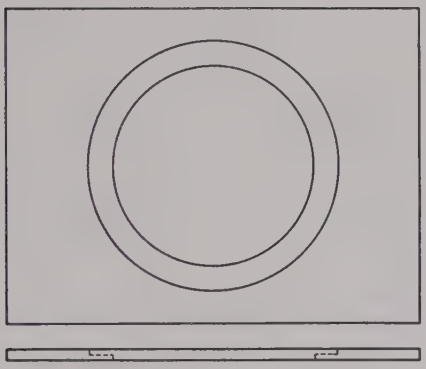

Fig. 6. Sample holder (lucite).

The stability of the tubes was checked by counting a uranium standard every day. The stability of each tube was good for many months. The background count was also taken every day.

3. SAMPLE CHANGER

An automatic sample changer was used to follow the decay of the samples. The sample changer could count up to twenty-four samples repeatedly. The arrangement was used only to check the half-lives of the nuclides. It could not be used to measure disintegration rates for cross section determinations, because the samples were put into small lead cups, and this caused a large amount of β-particle scattering and γ-ray conversion.

D. *Chemical Separations in General*

1. COMMON TECHNIQUE

The experiments were carried out in the following way. After the irradiation in the cyclotron, the target was dissolved in nitric acid containing the carriers, *i.e.* measured amounts of the elements to be studied in the actual experiment. After complete exchange between the active isotopes of each element and the carrier atoms, the different elements were separated and purified by a series of chemical procedures: precipitations, scavengings, extractions, distillations, etc. When an element had been isolated and purified, it was mounted in a suitable manner for particle counting. From the activity measurement the disintegration rates of the different isotopes in the sample were determined, and the cross sections were calculated using Eq. (17).

It is tacitly assumed that no activity is lost from the target by evaporation during the irradiation. The target is in a vacuum, and one might think that at least gaseous spallation products would diffuse through the target and get lost. The experimental investigations of this effect are somewhat contradictory. Seagrave (74) found the loss of N^{13} from the graphite in the reaction $C^{12}(p,\gamma)N^{13}$ to be negligible. On the other hand Hintz and Ramsey (63) bombarded sodium sulphate in a cyclotron to produce chlorine, and they found that

a target enclosed in a vacuum tight capsule gave fifteen per cent larger yield of Cl^{34} than a target at vacuum.

In the present bombardments the only element which might get lost is just chlorine. Judging from the investigation by Hintz and Ramsey there should be a certain possibility of losing some chlorine by evaporation during the bombardment. The effect is fairly small, however, and it is neglected here.

2. CHEMICAL SEPARATION WITH SMALL AMOUNTS OF CARRIERS

Absolute particle counting will be treated later. It must be pointed out now, however, that the determination of disintegration rates is simplified if the samples for counting are very thin (about 0.1 mg/cm^2) and are mounted on thin foils with little backscattering. For this reason a method using "collector" substances (known from analytical chemistry) was used, which gives thin samples mounted on thin aluminium foils for the activity measurement. In the early experiments (the bombardments of vanadium and some of the bombardments of manganese and cobalt) 10 mg amounts of carriers were used. Then the samples for counting consisted of a precipitate on an aluminium dish (50 mg/cm^2) or a platinum dish (400 mg/cm^2). The thickness of the samples was several milligrams per square centimeter. With the new method the thickness of the samples could be considerably reduced by using small amounts (only 0.1 or 0.2 mg) of carriers.

The chemical methods have to be worked out with special regard to the small amounts of carriers. Extractions, distillations, and scavengings are carried out in the usual way, but precipitations require special care. The amount of precipitate is often so small that it might easily get lost. For this reason it is advisable to add a few milligrams of another element which is precipitated together with the element of interest either by the same or by a different precipitating reagent. This element will serve as a collector for the element to be separated, and the combined precipitates can now easily be centrifuged and washed. Afterwards, the collector is removed by a suitable

chemical procedure. Thus it is possible to use several precipitation steps with the same or with different collectors in the separation procedure of an element. The action of the collector as described above is purely mechanical. It is also possible to choose a collector which will precipitate the actual element by coprecipitation (formation of mixed crystals, etc.). Such a collector is effective and can often precipitate elements which would otherwise not be precipitated.

When the separation and purification procedure has been completed, one should end with a final solution containing the element of interest free from all impurities. This final solution, from now on called the test solution, may be ammoniacal, neutral, or acidified with nitric acid, but it must not contain salts such as ammonium nitrate. For low activities the volume of the test solution should be small, about 0.3 ml. For high activities the test solution is diluted to a suitable volume, for instance 1–1.5 ml.

The test solution is analysed quantitatively to determine the concentration of the element of interest, and samples for particle counting are taken from it.

3. ISOTOPIC EXCHANGE

It is important that a complete isotopic exchange be obtained between the active isotopes of an element and the carrier atoms, because only then can one be sure that the carrier works properly. The exchange may be considered complete if the active atoms can be brought to the same physical and chemical form as the carrier atoms.

If the incident proton in a spallation reaction were completely captured by the nucleus (which is quite improbable for high energy protons), the nucleus would acquire a relatively high speed, of the same order as the speed of the valency electrons. The speed should then be high enough to ionize the atom (75, 76). There are indications, however, that the spallation products will be formed in a low oxidation state. One might perhaps expect the chemical form of the spallation

products to be about the same as the chemical form of the (n, γ)-products found in Szilard-Chalmers reactions or of (p, n)-products. In such reactions the products are usually formed in a low oxidation state or in elementary form. Examples of this are found in the review article by Edwards and Davies (77) and in the reference book by Wahl and Bonner (78). Investigations of the chemical form of spallation products formed in high energy bombardments are rare. However, G. A. Chackett and K. F. Chackett (79) irradiated aluminium metal with 100 Mev N^{14}-ions and found that the phosphorus formed is mainly in the elementary state or in a low oxidation state.

From these investigations one may assume the spallation products to be formed in a low oxidation state at the bombardment, especially if the target is metallic and thus forms a reducing medium. The chlorine may be assumed to be formed as chloride or possibly as elementary chlorine, which, however, would rapidly exchange with chloride ions (80, 81).

It is suitable to add the carrier in the chemical form to be expected for the spallation product after the dissolution of the target. In the actual bombardments the targets were dissolved in nitric acid. One might then expect the following chemical form of the spallation products: SeO_3^{2-}, Ge^{4+}, Ga^{3+}, Zn^{2+}, Cu^{2+}, Ni^{2+}, Co^{2+}, Fe^{3+}, Mn^{2+}, Cr^{3+}, VO^{2+} or VO_2^{+}, Ti^{4+}, Sc^{3+}, Ca^{2+}, K^{+}, Cl^{-}, SO_4^{2-}, PO_4^{3-}, SiO_3^{2-}, Mg^{2+}, Na^{+}. The carriers were added in the same form (vanadium as quadrivalent), except silicon, which was added as fluosilicate. This was then converted to silica by addition of boric acid.

4. CHEMICAL YIELD

The chemical yield has to be measured, since it is necessary to know how large a part of the total activity formed is found in the sample for particle counting.

When 10 mg amounts of carriers were used, the final precipitate of an element was chosen so as to be suitable for gravimetric analysis. The sample was spread out on an aluminium or a platinum dish depending on whether it was sufficient to

dry the precipitate at a fairly low temperature or it was necessary to ignite it. For the experiments with small amounts of carriers a more sensitive method of analysis had to be used. Spectrophotometry was found suitable for the purpose. Since the solution to be analysed is completely free from interfering impurities, it is often possible to make spectrophotometric analyses with an accuracy of 2–3 per cent or better (if the concentration is not too low owing to small chemical yield).

Since the carrier solution can be used as a standard in the spectrophotometric analysis, it is not necessary to know its concentration exactly. One obtains directly the ratio between the amount of the actual element in a given volume of the test solution and the amount added as carrier. By using the carrier solution as a standard in the analysis, those errors that might arise from concentration changes in the carrier solution are eliminated.

5. SAMPLES FOR PARTICLE COUNTING

In the early experiments the samples consisted of precipitates spread out as evenly as possible on aluminium or platinum dishes. The dish was fastened with tape at the center of a mounting card designed to fit into the shelves of the counter arrangement.

When the technique with small amounts of carriers was used, the samples for counting were prepared in the following way. A thin aluminium foil (2.4 mg/cm^2) was stretched over an aluminium frame, and 0.05 ml of the test solution was pipetted on to the foil with a micropipette. A fine air stream was directed to the under side of the foil right below the liquid drop, and the drop was evaporated to dryness under a heating lamp. The air stream helps to give good samples by keeping the liquid centered and preventing boiling. After the evaporation the foil was fastened with small strips of tape to a ring of lucite (outer diameter: 50 mm; inner diameter: 40 mm; thickness: 0.5 mm), so that the sample was placed at the center of the ring. The rings fitted into the lucite holder shown in Fig. 6.

The evaporation method described above usually gave evenly spread samples of about the same diameter. Sometimes the active material tended to form a ring, however. To avoid this, the center of the foil was wetted with insulin as recommended by Langer (82). Very good samples were obtained from ammoniacal or neutral test solutions by the addition of about 20 micrograms of copper (II) ferrocyanide in ammoniacal solution to the drop.

The diameter of the samples did not vary much. The average diameter of 231 samples was 8.3 mm with a standard deviation of 1.1 mm.

Figs. 7 and 8 can be used to estimate the effect of uneven spreading and differences in the diameter of the samples. Both figures refer to the counting arrangement using the Victoreen tube (tube diameter: 29 mm; distance from the sample to the sensitive volume of the tube: 27 mm). Fig. 7 shows the efficiency of detecting planar circular sources of different diameters. 100 per cent efficiency corresponds to a point source. Fig. 8 shows the efficiency of detecting a point source which is located at different distances from the symmetry axis. 100 per cent efficiency corresponds to a source on the axis. The curves in Figs. 7 and 8 are constructed from the solid angle calculations by Cook, Duncan, and Hewitt (83).

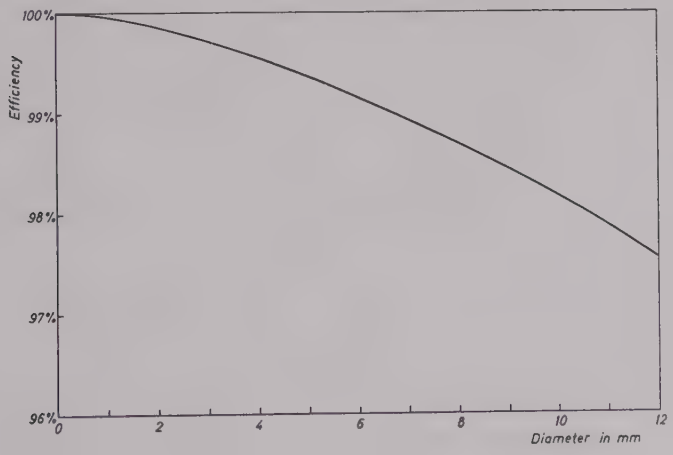

Fig. 7. Efficiency of detection of a planar circular source.

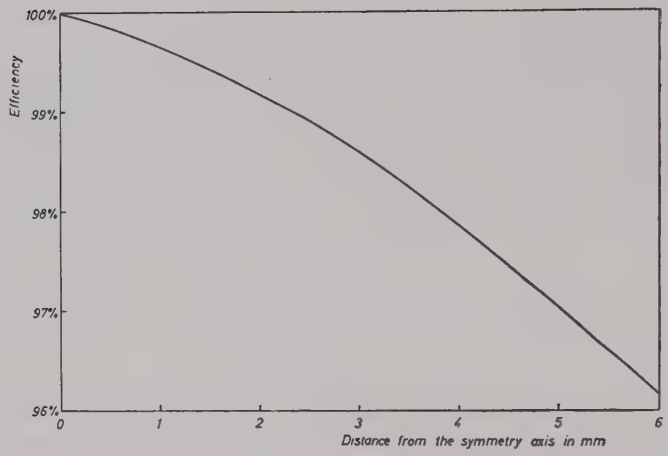

Fig. 8. Efficiency of detection of a point source.

From Fig. 7 it is evident that a deviation from the average value of the diameter of at least 4 mm is needed to cause a difference in counting efficiency of 1 per cent. Since such large deviations never occurred in the actual work, no correction for differences in diameter was considered necessary.

Figs. 7 and 8 show that uneven spreading is not likely to cause large errors in the determinations. In the extreme case that the source is a point source, it will give 1.4 per cent higher count than the standard planar sample with the diameter 8.3 mm. On the other hand, if the sample is in the form of a ring with the same diameter as the planar source, it would give a count which is only 0.9 per cent lower than the count from the planar source.

At least three samples for particle counting were taken from each test solution. The activity was measured, and the average count was determined. The error of this average value was usually less than 1 per cent. In a test of the reproducibility of the technique of preparing samples, 38 samples were prepared from a Co^{60}-solution. The standard deviation of the activity data turned out to be 1.7 per cent. This error includes errors in the pipetting, uneven spreading, variation of the sample diameter, etc.

6. CASES WHERE THE AMOUNT OF CARRIER CANNOT BE SMALL

The technique with small amounts of carriers is not always applicable. The reason for this may be:

1) it is not possible to work out a satisfactory chemical separation procedure using small amounts of carriers;
2) there is no suitable way of determining the chemical yield;
3) the isotopes to be studied belong to the target element.

In the chemistry for sodium and potassium precipitation steps were used where the amount of these elements should not be too small. A somewhat larger amount of sodium and potassium was also called for by the chemical analysis. Another reason against working with a very small amount of sodium is that the solutions might get contaminated with sodium-containing dust. For these reasons the amount of sodium and potassium used as carrier was 2 mg.

Selenium is another example where 2 mg of carrier was needed for the chemical separation procedure, which involved the precipitation of selenium in elementary form.

Even if relatively large amounts of carriers were used in the case of the elements mentioned above, the samples for particle counting were quite thin. Only a small amount of the test solution, at most 5 per cent, was namely taken for each sample. With 2 mg of carrier, a chemical yield of 50 per cent, and 5 per cent of the test solution in a sample, the thickness of the sample would be about 0.2 mg/cm^2.

When isotopes belonging to the target element were to be studied, only a very small part, at most 0.05 per cent, of the total amount (100–200 mg) of this element was used in each sample for counting in order to get thin samples.

E. *Special Chemical Methods*

1. GENERAL REMARKS

The target was dissolved in nitric acid, containing carriers, after the irradiation. The different elements were then sepa-

rated and purified. The separation and purification procedure depended on which elements were to be separated in the experiment. In some bombardments only two different elements were studied, in others up to eight. As an example of the separation procedure, the isolation of selenium, germanium, gallium, zinc, copper, nickel, and cobalt from the same target (arsenic) will be described at first. The purification methods for the different elements will then be given in some detail.

In the experiments with small amounts of carriers, all reagents have to be as pure as possible. Analytical grade reagents were always used, and all solutions were made with redistilled water. The nitric acid and the hydrochloric acid were also distilled. All solutions were kept in pyrex glass in order to avoid contamination from the glass. Care was taken not to introduce chromium from the washing of the glass.

The test solutions were kept in small glass-stoppered pyrex tubes. The solutions should be analysed as soon as possible after the preparation of samples for particle counting to avoid errors arising from concentration changes. The concentration might decrease due to adsorption on the walls of the tube, or increase due to evaporation of water. The first effect is negligible because the maximum loss (corresponding to a monomolecular layer on the walls of the tube) would be about 0.001 mg (73). The second effect was corrected for by measuring the loss of weight of the test solution in the time interval between the preparation of samples for counting and the chemical analysis.

2. SEPARATION OF SPALLATION PRODUCTS FROM ARSENIC

The elements to be separated are: selenium, germanium, gallium, zinc, copper, nickel, and cobalt.

1) The target, consisting of metallic arsenic, is dissolved in 8 N nitric acid containing 2 mg of selenium and 0.2 mg of each of the elements germanium, gallium, zinc, copper, nickel, and cobalt. The solution is evaporated nearly to

dryness, and the residue taken up into about 5 ml of 6 N hydrochloric acid.

2) The solution is transferred to a small distillation apparatus. A few crystals of potassium chlorate are added, and *germanium* is distilled with an air stream into an ice-cooled centrifuge tube with water.
3) The remainder is mixed with more 6 N hydrochloric acid and transferred to a separatory funnel. *Gallium* is then extracted with ether.
4) The water phase is diluted with the same volume of water, and a few milligrams of silver nitrate (collector) are added. Hydrogen sulphide is bubbled through the solution to precipitate the sulphides of arsenic, selenium, copper, and silver. The combined precipitate is washed three times with 1 N hydrochloric acid.
5) The supernate is boiled down to a small volume, about two milliliters, and then transferred to a centrifuge tube. A few milligrams of iron (III) chloride (collector) are added, and the solution is made alkaline with 6 N sodium hydroxide. The solution is treated with a few drops of hydrogen peroxide and heated on the water bath. The supernate after centrifugation contains *zinc*.
6) The precipitate is washed twice with 1 N sodium hydroxide and then dissolved in a few drops of hydrochloric acid. About one milliliter of a saturated solution of β-nitroso-α-naphthol in acetic acid is added, and the pH is adjusted to 4–6 with ammonia. *Cobalt* is extracted with carbon tetrachloride. The water phase contains *nickel*.
7) The precipitate from (4) is treated with 1 N sodium hydroxide plus a few drops of ammonium sulphide. *Copper* sulphide remains undissolved together with silver sulphide.
8) The supernate is acidified with hydrochloric acid, and the precipitate formed is washed twice with 6 N hydrochloric acid. It is then dissolved in a small amount of nitric acid. After evaporation nearly to dryness, the residue is dissolved in 1 N hydrochloric acid.

9) Solid hydroxylamine hydrochloride is added to precipitate *selenium*. *Arsenic* is left in solution.

3. SEPARATION AND PURIFICATION METHODS

The separation and purification procedures for the different elements are given below. For the working out of such chemical procedures reference must be made to the ordinary textbooks of analytical chemistry, especially the one by Lundell and Hoffman (84).

The chemical yield was usually 10–50 per cent.

Selenium. The arsenic target was dissolved in dilute nitric acid containing 2 mg of selenium as selenious acid. The solution was evaporated almost to dryness. The residue was then taken up into 6 N hydrochloric acid, and germanium carrier was added. Evaporation nearly to dryness removed germanium. The solution was then mixed with more 6 N hydrochloric acid, and hydrogen sulphide was bubbled through. The precipitate was washed three times with 1 N hydrochloric acid and then dissolved in a few drops of nitric acid. The nitric acid was evaporated, and the residue was taken up into 1 N hydrochloric acid. Solid hydroxylamine hydrochloride was added to the solution, which was then heated to precipitate elementary selenium. The precipitate was washed twice with 1 N hydrochloric acid. It was then dissolved in nitric acid, which was evaporated as before. Elementary selenium was again precipitated from 1 N hydrochloric acid and washed. After this the selenium was dissolved in a few drops of nitric acid. The nitric acid was evaporated, and the residue taken up into 1–1.5 ml of water. This solution was used as test solution for selenium.

Arsenic. Since the target consisted of arsenic, no carrier was added. The purification procedure was the same as for selenium down to the first precipitation of selenium with hydroxylamine hydrochloride. In the arsenic procedure a few milligrams of selenium carrier were added to the solution containing the arsenic and then precipitated with hydroxylamine hydrochloride. The precipitation was repeated with more selenium. The solution was then made 6 N in hydrochloric acid, copper carrier was added, and the sulphides were precipitated with hydrogen sulphide. The precipitate was washed three times with 6 N hydrochloric acid and three times with water. It was then treated with 10–20 ml of 6 N ammonia. The copper sulphide was centrifuged off, and the supernate was used as test solution for arsenic.

Germanium. The target (arsenic) was dissolved in dilute nitric acid

containing 0.2 mg of germanium as Ge(IV). The solution was evaporated nearly to dryness and then mixed with about 5 ml of 6 N hydrochloric acid. This solution was transferred to a distallation apparatus, a few crystals of potassium chlorate were added, and germanium tetrachloride was distilled into an ice-cooled receiver with water. A few milligrams of manganese carrier (collector) were added, and the solution was made strongly ammoniacal and treated with hydrogen peroxide under heating. The precipitate, consisting of manganese dioxide together with germanium hydroxide, was centrifuged and washed twice with water. It was then treated with 0.5–1 ml of 1 N nitric acid for a few minutes. The nitric acid dissolves the germanium hydroxide and leaves the manganese dioxide undissolved. The solution was filtered and used as test solution for germanium.

Gallium. The target (arsenic) was dissolved in dilute nitric acid containing 0.1 or 0.2 mg of gallium. The solution was evaporated nearly to dryness. The residue was taken up into 6 N hydrochloric acid and transferred to a separatory funnel. Gallium was extracted with ether, previously saturated with 6 N hydrochloric acid. The ether layer was washed three times with 6 N hydrochloric acid and then transferred to a centrifuge tube and evaporated on the water bath. The residue was dissolved in 6 N hydrochloric acid. Arsenic carrier was added, and arsenic sulphide was precipitated with hydrogen sulphide. The supernate was filtered down into a separatory funnel, and gallium was again extracted with ether. After washing three times with 6 N hydrochloric acid, the ether was evaporated as before. Care was taken to remove all traces of hydrochloric acid. The residue was then dissolved in eight drops of water and two drops of ammonia. This solution was used as test solution for gallium.

Zinc. The target (arsenic) was dissolved in nitric acid containing 0.1 or 0.2 mg of zinc. After evaporation nearly to dryness the residue was made 3 N in hydrochloric acid, and about 1 mg each of selenium and copper carriers were added. Arsenic, selenium, germanium, and copper were removed as sulphides. Gallium was extracted with ether from 6 N hydrochloric acid. The water phase was boiled down to a small volume, iron carrier was added and then ammonia to precipitate iron hydroxide. The solution was scavenged twice with iron hydroxide and then transferred to a separatory funnel. Cobalt and nickel carriers were added. The cobalt β-nitroso-α-naphthol complex was extracted from an acetic acid solution and nickel dimethylglyoxime from an ammoniacal solution into chloroform. Zinc was then extracted from the water phase with a solution of dithizone in carbon tetrachloride. The organic phase was washed twice with a solution containing some sodium diethyldithiocarbamate and ammonium citrate. Then the zinc was re-extracted into 0.01 N hydrochloric acid. The hydrochloric acid was evaporated, and the residue taken

up into 0.5 ml of water. This solution was used as test solution for zinc.

Copper. The arsenic target was dissolved in dilute nitric acid containing 0.1 or 0.2 mg of copper carrier. After evaporation nearly to dryness the residue was dissolved in 3 N hydrochloric acid, and about 1 mg of silver nitrate was added. Hydrogen sulphide was bubbled through to precipitate the sulphides. The precipitate was washed three times with 1 N hydrochloric acid and afterwards treated twice with 1 N sodium hydroxide containing a few drops of ammonium sulphide. It was then dissolved in nitric acid. The solution was diluted to 1 N, and the silver was precipitated with hydrochloric acid. The supernate was filtered down into a centrifuge tube, potassium ferrocyanide was added and then some barium chloride and a few drops of 1 N sulphuric acid. The precipitate, consisting of cupric ferrocyanide and barium sulphate, was centrifuged and then washed three times with 1 N nitric acid. The last trace of the wash liquid was removed by evaporation at about 120°, and copper was dissolved out of the precipitate into eight drops of water and two drops of ammonia. This solution was the test solution for copper.

Nickel. The arsenic target was dissolved in dilute nitric acid containing 0.2 mg of nickel. Arsenic, selenium, germanium, and copper were precipitated, and gallium was extracted with ether just as described in the zinc procedure. The solution was boiled down to about 2 ml, and 1–2 mg of iron carrier was added. The solution was made alkaline with 6 N sodium hydroxide and treated with hydrogen peroxide. The precipitate, containing iron, nickel, and cobalt as hydroxides, was washed twice with 1 N sodium hydroxide, and then dissolved in a few drops of hydrochloric acid. 1 mg of cobalt carrier was added, and cobalt β-nitroso-α-naphtholate was extracted from an acetic acid solution into chloroform. The water phase was made ammoniacal, and nickel was precipitated with dimethylglyoxime (2 per cent solution in alcohol). The precipitate was washed twice with water. Then 1 ml of 0.5 N ammonium citrate and 1 ml of dimethylglyoxime were added, and nickel dimethylglyoxime was extracted into chloroform. The chloroform layer was washed twice with 0.3 N ammonia. The nickel was then re-extracted into a few drops of nitric acid. The water phase was washed once with chloroform and then used as test solution for nickel.

Cobalt. The target (arsenic) was dissolved in dilute nitric acid containing 0.2 mg of cobalt carrier. The purification procedure was the same as for nickel down to the extraction of cobalt β-nitroso-α-naphtholate with chloroform, which, of course, was carried out without addition of more cobalt carrier. The chemical procedure was continued as follows. The organic phase was washed once with 1 N and three times with 6 N hydrochloric acid and then transferred to a

porcelain crucible. A few drops of nitric acid were added, and the liquid was evaporated to dryness. 2 ml of 3 N sulphuric acid and 2 drops of nitric acid were added, and the solution was again taken to dryness. The residue was dissolved in 0.5 ml of 1 N nitric acid. This solution was used as test solution for cobalt.

Iron. The arsenic target was dissolved in dilute nitric acid containing 0.1 or 0.2 mg of iron carrier. The iron was extracted into ether in exactly the same way as gallium. The ether phase was washed with 6 N hydrochloric acid, then transferred to a centrifuge tube and evaporated to dryness. The residue was dissolved in water, and about 1 mg each of gallium and manganese carriers were added. The solution was made alkaline with 6 N sodium hydroxide and treated with hydrogen peroxide to precipitate manganese dioxide together with iron hydroxide. The precipitate was washed twice with 1 N sodium hydroxide and then dissolved in 6 N hydrochloric acid. The ether-extraction and hydroxide-precipitation cycle was repeated twice. The ether layer in the last extraction was removed and evaporated to dryness on the water bath. The test solution was obtained by dissolving the residue in 0.5 ml of water.

Manganese. The cobalt target was dissolved in dilute nitric acid containing 0.4 mg of manganese carrier. Some iron carrier was added and then solid ammonium chloride and ammonia to precipitate the hydroxides. Manganese here almost completely follows iron in the hydroxide precipitate, whereas most of the cobalt remains in solution. The precipitate was washed twice with dilute ammonia. It was then dissolved in 1 N nitric acid, and holdback carriers of nickel, iron, chromium, vanadium, titanium, and scandium were added. Manganese dioxide was precipitated by the addition of solid potassium bromate and heating on the water bath for ten minutes. The precipitate was well washed with 1 N nitric acid and then dissolved in hydrochloric acid plus two drops of hydrogen peroxide. After evaporation of the hydrochloric acid, the manganese dioxide precipitation and the dissolution of the precipitate in hydrochloric acid and hydrogen peroxide were repeated. At last the hydrochloric acid was evaporated, and the residue was dissolved in water to form the test solution for manganese.

Chromium. The target (cobalt) was dissolved in dilute nitric acid containing 0.2 mg of chromium carrier. Iron carrier was added, and the hydroxides were precipitated with ammonia and ammonium chloride. The precipitate was washed twice with dilute ammonia and then boiled with 1 N sodium hydroxide and two drops of hydrogen peroxide. The solution was scavenged twice with iron and titanium hydroxides, then neutralized and made acid with 0.5 ml of 1 N sulphuric acid. Two drops of hydrogen peroxide were added, and chromium was extracted with 10 ml of ethyl acetate. The organic

layer was washed twice with very dilute sulphuric acid. Chromium was then re-extracted into dilute ammonia. The extraction of chromium was repeated. This time chromium was re-extracted into eight drops of water and two drops of ammonia. This solution was used as test solution for chromium.

Vanadium. The first part of the chemical procedure for vanadium was the same as for chromium except that 0.2 mg of vanadium was added as carrier instead of chromium. Vanadium was oxidized by hydrogen peroxide and dissolved in sodium hydroxide just as chromium. The solution was scavenged twice with iron and titanium hydroxides and then made 1 N in hydrochloric acid. 1 ml of a 6 per cent cupferron solution was added, and vanadium cupferrate was extracted into chloroform. The chloroform phase was washed twice with 1 N hydrochloric acid and then transferred to a porcelain crucible. The chloroform was evaporated, and the residue was ignited. It was then taken up into 0.5 ml of 1 N nitric acid. This solution was used as test solution for vanadium.

Titanium. The target (cobalt) was dissolved in dilute nitric acid containing 0.2 mg of titanium carrier. Carriers of iron and vanadium were added, and the solution was made ammoniacal. The precipitate was washed twice with dilute ammonia and then boiled with 1 N sodium hydroxide and hydrogen peroxide. After washing, the precipitate was dissolved in hydrochloric acid, and more vanadium carrier, sodium hydroxide, and hydrogen peroxide were added. After boiling, the precipitate was centrifuged, washed, and then dissolved in 6 N hydrochloric acid. All iron was removed by repeated extractions with ether. The water phase was made 1 N in hydrochloric acid, 1 ml of a 6 per cent cupferron solution was added, and titanium was extracted with chloroform. The chloroform layer was washed twice with 1 N hydrochloric acid and then transferred to a porcelain crucible for evaporation and ignition. The residue was dissolved in 1 N nitric acid, which was evaporated to a volume of 0.5 ml to form a test solution for titanium.

Scandium. The scandium chemistry (cobalt target) was very similar to the titanium chemistry in the first steps (carrier: 0.2 mg of scandium). The hydroxides were precipitated, and chromium and vanadium were removed after oxidation with hydrogen peroxide. Iron chloride was extracted with ether and titanium cupferrate with chloroform. The water phase after the titanium extraction was made ammoniacal, and the precipitate was washed with water. It was then dissolved in 3 ml of 1 N hydrochloric acid. 3 g of ammonium thiocyanate was added, and the scandium thiocyanate was extracted with ether. The ether phase was washed twice with 1 N hydrochloric acid containing 0.5 g of ammonium thiocyanate per milliliter. A few drops of hydrochloric acid were added, and

the ether was evaporated on the water bath. The thiocyanate was destroyed with nitric acid, and then scandium was precipitated with ammonia again. After washing with water, the precipitate was dissolved in 0.5 ml of 1 N nitric acid to form the test solution for scandium.

Calcium. Calcium was separated from cobalt, manganese, and vanadium using 10 mg of carrier. The separation procedure from a cobalt target was as follows. The target was dissolved in nitric acid containing 10 mg of calcium. The solution was made ammoniacal and scavenged three times with iron and titanium hydroxides. Cobalt was precipitated as the sulphide. The supernate was boiled down to a small volume, and calcium oxalate was precipitated with ammonium oxalate. The calcium oxalate was washed with a solution containing ammonium oxalate. It was then dissolved in dilute nitric acid, and the oxalate was destroyed with potassium permanganate. Iron and titanium carriers were added, and the solution was made ammoniacal. After scavenging with more iron hydroxide, the precipitation of calcium oxalate and then the destruction of the oxalate were repeated. At last calcium was again precipitated as the oxalate, which was washed with water, alcohol, and ether and then spread out on an aluminium dish, dried at 110°, weighed, and mounted for particle counting.

Potassium. The target (cobalt) was dissolved in nitric acid containing 2 mg of potassium carrier. Iron carrier was added, and the solution was made ammoniacal to precipitate the hydroxides. The supernate was scavenged twice with iron hydroxide. After this, hydrogen sulphide was bubbled through to precipitate cobalt. The supernate was strongly acidified with nitric acid and hydrochloric acid and then evaporated to dryness in a porcelain crucible. All ammonium salts were fumed off. The residue was dissolved in 1 ml of water. This solution was cooled in an ice-bath, and potassium perchlorate was precipitated with perchloric acid and alcohol. The precipitate was washed twice with absolute alcohol and then dissolved in 1 ml of hot perchloric acid. Potassium perchlorate was again precipitated on cooling and addition of alcohol. The cycle was repeated once more. Then the potassium perchlorate was washed well with absolute alcohol, dried at 120°, and dissolved in 1–1.5 ml of water. This solution was the test solution for potassium.

Chlorine. The target (vanadium) was transferred to a distillation apparatus and dissolved in dilute nitric acid containing 10 mg of chlorine as hydrochloric acid. When the target had been completely dissolved, the hydrochloric acid was distilled into a receiver containing a solution of silver nitrate. The silver chloride was washed twice with 1 N nitric acid and then dissolved in 5 N ammonia. After two scavengings with iron hydroxide the solution was acidified with nitric

acid, and more silver nitrate was added. The precipitate was washed with 1 N nitric acid, water, alcohol, and ether. It was transferred to an aluminium dish, dried, weighed, and mounted for particle counting.

Sulphur. The target (vanadium or manganese) was dissolved in dilute nitric acid containing 10 mg of sulphur as sulphuric acid. Barium chloride was added to precipitate barium sulphate. The precipitate was well washed with dilute hydrochloric acid and then boiled for one hour with a 50 per cent solution of potassium carbonate. The supernate was acidified with hydrochloric acid, and barium sulphate was precipitated with barium chloride. The barium sulphate was converted to barium carbonate as before, and the sulphate in the supernate was again precipitated with barium chloride. The precipitate was well washed, dried at 110°, and weighed on an aluminium dish.

Phosphorus. The target (vanadium or manganese) was dissolved in dilute nitric acid containing 10 mg of phosphorus as phosphate. The solution was made 1 N in nitric acid, and phosphorus was precipitated with ammonium molybdate. The precipitate was washed with nitric acid and then dissolved in ammonia. Holdback carrier of vanadium was added, and magnesium ammonium phosphate was precipitated with magnesia mixture. The precipitate was washed and then dissolved in 1 N nitric acid. The ammonium phosphomolybdate–magnesium ammonium phosphate cycle was repeated twice. The last precipitate of magnesium ammonium phosphate was washed, ignited on a platinum dish, and weighed as magnesium pyrophosphate.

Silicon. The target (vanadium or manganese) was dissolved in nitric acid containing 10 mg of silicon as fluosilicate. Boric acid and ammonia were added to precipitate silica. The precipitate was washed twice with concentrated nitric acid and then dissolved in sodium hydroxide. After two scavengings with titanium hydroxide the supernate was acidified with hydrochloric acid and evaporated to dryness. The residue was treated with hydrochloric acid and then washed with nitric acid. The dissolution in sodium hydroxide and evaporation to dryness after scavenging with titanium hydroxide was repeated. The residue was washed with nitric acid, water, alcohol, and ether and then dried, ignited on a platinum dish, and weighed as silica.

Magnesium. The target (vanadium) was dissolved in dilute nitric acid containing 10 mg of magnesium carrier. Iron carrier was added, and the solution was made ammoniacal. The supernate was scavenged three times with iron and titanium hydroxides. Diammonium phosphate was then added to precipitate magnesium ammonium phosphate. The precipitate was washed with water and then dissolved in hydrochloric acid. Chromium carrier and a few drops of hydrogen peroxide were added, and the solution was made ammoniacal.

Magnesium was again precipitated with diammonium phosphate. The cycle was repeated twice. The last precipitate was washed with water, alcohol, and ether, then ignited on a platinum dish and weighed as magnesium pyrophosphate.

Sodium. The target consisted of a mixture of arsenic (cobalt, manganese) and aluminium (magnesium). It was dissolved in nitric acid and hydrochloric acid containing 2 mg of sodium carrier. Iron carrier was added, and the solution was made ammoniacal to precipitate the hydroxides. The supernate was scavenged twice with iron hydroxide and twice with zinc sulphide. Then it was strongly acidified with hydrochloric acid and nitric acid and evaporated to dryness in a porcelain crucible. The ammonium salts were fumed off, and the residue was dissolved in 1 ml of water. The solution was cooled in an ice-bath, and a solution of zinc uranyl acetate was added to precipitate sodium zinc uranyl acetate. The precipitate was washed with the reagent and then dissolved in absolute alcohol, which had previously been saturated with hydrogen chloride gas. After a short time sodium chloride was precipitated. The precipitate was washed twice with the hydrogen chloride saturated alcohol. It was then dissolved in a few drops of water. The sodium zinc uranyl acetate--sodium chloride cycle was repeated twice. When the last sodium chloride precipitate had been washed with hydrogen chloride saturated alcohol, it was washed twice with absolute alcohol. The last trace of the wash liquid was removed by heating at 120° for ten minutes. The residue was then dissolved in 1–1.5 ml of water to form the test solution for sodium.

4. METHODS OF ANALYSIS

The analyses of the test solutions were generally carried out with spectrophotometric methods. Unless stated, the methods used are modifications of the methods described by Sandell (85). Since all solutions were very pure, the standard methods could often be simplified.

The method used for each element is shortly indicated below.

Selenium. A turbidimetric method described by De Meio (86), was used. The selenious acid was reduced to elementary selenium with stannous chloride, and the colloidal solution was stabilized by the addition of gum arabic.

Arsenic. Since arsenic was available in rather large quantities, a gravimetric method of analysis was chosen, namely the

precipitation of magnesium ammonium arsenate as described by Scott (87).

Germanium. A blue colour is developed by the addition of ammonium molybdate and ferrous ammonium sulphate to a germanium solution. This reaction was used in the spectrophotometric analysis.

Gallium. Gallium was determined as the oxinate in chloroform. The method is described by Moeller and Cohen (88).

Zinc. The mixed-colour method using zinc dithizonate, extracted into carbon tetrachloride, was used.

Copper. Copper was analysed as the diethyldithiocarbamate in isoamylalcohol.

Nickel. Also nickel was analysed as the diethyldithiocarbamate in isoamylalcohol.

Cobalt. Cobalt gives a red colour with nitroso-R salt. This reaction forms the basis for the method of analysis used.

Iron. The orange-red complex formed by ferrous iron and *o*-phenanthroline was used in the spectrophotometric analysis.

Manganese. The manganese was oxidized to permanganate with periodate, and the permanganate solution was used in the spectrophotometric analysis.

Chromium. The chromium was oxidized to chromate with ammonium persulphate, and the red-violet colour developed by chromate and diphenylcarbazide was used in the analysis.

Vanadium. Vanadium, treated with hydrogen peroxide, gives a yellow colour with phosphoric acid and a solution of sodium tungstate. This reaction was used in the analysis.

Titanium. For the analysis of titanium the method by von Endrédy and Brugger (89) was used. This method uses the red colour developed by titanium and chromotropic acid in a sulphuric acid solution.

Scandium. Eberle and Lerner (90) describe a spectrophotometric method of analysis for scandium using the coloured complex with alizarin-red S. This method was used.

Potassium. The potassium was converted to potassium sulphate by evaporation with sulphuric acid in a weighed platinum crucible. The analysis was simply carried out by weighing

the sulphate on a microchemical balance (amount of potassium sulphate: 1–2 mg).

Sodium. Sodium was precipitated as sodium zinc uranyl acetate, which was then dissolved in water. This yellow solution was used in the analysis.

F. *Determination of Disintegration Rates*

1. CONVERSION OF COUNTING RATES TO DISINTEGRATION RATES

With the counting equipment previously described the activity of different nuclides can be determined. If there is more than one radioactive isotope in a sample, and these isotopes have sufficiently different half-lives, it is often possible to determine the activity of each isotope by analysis of the gross disintegration curve. The activity, or counting rate, has to be converted to disintegration rate for the cross section determination. Zumwalt (70), Burtt (91), Cook and Duncan (92), Pappas (71), and others have investigated absolute determinations of disintegration rates with counting equipments of a similar type as the one used here. They find that the activity A of a β-emitting nuclide, after correction for coincidence loss and background count, can be written in the following way:

$$A = G\,D\,f_W f_A f_H f_S f_B f_E = G\,D\,F;$$
$$F = f_W f_A f_H f_S f_B f_E. \qquad (19)$$

D is the disintegration rate. The other factors appearing in Eq. (19) correct for the following effects:

f_W: absorption in the window of the GM-tube and in the air between the sample and the window;

f_A: scattering from the air between the sample and the window;

f_H: scattering from the sample holder and from the walls of the lead housing;

f_S : scattering and absorption in the sample;
f_B : backscattering from the support of the sample;
f_E : the efficiency of the counter for different kinds of radiation. f_E is defined as the ratio between the number of particles counted and the number of particles that reach the sensitive volume of the counting tube.

The factor G is a geometry factor, which can be calculated from the geometry of the counting arrangement or may be determined by a suitable experiment (91, 93, 94). In the present work only relative disintegration rates were measured, and it was not necessary to determine the geometry factor (its value was about seven per cent).

Nuclides can emit radiation of different kind: β-particles (positive or negative), conversion electrons, γ-rays, and x-rays.[1] The total counting rate of a nuclide, A_{tot}, will be the sum of a series of terms of the type (19), one for each kind of radiation in the disintegration.[2]

$$A_{tot} = G\,D\,(\Sigma a_\beta F_\beta + \Sigma a_e F_e + \Sigma a_\gamma F_\gamma + \Sigma a_x F_x) = G\,D\,\Sigma a_j F_j. \tag{20}$$

a_j is here the fraction of the disintegrations giving rise to radiation of the kind j. $\Sigma a_\beta F_\beta$ consists of a series of (aF)-values, one for each β-group, etc. The disintegration rate D can thus be calculated from a measurement of A and a determination of the different F-values, provided that the disintegration scheme for the actual nuclide is known.

In most cases the (aF)-values of the β-particles give by far the most important contribution to $\Sigma a_j F_j$. The contribution from other kinds of radiation is then to be considered only as a small correction. Sometimes, however, there are no β-particles in the disintegration of the nuclide. Then the other terms in the sum $\Sigma a_j F_j$ will, of course, be important.

[1] α-particles and Auger electrons are of no interest here.

[2] This is not strictly true because of possible coincidences between different kinds of radiation. However, if the geometry used is small, the number of coincidences will be low and can be neglected.

2. CORRECTION FACTORS FOR β-PARTICLES

a. *The Disintegration Scheme*

For many nuclides, which decay 100 per cent by β-radiation but which have several β-groups, the percentage of the different β-groups is not well known. The values of a_β are uncertain. The uncertainty in the cross section determination, arising from this, might be small because the factors F_β do not depend strongly on the β-energy (if this is not very low) and the sum Σa_β is equal to unity. However, for K-capturing nuclides the ratio between the probability of K-capture and the probability of positron (negatron) emission is often quite uncertain. In such cases this, as a rule, will be the main source of error in the cross section determinations.

b. *Absorption in Air and Window*

The factor f_W, which corrects for the absorption of β-particles in the counter window and in the air between the sample and the window, does not differ much from unity except for low energy radiation. It can be determined from an absorption curve (70, 71, 91). The sample is placed in the standard position (on the second shelf from the window), an aluminium absorber is placed immediately below the window, and the activity is measured for different absorber thicknesses. The absorption curve is then obtained by plotting the activity on a logarithmic scale as a function of the absorber thickness (in mg/cm^2). It is important that the absorbers be placed as close as possible to the window in order to decrease the effect of scattering. If the absorber is placed close to the sample, the absorption curve will often show a maximum for a thickness of a few milligrams per square centimeter. Such a curve cannot be used to determine f_W.

The factor f_W is now determined in the following way. The absorption curve is extrapolated back to a (negative) thickness which is equal to the combined thickness d of the window and the air in the air gap. f_W is then equal to the ratio between the activity at the absorber thickness zero and the extrapolated activity at the thickness $-d$. The extrapolation is simplified

by the fact that the absorption curve is almost linear in its first part, *i.e.* the absorption is exponential. Owing to this exponential absorption f_W can be determined from the formula

$$f_W = \exp\left(-\frac{d \ln 2}{d_{1/2}}\right), \tag{21}$$

where $d_{1/2}$ is the initial half-thickness, *i.e.* the absorber thickness needed to decrease the activity by a factor of two. The initial half-thickness is determined graphically from the first part of the absorption curve. If the curve is not linear, the tangent should be drawn at the point zero and $d_{1/2}$ determined from this tangent.

Zumwalt (70) found that the absorption curves showed a tendency to bend upwards for small absorber thicknesses. This would mean that f_W determined from (21) would be too large. Zumwalt introduced a second order correction for this effect. On the other hand, Gleason, Taylor, and Tabern (95) found exponential absorption for thin absorbers even if the air was replaced by helium. Graf, Comar, and Whitney (96) used a windowless counter to determine absorption curves for Ca^{45}, S^{35}, and C^{14} between 0 and 3 mg/cm^2. Their absorption curves for S^{35} and C^{14} are approximately linear in the whole region, but the absorption curve for Ca^{45} bends upwards for absorbers thinner than 0.3 mg/cm^2. In the absorption curves determined in the present work no deviation from an initially exponential absorption was seen, and consequently f_W was determined from (21).

Zumwalt and Pappas took the oblique path of the β-particles into account in the determination of d. No such correction is necessary here, however, since the path of the β-particles is oblique also in the absorbers. Thus $d_{1/2}$ should be multiplied by the same factor as d, and this factor would drop out of the formula (21).

For nuclides with a complex β-spectrum f_W has to be determined for each of the β-groups. This is not easily done from the absorption curve, however. In such cases f_W was determined from an experimental curve of $d_{1/2}$ as a function of the maximum energy of the β-particles. For the determination of this

curve only nuclides with a single β-group were used. The data chosen for this empirical curve are tabulated in Table 3.

Table 3

Experimental determinations of $d_{1/2}$

Nuclide	Maximum β-energy	$d_{1/2}$ mg/cm²
S^{35}	0.17 Mev	3.0
Ca^{45}	0.26 „	5.8
Co^{60}	0.31 „	8.6
Zn^{65}	0.33 „	7.5
Sc^{46}	0.36 „	10.3
Cu^{64}	0.60 „	23
	(average of β^- and β^+)	
V^{48}	0.69 Mev	34
Tl^{204}	0.76 „	34
Zn^{69}	0.90 „	58
Pr^{143}	0.92 „	52
Ti^{45}	1.02 „	66
Bi^{210}	1.17 „	58
Na^{24}	1.39 „	95
Ga^{68}	1.88 „	178
V^{47}	1.89 „	132
Y^{90}	2.25 „	240
Pr^{144}	2.97 „	375
Rb^{82m}	3.15 „	380

The values of the half-thicknesses are plotted on a log-log-scale *versus* the maximum β-energy in Fig. 9. A linear relationship between log $d_{1/2}$ and log E_{max} is indicated. The line drawn in the figure corresponds to the formula

$$d_{1/2}\,(\mathrm{mg/cm^2}) = 57\ E^{1.71}\,(\mathrm{Mev}). \tag{22}$$

Gleason *et al.* (95) also noted this relationship. They give a formula which in our notation can be written

$$d_{1/2}\,(\mathrm{mg/cm^2}) = 41\ E^{1.43}\,(\mathrm{Mev}). \tag{23}$$

This curve is also shown in Fig. 9 as is the empirical curve given by Coryell and Sugarman (97). The deviation between

the curves might be due to slight differences in the way of measuring the half-thicknesses. The differences in f_W computed from these three curves would be quite small, however, since the curves almost coincide at low energies, *i.e.* where f_W deviates appreciably from unity.

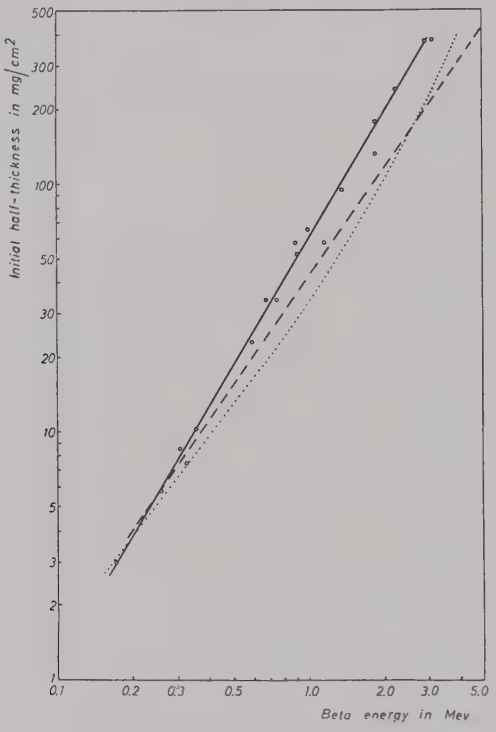

Fig. 9. The initial half-thickness *versus* the maximum β-energy.
Solid line: This work.
Broken line: Gleason, Taylor, and Tabern (95).
Dotted line: Coryell and Sugarman (97).

It is interesting to see what would be the value of $d_{1/2}$ obtained from the absorption curve of a nuclide with a complex β-spectrum. A nuclide is assumed to have several β-groups with the relative probability a_i and the half-thickness d_i (the ab-

sorption is assumed to be exponential for all components) for the i^{th} β-group.

If $A(x)$ is the counting rate with the absorber x, one obtains

$$A(x) = A(0) \sum_i a_i \exp\left(-\frac{x \ln 2}{d_i}\right). \tag{24}$$

If the total absorption is approximately exponential for small values of x (which is often the case (71)) and has the half-thickness d_0, one can write

$$A(x) = A(0) \exp\left(-\frac{x \ln 2}{d_0}\right). \tag{25}$$

Equating the expressions for

$$\left(\frac{d \ln A(x)}{dx}\right)_{x=0}$$

obtained from (24) and (25) gives the following relation between the initial half-thickness of the complex β-spectrum and the half-thicknesses of the components:

$$\frac{1}{d_0} = \sum_i \frac{a_i}{d_i}. \tag{26}$$

Measured values of the half-thickness and values calculated from (26) are compared in Table 4.

c. *Air- and House-Scattering*

The factors f_A and f_H correct for scattering effects from the air between the sample and the window and from the walls of the aluminium-lined lead housing. These factors have been determined by Zumwalt (70). Since the counting arrangement used by Zumwalt was very similar to the one used here, his data (in the form of a curve given by Pappas (71)) were used in the present work. These scattering effects are small. f_A and f_H deviate from unity by 2.5 per cent at most.

Table 4

Comparison between measured and calculated half-thicknesses for nuclides with a complex β-spectrum

Nuclide	Maximum β-energy	a	(d_o) obs mg/cm²	(d_o) calc mg/cm²
Cr^{49}	0.73 Mev	0.15	101	82
	1.39 „	0.35		
	1.54 „	0.50		
Fe^{59}	0.26 „	0.48	9.3	8.6
	0.46 „	0.52		
Co^{61}	1.00 „	0.45	81	77
	1.45 „	0.55		
Ni^{65}	0.60 „	0.29	61	54
	1.01 „	0.14		
	2.10 „	0.57		

d. *Self-Scattering and Self-Absorption*

The factor f_S corrects for scattering and absorption in the sample itself. It depends on the thickness and composition of the sample and on the β-energy. This correction factor has been investigated especially by Nervik and Stevenson (98), by Pappas (71), and by Baker and Katz (99).

For a given sample composition and β-energy f_S increases at first with the thickness of the sample (the scattering outweighs the absorption). It passes through a maximum and decreases afterwards owing to the increasing importance of the absorption. It has been found by several investigators that this ultimate decrease is approximately exponential (100, 101). The factor f_S depends also on the atomic number of the sample. This is to be expected, since the scattering effect is strongly dependent on the atomic number. There is also a strong dependence of f_S on the β-energy.

The magnitude of f_S and its dependence on various factors is indicated in Table 5, the data of which are taken from the work by Nervik and Stevenson.

Table 5

The correction factor for self-scattering and self-absorption

Maximum β-energy	Sample	Sample thickness giving maximum f_S	Maximum of f_S
0.3 Mev	NaCl	1.2 mg/cm²	1.02
2.5 „	NaCl	20.5 „	1.19
0.3 „	$Pb(NO_3)_2$	2.0 „	1.12
2.5 „	$Pb(NO_3)_2$	8 „	1.30

It is seen from the table that the self-scattering and self-absorption effect is quite large even for relatively thin samples.

Evidently f_S is a very complex function of the variables just mentioned. Whether it also depends on the kind of β-radiation, has not been investigated. Positrons and negatrons might give different f_S under otherwise identical conditions, however, in analogy with the difference in the backscattering effect (compare p. 54). It would be very laborious to make up general curves of f_S as a function of the thickness and composition of the sample and of the β-energy. For accurate work it should be better to determine f_S experimentally for each nuclide and sample to be studied. This difficulty in the determination of f_S was the main reason for the method, previously described, of using small amounts of carriers and consequently thin samples for counting. For thin samples f_S will tend towards unity.

In order to evaluate the variation of f_S with the sample thickness for thin samples, the self-scattering and self-absorption was investigated in the following way. A series of test solutions containing known amounts of a suitable compound and of the same volume were made up, and the same amount of a carrier-free tracer solution was added to each test solution. Five or more samples for counting were prepared from each solution in the usual way, and the activity of the samples was measured. For each test solution the average activity was determined. This average value was divided by the corresponding average activity for a solution which did not contain any added compound and which gave essentially weightless samples. Thus one value of f_S was obtained for each test solution. The added compound

was chosen so as to have about the same "effective" atomic number as the samples to be investigated in the present work. The definition by Pappas (71) was used for the "effective" atomic number Z_{eff}, namely

$$Z_{eff} = \frac{\sum_i n_i A_i Z_i}{\sum_i n_i A_i} \tag{27}$$

for a sample of the composition

$$n_1 Z_1^{A_1} + n_2 Z_2^{A_2} + n_3 Z_3^{A_3} + \ldots .$$

The results with different tracers are tabulated in Table 6.[1] The added compound was potassium nitrate, which has an effective atomic number of 12.1.

Table 6

Determination of f_S

Tracer	Maximum β-energy	Thickness of the sample	f_S
Co^{60}	0.31 Mev	0 mg/cm²	1.000
		0.34 „	1.013 ± 0.002
		0.46 „	1.016 ± 0.005
Sr^{89}	1.46 Mev	0 „	1.000
		0.21 „	1.012 ± 0.004
		0.40 „	1.019 ± 0.005
		0.71 „	1.029 ± 0.004
Pr^{144}	2.97 Mev	0 „	1.000
		0.18 „	1.014 ± 0.005
		0.36 „	1.016 ± 0.005

The work by Nervik and Stevenson (98) indicates that f_S does not depend strongly on the β-energy for very thin samples. Therefore all f_S-values of Table 6 have been plotted *versus* the

[1] The error given in the tables and figures is always the standard deviation.

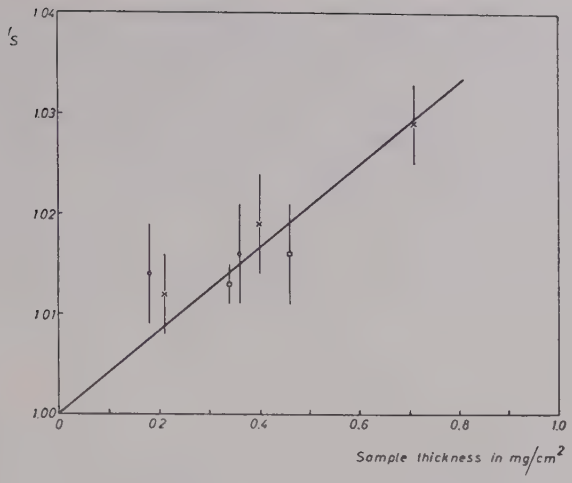

Fig. 10. The correction factor for self-scattering and self-absorption *versus* the sample thickness. Co^{60} (squares), Sr^{89} (crosses), and Pr^{144} (circles) were used in the determinations.

sample thickness in Fig. 10. The solid line in the figure was used to correct the samples for the effect of self-scattering and self-absorption in the present work.

In order to correct for self-scattering and self-absorption the weight of the samples had to be approximately determined. This was done by weighing them on a microchemical balance. Most samples were thin enough so that f_S could be put equal to unity.

For the thick samples obtained with 10 mg amounts of carriers the f_S -values were taken from the curves given by Nervik and Stevenson.

e. Backscattering

The factor f_B corrects for the backscattering of β-particles from the sample support. This effect depends on the kind and energy of the β-particles and on the thickness and composition of the support. The backscattering effect has been investigated by Zumwalt (70), Pappas (71), Burtt (91), Yaffe and Justus (102), and others. The main features of f_B are the following.

For a given kind of support and β-energy f_B increases with the thickness of the support until the thickness corresponds to 1/8–1/4 of the range of the β-particles in the substance. Then a saturation value is reached, and f_B becomes a constant. The saturation value is independent of the β-energy if this is above 0.2 Mev as shown by Glendenin and Solomon (103), but a thicker support is, of course, required to reach this saturation value for higher β-energies. The saturation value increases with the atomic number. Müller (104) has shown that the saturation value increases with the effective atomic number as defined by Eq. (27) approximately as $Z_{eff}^{1/3}$.

The saturation value of f_B is often high. For lead Yaffe and Justus give the value 1.65.

Seliger (105) found that f_B depends on the kind of β-particle. The scattering effect is about thirty per cent lower for positrons than for negatrons.

Seliger (106) has also pointed out that the backscattering is anisotropic. For this reason f_B will depend on the geometry of the counting arrangement.

It is thus seen, that the backscattering effect is quite complex. Some investigators use thick supports in order to get saturation backscattering. The backscattering factor will then be high, however, and large errors in the determinations might arise from erroneous determinations of f_B. Ideally all correction factors should be as close to unity as possible. In the method of sample preparation, previously described, the samples were prepared by the evaporation of a measured amount of the test solution on a thin aluminium foil. The average thickness of the foil used was 2.40 mg/cm^2. Since the support was so thin f_B was always close to unity. The backscattering effect cannot be neglected, however, and a series of experiments were carried out in order to determine the factor f_B.

Since the thickness and composition of the support was always the same, the only variable for f_B was the kind and energy of the β-particles. The backscattering factor was determined for a few nuclides with simple β-spectra in the following way. One drop of a suitable carrier-free tracer solution was

evaporated on a thin film of tygon or rubber hydrochloride. The sample was placed in the standard position of the counter arrangement, and the activity was measured. Then the aluminium foil was placed immediately below the thin film, and the activity was again measured. The activity measurements were corrected for background and gamma count, and f_B was then obtained as the ratio between the activity with and without the aluminium foil.

The tracers used for the experiment are tabulated in Table 7.

Table 7

Tracers for the determination of the backscattering factor

Nuclide	Maximum β-energy	Support	
		Kind	Thickness
Co^{60}	0.31 Mev	tygon	0.2 mg/cm²
Tl^{204}	0.77 „	„	0.2 „
Sr^{89}	1.46 „	rubberhydrochloride	0.5 „
Y^{90}	2.24 „	„	0.5 „
Pr^{144}	2.97 „	„	0.5 „

The results of the measurements are given in Table 8.

Table 8

Determination of f_B

β-Energy	0.31 Mev	0.77 Mev	1.46 Mev	2.24 Mev	2.97 Mev
f_B	1.053	1.033	1.012	1.017	1.003
	1.029	1.038	1.026	1.013	1.005
	1.022	1.030	1.010	1.011	0.998
	1.039	1.034	1.012	1.005	1.014
	1.027	1.038	1.031	1.004	1.004
	1.047	1.028	1.029	1.017	0.995
		1.028	1.024	1.008	
		1.028	1.027		
(f_B) Av	1.036 ± 0.005	1.032 ± 0.002	1.021 ± 0.003	1.011 ± 0.002	1.003 ± 0.003

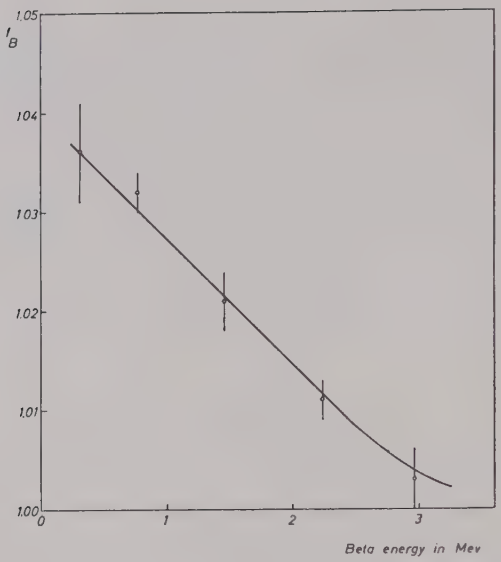

Fig. 11. The backscattering factor *versus* the maximum β-energy.

A correction should be made for the scattering from the thin film. This correction, however, turned out to be negligible.

The method of determining the backscattering factor used here is not quite free from criticism. Glendenin and Solomon (103) have shown that a sample directly evaporated on a metal foil has a higher value of f_B than a sample evaporated on a thin film with the metal foil below. This depends probably on the fact that the surface of the metal foil is more uneven than the film and gives more small-angle scattering. Yaffe and Justus (102) also noted this, but they claim that the method can be used for aluminium.

The factor f_B is plotted as a function of the maximum β-energy in Fig. 11. The curve drawn through the points was used to estimate f_B in the present work. The curve is valid for negatrons. For positrons the scattering effect was assumed to be thirty per cent lower than for negatrons.

For the thick samples mounted on aluminium (50 mg/cm^2) or platinum (400 mg/cm^2) dishes f_B was estimated from the investigations by Burtt, Yaffe and Justus, and Seliger.

f. *The Efficiency of the GM-Tube*

The factor f_E is assumed to be equal to unity for both positrons and negatrons, *i.e.* those particles which have reached the sensitive volume of the counter are counted with 100 per cent efficiency. The efficiency might perhaps be expected to be slightly lower than 100 per cent, but this should not affect the measurements much provided that the sensitivity of the counter tube is not energy dependent. Zumwalt's data (70) show that the energy dependence is negligible.

g. *The F-Values for* β*-Particles*

For practical use it is convenient to multiply together all the correction factors except f_S to give a factor F_1, which then only depends on the maximum β-energy if the counting arrangement is not changed.

$$F_1 = f_W f_A f_H f_B f_E. \tag{28}$$

Fig. 12 shows F_1 as a function of the β-energy. It is valid for negatrons counted with the Victoreen tube with d equal to 5.7 mg/cm^2.

3. CORRECTION FACTORS FOR CONVERSION ELECTRONS

The conversion electrons are monoenergetic. For this reason different correction factors are required for conversion electrons than for β-particles. How the correction factors depend on the energy, has not been investigated in the present work. Usually the conversion electrons do not contribute very much to the total activity, and it is not necessary to know the correction factors as well as for β-particles (this remark also applies to γ-rays and x-rays). It should therefore be sufficient to estimate the correction factors for conversion electrons from the corresponding factors for β-particles.

The absorption of monoenergetic electrons is linear in the absorber thickness (107). This means that a linear extrapola-

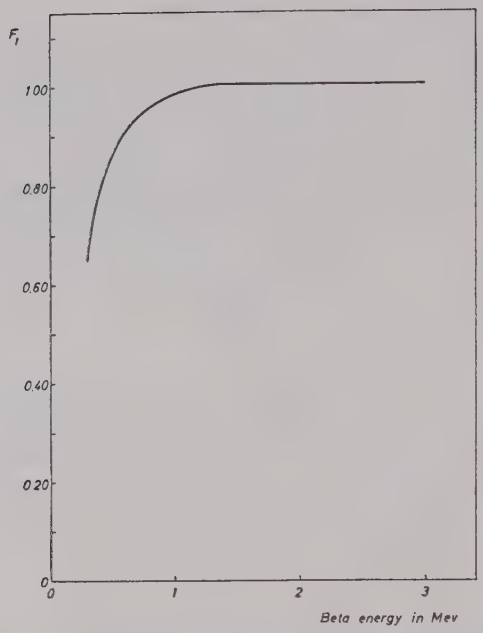

Fig. 12. The factor F_1 (for β-particles) *versus* the maximum β-energy.

tion should be carried out instead of an exponential one for the determination of f_W. Thus f_W is easily calculated from the range of the monoenergetic electrons, which can be obtained from the reference (107).

For the factors f_A, f_H, f_B, and f_S the same curves were used for conversion electrons as for β-particles after a change of the energy scale. For conversion electrons of energy E the values of the correction factors corresponding to the maximum β-energy 3 E were used, because the average energy in the β-spectrum is about one third of the maximum energy. This procedure is justified at least for the backscattering effect as shown by Balfour (108).

The efficiency factor f_E was put equal to unity for conversion electrons.

4. CORRECTION FACTORS FOR γ-RAYS

For γ-rays the effects of absorption and scattering are negligible. The factors f_W, f_A, f_H, f_S, and f_B can be put equal to unity. The only correction factor of importance is the counter efficiency of detecting γ-rays.

The γ-sensitivity of a GM-tube of a similar type as the ones used in this work has been calculated by Studier and James (109). They found that f_E can be put equal to E (Mev)/100 for energies larger than 0.5 Mev. Below 0.5 Mev the sensitivity is constant, and the value $f_E = 0.005$ should be used.

In this work the γ-sensitivity of the tubes was checked experimentally by comparing the γ-activity and the β-activity for nuclides with known disintegration schemes. Some results are given in Table 9.

Table 9

Comparison between observed and calculated γ-sensitivity

Nuclide	γ-energy	$\frac{\gamma\text{-activity}}{\beta\text{-activity}}$ in per cent	
		Experimental data	Calculated data
Na^{24}	1.37 Mev 2.75 „	4.3	4.3
V^{48}	0.99 „ 1.32 „	4.9	5.2
Cr^{49}	0.15 „ 0.61 „	1.0	0.84
$Fe^{52} + Mn^{52m}$	0.94 „ 1.46 „	2.0	2.2
Fe^{59}	1.10 „ 1.30 „	1.1	1.2
Co^{60}	1.17 „ 1.33 „	2.3	2.5
Co^{61}	0.45 „	0.3	0.23
$Ni^{66} + Cu^{66}$	1.09 „	0.0	0.05
Cu^{67}	0.09 „ 0.18 „	0.19	0.25

The agreement between the observed and the calculated γ-sensitivity is good. Thus the factor f_E can be calculated in the simple way described above. The standard deviation is estimated to be about twenty per cent.

5. CORRECTION FACTORS FOR X-RAYS

For x-rays the scattering effects were neglected. Thus the factors f_A, f_H, f_S, and f_B were all put equal to unity. The factor f_W, on the other hand, will often be quite small, because a large part of the low-energy x-rays found in the actual region of the periodic system is absorbed in the window and in the air between the sample and the window. The absorption of x-rays is exponential so that f_W can be written in the form

$$f_W = e^{-kd}, \tag{29}$$

where k is the mass absorption coefficient and d is the thickness of the absorbing medium in g/cm^2. Since the absorption is strongly dependent on the atomic number of the absorbing medium, the absorption factor was calculated for the air and for the window separately. The mass absorption coefficients for the constituents of the air and for mica were taken from the textbook by Compton and Allison (110).

The factor f_E for the counter efficiency of detecting x-rays will be calculated under the assumption (111) that an x-ray quantum is counted if it is absorbed in the gas of the counter, and that the contribution to the counting rate from electrons emitted from the walls and the window by x-ray absorption can be neglected.

Let s be the density of the gas in the counter and x be the length traversed by the x-rays. Then the sensitivity is equal to

$$1 - e^{-ksx}, \tag{30}$$

since this expression is equal to the ratio between the number of absorbed quanta and the number of incident quanta.

The geometrical arrangement is shown in Fig. 13. The x-rays are assumed to come from a point-source situated at P.

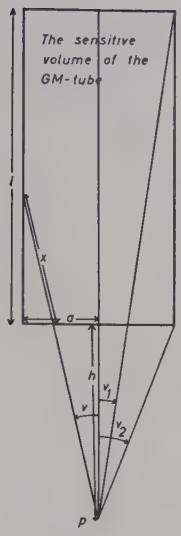

Fig. 13.

The efficiency of detecting x-rays can now be written

$$f_E = \frac{\int_0^{v_2} (1 - e^{-ksx}) \sin v \, dv}{\int_0^{v_2} \sin v \, dv}. \tag{31}$$

In the region

$$0 \leq v \leq v_1$$

the path through the tube is assumed to be equal to the length of the tube. Thus

$$f_E = \frac{(1 - \cos v_1)(1 - e^{-ksl}) + I}{1 - \cos v_2}, \tag{32}$$

where

$$I = \int_{v_1}^{v_2} (1 - e^{-ksx}) \sin v \, dv. \tag{33}$$

The integral can be solved after expansion of $(1 - e^{-ksz})$. The result is

$$I = k\,s\left[a\,(v_2 - v_1) + h\,\ln\left(\frac{\cos v_2}{\cos v_1}\right)\right] - \frac{(k\,s)^2}{2}\left[a^2 \ln \frac{\operatorname{tg}(v_2/2)}{\operatorname{tg}(v_1/2)} + \right.$$

$$\left. + h^2\left(\frac{1}{\cos v_2} - \frac{1}{\cos v_1}\right) - 2\,a\,h \ln\left\{\frac{\operatorname{tg}(v_2/2 + \pi/4)}{\operatorname{tg}(v_1/2 + \pi/4)}\right\}\right] +$$

$$+ \frac{(k\,s)^3}{6}(\ldots) \pm \ldots . \qquad (34)$$

Since (ks) is usually small, the series converges rapidly. The factor F for x-rays is now obtained:

$$F = (f_W)_{air}\,(f_W)_{window}\,f_E . \qquad (35)$$

Often one is not directly interested in the x-ray sensitivity but in the efficiency of detecting K-capture. This efficiency is obtained by multiplying the factor F by the fluorescent yield w_x, which can be obtained from the reference (112).

As an example the efficiency of detecting K-capture of the Victoreen tube in the standard counting arrangement is plotted *versus* the atomic number Z of the K-capturing nuclide in Fig. 14.

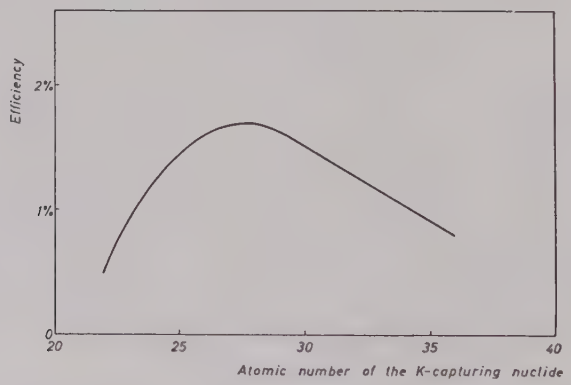

Fig. 14. Efficiency of detection of K-capture.

The error of the efficiency of detecting K-capture was taken to be about fifty per cent.

G. *Identification of Nuclides*

1. HALF-LIFE

The nuclides in the samples were identified by means of their half-lives and β-energies.

The half-life was usually determined graphically from the decay curves. For most nuclides, however, a few half-life determinations were also made using the method of least squares. This method can be immediately applied to the disintegration law in the logarithmic form:

$$\ln A(t) = \ln A(0) - \lambda t. \tag{36}$$

$A(t)$ is the counting rate at the time t.

For simplicity all data were assumed to have the same weight.

In the determination of $A(t)$ the time t was taken to be the middle point of the time interval during which the sample was counted, as proposed by Pappas (71).

2. β-ENERGY

The β-energy of a nuclide can be determined from the absorption curve in different ways (107, 113–115). In the present work two methods were used, namely the determination of the initial half-thickness and the determination of the range by means of the Feather analysis (116).

In the first method the experimental curve in Fig. 9 was used to relate the measured value of the half-thickness and the maximum β-energy.

For the Feather analysis two different comparison curves were used, namely Bi^{210} with the range 510 mg/cm^2 (117) and Y^{90} with the range 1065 mg/cm^2 (115). Bi^{210} has an absorption curve which is linear over almost the entire range, whereas the absorption curve of Y^{90} is concave downwards. The comparison curve most similar to the one to be analysed was chosen.

The empirical relationship given by Katz and Penfold (115)

was used to relate the range R (mg/cm^2) and the maximum β-energy E (Mev). This relationship is as follows:

$$\begin{aligned} R &= 412\, E^{1.265 - 0.0954 \ln E}, \quad \text{for } E < 2.5 \text{ Mev}; \\ R &= 530\, E - 106, \qquad\qquad \text{for } E > 2.5 \text{ Mev}. \end{aligned} \tag{37}$$

H. *Estimation of the Error (Standard Deviation) of the Cross Section Determinations*

If an internal monitor is used, the cross sections are obtained from Eq. (17). The disintegration rate D has now to be written (compare with Eq. (20)):

$$D(t) = \frac{A(t)}{G\, F_0\, f_k}, \tag{38}$$

with

$$F_0 = \sum_j a_j F_j. \tag{39}$$

The factor f_k has to be introduced as a chemical correction factor. It is defined as the ratio between the amount of the actual element in the sample and the amount added as carrier, and is obtained from the chemical analysis.

Eqs. (17) and (38) now give

$$\sigma_a = \sigma_b \frac{A_a(t)}{A_b(t)} \frac{F_{0b}\, f_{kb}}{F_{0a}\, f_{ka}} \frac{Q_b(t)}{Q_a(t)}. \tag{40}$$

The time t in the above formula was always chosen to be the end point t_e of the bombardment.

The standard deviation of σ_a is obtained as follows (the standard deviation of a quantity K is denoted by ΔK):

$$\left(\frac{\Delta \sigma_a}{\sigma_a}\right)^2 = \left(\frac{\Delta \sigma_b}{\sigma_b}\right)^2 + \left(\frac{\Delta A_a(t_e)}{A_a(t_e)}\right)^2 + \left(\frac{\Delta F_{0a}}{F_{0a}}\right)^2 + \left(\frac{\Delta f_{ka}}{f_{ka}}\right)^2 +$$

$$+ \left(\frac{\Delta Q_a(t_e)}{Q_a(t_e)}\right)^2 + \text{similar terms with } a \text{ exchanged for } b. \tag{41}$$

The different terms in (41) will now be investigated:

$\Delta \sigma_b/\sigma_b$. This is obtained from the determination of the absolute cross section of the monitor.

$\Delta A/A$. The activity $A(t_e)$ is calculated from the measured activity $A(t)$ by means of the formula

$$A(t_e) = A(t)\, e^{\lambda(t-t_e)}. \tag{42}$$

Thus

$$\left(\frac{\Delta A(t_e)}{A(t_e)}\right)^2 = \left(\frac{\Delta A(t)}{A(t)}\right)^2 + [\lambda \Delta (t-t_e)]^2 + [(t-t_e)\Delta \lambda]^2. \tag{43}$$

$\Delta A(t)/A(t)$ is estimated graphically from the decay curve or obtained from a "least squares" analysis.

$\Delta F/F$. Differentiation of F_0 gives

$$d F_0 = \sum_j (a_j\, d F_j + F_j\, d a_j), \tag{44}$$

which is substituted for ΔF_0. $\Delta F/F$ is thus estimated from the errors of the correction factors (dF_j) and of the disintegration scheme (da_j). It must be remembered that $\sum_\beta da_\beta = 0$ for a nuclide which decays 100 per cent by β-emission.

$\Delta f_k/f_k$. This is obtained from the chemical analysis.

$\Delta Q/Q$. If the ion current is constant during the irradiation, Q is very simple:

$$Q(t_e) = (1 - e^{-\lambda T}), \tag{45}$$

where T is the length of the irradiation time.
Thus

$$\left(\frac{\Delta Q(t_e)}{Q(t_e)}\right)^2 = \left(\frac{e^{-\lambda T}}{1-e^{-\lambda T}}\right)^2 [(\lambda \Delta T)^2 + (T \Delta \lambda)^2]. \tag{46}$$

For the more general case $\Delta Q/Q$ is obtained from Eq. (7) taking into account possible variation of λ, I_i, K_i, and T_i.

CHAPTER II

Experimental Results

A. *Decay Data of the Investigated Nuclides*

A knowledge of the decay schemes of the nuclides investigated is necessary for the determination of the correction factors used in converting counting rates into disintegration rates. The half-lives must be accurately known for the extrapolation of the counting rate back to the end of the irradiation time and for the evaluation of the factor Q (Eq. (7)). In the present work β-energies were determined only for identification purposes. The decay schemes for the different nuclides were obtained from the literature. More effort was spent, however, in determining half-lives accurately. This was done by analysing the experimental data using the method of least squares.

The nuclides investigated will now be considered in turn. The half-life determinations (with their standard deviation) are collected in tables together with half-lives reported in the literature and references to investigations from which the decay schemes were obtained.

Selenium

Table 10

Selenium isotopes

Isotope	Decay scheme References	Half-life		
		Reported in literature	Determined in this work	Chosen for the calculations
Se^{72}	(48)	9.7 d (48)	8.64 ± 0.06 d	8.64 ± 0.06 d
Se^{73}	(118)	6.7 h (48)	6.37 ± 0.10 h	6.37 ± 0.10 h

Two activities were always found in the selenium samples, namely Se^{72} and Se^{73}. On one occasion the selenium sample

was counted within two hours after the end of the bombardment. Then traces of an activity with short half-life, possibly Se^{70} or 44 m Se^{73} (119), were seen. The activity could not be identified, however, and its cross section must be very small.

Arsenic

Table 11

Arsenic isotopes

Isotope	Decay scheme References	Half-life		
		Reported in literature	Determined in this work	Chosen for the calculations
As^{70}	(120, 122)	52 ± 1 m (121) 47 ± 2 m (122)		52 ± 1 m
As^{71}	(123, 124)	62 ± 3 h (123) 59.5 ± 2 h (125) 48.2 ± 1.2 h (126)		48.2 ± 1.2 h
As^{72}	(127)	25.8 ± 0.2 h (126)		25.8 ± 0.2 h
As^{74}	(128)	17.82 ± 0.13 d (126) 17.5 ± 0.1 d (129)	18.7 ± 0.2 d	18.7 ± 0.2 d

Germanium

Table 12

Germanium isotopes

Isotope	Decay scheme References	Half-life		
		Reported in literature	Determined in this work	Chosen for the calculations
Ge^{67}	(130)	19 m (130)	18.2 ± 1.2 m	18.2 ± 1.2 m
Ge^{68}	(131)	275 ± 20 d (131)	288 ± 6 d	288 ± 6 d
Ge^{69}	(129, 132)	1.65 ± 0.02 d (129)	1.641 ± 0.009 d	1.641 ± 0.009 d
Ge^{71}	(129)	11.4 ± 0.1 d (129) 12.5 ± 0.1 d (133)	10.5 ± 0.4 d	11.4 ± 0.1 d

No trace of 150 m Ge^{66} was seen.

Table 13

Gallium isotopes

Isotope	Decay scheme References	Half-life		
		Reported in literature	Determined in this work	Chosen for the calculations
Ga^{66}	(134—136)	9.45 h (134)	9.57 ± 0.06 h	9.57 ± 0.06 h
Ga^{67}	(137)	78.2 ± 0.5 h (129) 77.9 ± 0.3 h (138)	79.0 ± 0.3 h	79.0 ± 0.3 h
Ga^{68}	(135)	68 ± 4 m (139)	67.7 ± 0.5 m	67.7 ± 0.5 m
Ga^{70}	(140)	20.3 m (141)	22.0 ± 0.9 m	22.0 ± 0.9 m
Ga^{72}	(142)	14.08 ± 0.02 h (143) 14.25 ± 0.10 h (144)		14.08 ± 0.02 h
Ga^{73}	(145)	5 ± 0.5 h (144)	4.77 ± 0.09 h	4.77 ± 0.09 h

Ordinarily the activities in the gallium samples could only be partly separated. The isotopes Ga^{67}, Ga^{68}, and Ga^{70} were always seen, but the isotopes Ga^{66} (9.6 h), Ga^{72} (14 h), and Ga^{73} (4.8 h) could not be separated. In order to determine the relative cross sections of these isotopes a few experiments were carried out in which the gallium isotopes were separated electromagnetically by Andersson and Burgman (146). The method is described by Andersson (147). The isotopes were collected on strips of 2.40 mg/cm^2 aluminium. The relative cross sections of the isotopes Ga^{66}, Ga^{67}, Ga^{68}, Ga^{70}, Ga^{72}, and Ga^{73} could be determined in this way and converted to absolute cross sections from the determination of the cross section of Ga^{68}.

Zinc

Table 14

Zinc isotopes

Isotope	Decay scheme References	Half-life		
		Reported in literature	Determined in this work	Chosen for the calculations
Zn^{65}	(148)	245.0 ± 0.8 d (149)		245.0 ± 0.8 d
Zn^{69m}	(150)	13.8 ± 0.4 h (151)	13.9 ± 0.2 h	13.9 ± 0.2 h
Zn^{69}	(150)	57 ± 2 m (151)	58.5 ± 1.2 m	58.5 ± 1.2 m

The isotopes Zn^{63}, Zn^{71} (3 h isomer), and Zn^{72} were never seen in the zinc samples. Their cross sections are probably small.

Copper

Table 15
Copper isotopes

Isotope	Decay scheme References	Half-life		
		Reported in literature	Determined in this work	Chosen for the calculations
Cu^{60}	(152)	24.6 ± 0.3 m (153)		24.6 ± 0.3 m
Cu^{61}	(154, 155)	3.35 ± 0.1 h (111) 3.33 h (156)	3.27 ± 0.10 h	3.27 ± 0.10 h
Cu^{64}	(157, 224)	12.80 ± 0.03 h (138) 12.88 ± 0.03 h (158) 12.74 ± 0.07 h (159)	12.90 ± 0.06 h	12.88 ± 0.03 h
Cu^{66}	(160)	5.07 ± 0.02 m (161)		
Cu^{67}	(162)	58.6 ± 0.5 h (163)	61.6 ± 0.3 h	61.6 ± 0.3 h

Nickel

Table 16
Nickel isotopes

Isotope	Decay scheme References	Half-life		
		Reported in literature	Determined in this work	Chosen for the calculations
Ni^{57}	(164)	36.2 ± 1 h (164)	37.6 ± 0.5 h	37.6 ± 0.5 h
Ni^{65}	(165)	2.564±0.005 h (158)	2.56 ± 0.02 h	2.564 ± 0.005 h
Ni^{66}	(166)	55.1 ± 1.0 h (166) 54.8 ± 0.3 h (167)	53.5 ± 0.7 h	54.8 ± 0.3 h

The isotope Ni^{56} was not found in the samples from the cobalt bombardments. Its cross section is probably very small.

Cobalt

Table 17

Cobalt isotopes

Isotope	Decay scheme References	Half-life		
		Reported in literature	Determined in this work	Chosen for the calculations
Co^{61}	(168)	99.0 ± 0.3 m (169)	98.7 ± 0.4 m	98.7 ± 0.4 m

The cobalt samples contained a long-lived activity, presumably a mixture of Co^{56}, Co^{57}, and Co^{58}. These activities could not be resolved. An activity with a half-life of 12–14 hours was found after the subtraction of the long-lived activity. This activity probably consisted of a mixture of Co^{55} and Co^{58m}. It was not resolved.

Iron

Table 18

Iron isotopes

Isotope	Decay scheme References	Half-life		
		Reported in literature	Determined in this work	Chosen for the calculations
Fe^{52}	(170)	7.8 h (41)	8.53 ± 0.05 h	8.53 ± 0.05 h
Fe^{55}	(171)	2.94 ± 0.03 y (172)		2.94 ± 0.03 y
Fe^{59}	(173)	45.0 ± 0.2 d (149) 45.1 ± 0.2 d (159)	47.1 ± 0.3 d	45.1 ± 0.2 d

No 8.4 h Fe^{60} (26, 174) was found in the arsenic bombardments.

Manganese

Table 19

Manganese isotopes

Isotope	Decay scheme References	Half-life		
		Reported in literature	Determined in this work	Chosen for the calculations
Mn^{51}	(176)	44.3 ± 0.5 m (175) 45.2 m (176)	45.0 ± 0.6 m	45.0 ± 0.6 m
Mn^{52m}	(201)	21 ± 2 m (178) 21.3 m (177)	20.1 ± 0.8 m	20.1 ± 0.8 m
Mn^{52}	(179, 201)	5.60 ± 0.01 d (175) 5.72 ± 0.02 d (180)	5.82 ± 0.06 d	5.72 ± 0.02 d
Mn^{56}	(181)	2.581±0.003 h (161) 2.576±0.002 h (182) 2.574±0.003 h (183)		2.576 ± 0.002 h

Chromium

Table 20

Chromium isotopes

Isotope	Decay scheme References	Half-life		
		Reported in literature	Determined in this work	Chosen for the calculations
Cr^{48}	(184)	24 ± 1 h (185)		
Cr^{49}	(186)	41.7 ± 0.5 m (186) 41.9 ± 0.3 m (187)	41.7 ± 0.3 m	41.7 ± 0.3 m

The activity of the isotope Cr^{48} was determined by counting its daughter nuclide V^{48}.

Cr^{55} (2 h) was not found.

Vanadium

Table 21
Vanadium isotopes

Isotope	Decay scheme References	Half-life		
		Reported in literature	Determined in this work	Chosen for the calculations
V^{47}	(188)	31.1 m (176) 31 ± 1 m (188)	32.0 ± 0.3 m	32.0 ± 0.3 m
V^{48}	(189)	16.25 ± 0.17 d (190) 16.4 d (191)	16.18 ± 0.05 d	16.18 ± 0.05 d

No 16 h activity (192) or 23 h activity (193) was found in the vanadium samples.

Titanium

Table 22
Titanium isotopes

Isotope	Decay scheme References	Half-life		
		Reported in literature	Determined in this work	Chosen for the calculations
Ti^{45}	(194)	3.05 h (194) 3.09 ± 0.03 h (195)	3.09 ± 0.07 h	3.09 ± 0.03 h

Scandium

Table 23
Scandium isotopes

Isotope	Decay scheme References	Half-life		
		Reported in literature	Determined in this work	Chosen for the calculations
Sc^{43}	(196)	3.92 ± 0.02 h (197)		3.92 ± 0.02 h
Sc^{44m}	(198, 199)	57 ± 2 h (200)	58.7 ± 0.4 h	58.7 ± 0.4 h
Sc^{44}	(198, 199)	3.92 ± 0.03 h (197)		3.92 ± 0.03 h
Sc^{46}	(201)	84 d (202) 85 ± 1 d (203)	82.9 ± 1.6 d	82.9 ± 1.6 d
Sc^{47}	(204)	3.44 ± 0.05 d (205) 3.40 ± 0.05 d (206)		3.44 ± 0.05 d
Sc^{48}	(189)	44 ± 1 h (207)		44 ± 1 h

The disintegration curve of scandium is difficult to resolve owing to the large number of scandium activities present. The difficulty is the separation of Sc^{44m} (59 h), Sc^{47} (83 h), and Sc^{48} (44 h). It is, however, possible to determine the contribution of Sc^{44m} by counting the sample through an aluminium absorber which completely absorbs the β-particles from Sc^{47} and Sc^{48}. The counting efficiency of Sc^{44m} using this absorber was obtained from an absorption curve taken with scandium samples whose predominant activity consisted of Sc^{44}. Then, after the subtraction of the activities of Sc^{44m} and Sc^{46} from the gross disintegration curve, the activities of Sc^{47} and Sc^{48} could be determined.

Calcium

Table 24

Calcium isotopes

Isotope	Decay scheme References	Half-life		
		Reported in literature	Determined in this work	Chosen for the calculations
Ca^{45}	(208)	163.5 ± 4 d (209)		163.5 ± 4 d
Ca^{47}	(210)	4.3 ± 0.2 d (205) 4.7 ± 0.2 d (211)		4.7 ± 0.2 d

Potassium

Table 25

Potassium isotopes

Isotope	Decay scheme References	Half-life		
		Reported in literature	Determined in this work	Chosen for the calculations
K^{42}	(212)	12.516±0.007 h (213)		12.516 ± 0.007 h
K^{43}	(214)	22.4 h (215)		22.4 h

The potassium samples were not prepared early enough to see the short-lived isotope K^{44}.

Chlorine

Table 26

Chlorine isotopes

Isotope	Decay scheme References	Half-life		
		Reported in literature	Determined in this work	Chosen for the calculations
Cl^{34}	(216)	32.40 ± 0.04 m (216)		32.40 ± 0.04 m
Cl^{38}	(217)	37.29 ± 0.04 m (218)		37.29 ± 0.04 m
Cl^{39}	(219)	55.5 ± 0.2 m (220)		55.5 ± 0.2 m

It is difficult to separate the chlorine isotopes by analysing the decay curves since their half-lives are very similar. The cross sections of the chlorine isotopes from vanadium were determined by Arbman (221), who used a β-spectrometer for the determinations.

Sulphur

Table 27

Sulphur isotopes

Isotope	Decay scheme References	Half-life		
		Reported in literature	Determined in this work	Chosen for the calculations
S^{35}	(222)	87.1 ± 1.2 d (223)		87.1 ± 1.2 d

Phosphorus

Table 28

Phosphorus isotopes

Isotope	Decay scheme References	Half-life		
		Reported in literature	Determined in this work	Chosen for the calculations
P^{32}	(224)	14.35 ± 0.05 d (225) 14.30 ± 0.03 d (226)		14.30 ± 0.03 d
P^{33}	(227)	24.8 ± 0.5 d (227)		24.8 ± 0.5 d

Silicon

Table 29

Silicon isotopes

Isotope	Decay scheme References	Half-life		
		Reported in literature	Determined in this work	Chosen for the calculations
Si^{31}	(228)	157 ± 0.7 m (229)	153 ± 3 m	157 ± 0.7 m

Magnesium

Table 30

Magnesium isotopes

Isotope	Decay scheme References	Half-life		
		Reported in literature	Determined in this work	Chosen for the calculations
Mg^{27}	(230)	9.45 ± 0.03 m (231) 9.39 ± 0.03 m (183)		9.39 ± 0.03 m

The isotope Mg^{28} was not measured.

Sodium

Table 31

Sodium isotopes

Isotope	Decay scheme References	Half-life		
		Reported in literature	Determined in this work	Chosen for the calculations
Na^{24}	(232)	14.90 ± 0.05 h (138) 14.97 ± 0.02 h (183) 15.10 ± 0.04 h (218) 15.04 ± 0.06 h (233)	15.01 ± 0.06 h	15.01 ± 0.06 h

A long-lived activity which could be attributed to Na^{22} was found in the sodium samples. The activity was very low, however, and no identification was possible.

B. *Experimental Cross Sections*

1. INDEPENDENT CROSS SECTIONS

The nuclides investigated can be divided into three groups:

1) shielded nuclides;
2) nuclides for which the cross section of the parent nuclide is known;
3) nuclides for which the cross section of the parent nuclide is unknown.

The nuclides in the first group may be shielded by stable isobars or by isobars with very long half-lives. For the selenium isotopes the parent nuclides cannot be formed (except in very low yield (21) by secondary reactions). The same applies to the nickel isotopes at the bombardments of cobalt, etc. The cross sections measured for the nuclides in the first group can be regarded as independent. To this group belong: Se^{72}, Se^{73}, As^{74}, Ga^{68}, Ga^{70}, Cu^{64}, Ni^{57} (from Co), Fe^{52} (from Mn), Mn^{52}, Cr^{48} and Cr^{49} (from V), Sc^{44}, Sc^{46}, Sc^{48}, K^{42}, and P^{32}.

The cross sections of the nuclides in the second group were corrected for the parent effect using Eqs. (8)–(13) (the independent cross section of the parent nuclide was approximated by the measured one) and can be regarded as independent. To this group belong: As^{72}, Ge^{71}, Ga^{67}, Mn^{52m}, V^{48}, and Sc^{47}.

All the rest of the nuclides belong to the third group. As a rule, the reason why the cross sections of the parent nuclides were not measured is that these nuclides have very short half-lives. In such cases the cross section measured is the sum of the parent cross section and the daughter cross section (see Eq. (15)). In the next Chapter it will be shown how the cross sections of the nuclides belonging to this third group can be corrected by means of "spallation systematics".

2. IRRADIATION OF ARSENIC WITH 170 MEV PROTONS

The cross sections of the spallation products formed from arsenic at bombardments with 170 Mev protons are tabulated in Table 32. The cross sections given in the second and third columns of the table are cross sections relative to the cross

section of the monitor, whereas the cross sections in the fourth column are given in millibarns. The error (standard deviation) of the determinations in the second and third columns does not include the systematic error in the factor F. For many nuclides the error in F is large and arises from insufficiently known disintegration schemes. In the fourth column the total estimated error of the cross sections is given.

It is seen that the errors in the fourth column are much larger than the errors in the second and third columns. This is partly due to the error in F, partly to the estimated standard deviation of about fifteen per cent for the absolute formation cross section of Na^{24} from aluminium and magnesium. When more accurate determinations of these monitoring reactions are at hand, and the disintegration schemes are better known, the cross sections can be recalculated to yield more exact values.

The nuclide Cu^{64} was used as an internal monitor.

Table 32

Cross sections for the spallation group G (As; p; 170 Mev)

Nuclide	$\sigma/\sigma_{Cu^{64}}$	$(\sigma/\sigma_{Cu^{64}})_{Av}$	σ_{Av} in millibarns
Se^{73}	1.09 ± 0.12 1.20 ± 0.07	1.17 ± 0.06	8.4 ± 1.9
Se^{72}	1.19 ± 0.13 1.58 ± 0.10	1.43 ± 0.19	10 ± 4
As^{74}	9.3 ± 0.9 14.0 ± 0.8 15.0 ± 4.0	12.0 ± 1.7	90 ± 30
As^{72}	5.9 ± 0.8 10.1 ± 0.8	8.2 ± 2.0	58 ± 20
As^{70}	0.99 ± 0.15 1.24 ± 0.33	1.03 ± 0.14	7.4 ± 1.9
Ge^{71}	8.0 ± 0.9 11.1 ± 1.3 11.6 ± 1.5	9.5 ± 1.2	70 ± 40
Ge^{69}	6.9 ± 0.4 7.1 ± 0.5 7.6 ± 0.9	7.0 ± 0.3	50 ± 20

Nuclide	$\sigma/\sigma_{Cu^{64}}$	$(\sigma/\sigma_{Cu^{64}})_{Av}$	σ_{Av} in millibarns
Ge^{68}	3.16 ± 0.38 3.59 ± 0.43 3.66 ± 0.50 3.77 ± 0.60	3.47 ± 0.23	25 ± 5
Ge^{67}	0.29 ± 0.10 0.49 ± 0.08	0.41 ± 0.10	3.0 ± 0.9
Ga^{70}	2.0 ± 0.3 2.5 ± 0.4	2.2 ± 0.2	16 ± 3
Ga^{68}	3.7 ± 0.2 4.0 ± 0.2 4.4 ± 0.6 6.4 ± 0.6	4.0 ± 0.3	29 ± 6
Ga^{67}	5.0 ± 0.3 6.9 ± 0.9 7.5 ± 0.6 7.9 ± 0.2 8.0 ± 0.3	7.2 ± 0.6	52 ± 13
Zn^{69m}	0.141 ± 0.010 0.147 ± 0.012 0.147 ± 0.013 0.215 ± 0.029	0.148 ± 0.009	1.1 ± 0.2
Zn^{69}	0.171 ± 0.018 0.177 ± 0.015 0.193 ± 0.024 0.195 ± 0.038 0.208 ± 0.017	0.186 ± 0.009	1.3 ± 0.2
Cu^{67}		Average of 17 determinations: 0.077 ± 0.002	0.55 ± 0.10
Cu^{61}		Average of 24 determinations: 0.203 ± 0.006	1.5 ± 0.3
Cu^{60}	0.047 ± 0.023		0.34 ± 0.18
Ni^{66}	0.0031 ± 0.0002 0.0034 ± 0.0005 0.0034 ± 0.0004 0.0039 ± 0.0004	0.0033 ± 0.0002	0.024 ± 0.005

Nuclide	$\sigma/\sigma_{Cu^{64}}$	$(\sigma/\sigma_{Cu^{64}})_{Av}$	σ_{Av} in millibarns
Ni^{65}	0.0165 ± 0.0007	0.0185 ± 0.0009	0.13 ± 0.03
	0.0167 ± 0.0021		
	0.0186 ± 0.0007		
	0.0202 ± 0.0006		
Co^{61}	0.079 ± 0.005	0.082 ± 0.003	0.59 ± 0.10
	0.079 ± 0.006		
	0.084 ± 0.004		
	0.092 ± 0.013		
Fe^{59}	0.0123 ± 0.0037	0.0142 ± 0.0012	0.10 ± 0.02
	0.0137 ± 0.0016		
	0.0155 ± 0.0020		
Mn^{56}	0.015 ± 0.001	0.017 ± 0.004	0.12 ± 0.04
	0.025 ± 0.002		
	$\sigma/\sigma_{Ga^{68}}$		
Ga^{73}	0.0147 ± 0.0009		0.43 ± 0.09
Ga^{72}	0.0456 ± 0.0027		1.3 ± 0.3
Ga^{66}	0.548 ± 0.024		16 ± 3
	$\sigma/\sigma_{Na^{24}\text{ (from Al)}}$	$(\sigma/\sigma_{Na^{24}})_{Av}$	
Cu^{64}	0.71 ± 0.03	0.81 ± 0.07	7.2 ± 1.2
	0.72 ± 0.03		
	0.73 ± 0.04		
	1.00 ± 0.05		
	1.03 ± 0.04		
	1.17 ± 0.08		

3. IRRADIATION OF ARSENIC WITH 103 MEV PROTONS

The cross sections of the spallation products are tabulated in Table 33.

Table 33

Cross sections for the spallation group *G* (As; *p*; 103 Mev)

Nuclide	$\sigma/\sigma_{Cu^{64}}$	$(\sigma/\sigma_{Cu^{64}})_{Av}$	σ_{Av} in millibarns
Se^{73}	4.9 ± 0.6		11 ± 3
Se^{72}	5.1 ± 0.7 5.9 ± 0.7	5.5 ± 0.5	13 ± 5
As^{74}	30 ± 3 31 ± 4 33 ± 4 37 ± 8	31 ± 2	70 ± 25
As^{72}	18 ± 2 36 ± 18	18 ± 2	41 ± 10
As^{71}	21 ± 3 26 ± 6 29 ± 5 29 ± 5	24 ± 3	55 ± 25
Ge^{71}	4.5 ± 0.5 5.2 ± 1.1 6.8 ± 0.6	5.4 ± 0.8	12 ± 7
Ge^{69}	4.5 ± 0.2 4.8 ± 0.6 5.1 ± 0.3 5.9 ± 0.7	4.8 ± 0.2	11 ± 4
Ge^{68}	1.6 ± 0.2 2.3 ± 0.3	1.8 ± 0.3	4.1 ± 1.2
Ge^{67}	0.22 ± 0.05 0.31 ± 0.08	0.25 ± 0.04	0.58 ± 0.17
Ga^{70}	2.18 ± 0.76 2.44 ± 0.66 2.45 ± 0.34 2.58 ± 0.45	2.46 ± 0.24	5.7 ± 1.5
Ga^{68}	6.6 ± 0.7 6.9 ± 0.7 7.1 ± 0.9 7.3 ± 0.3 8.3 ± 0.8 9.9 ± 0.6	7.6 ± 0.4	17 ± 4

Nuclide	$\sigma/\sigma_{Cu^{64}}$	$(\sigma/\sigma_{Cu^{64}})_{Av}$	σ_{Av} in millibarns
Ga^{67}	7.8 ± 0.8	11.1 ± 0.5	25 ± 7
	8.1 ± 1.1		
	8.6 ± 0.8		
	9.0 ± 0.7		
	9.4 ± 0.9		
	9.9 ± 0.9		
	11.8 ± 0.7		
	11.8 ± 0.7		
	12.0 ± 1.0		
	12.1 ± 0.3		
	12.6 ± 1.0		
	12.7 ± 0.6		
Zn^{69m}	0.126 ± 0.022	0.146 ± 0.009	0.34 ± 0.08
	0.132 ± 0.012		
	0.155 ± 0.010		
	0.183 ± 0.024		
Zn^{69}	0.092 ± 0.016	0.110 ± 0.012	0.25 ± 0.07
	0.110 ± 0.013		
	0.138 ± 0.020		
Zn^{65}	2.88 ± 0.20		6.6 ± 2.5
Cu^{67}	0.069 ± 0.018	0.097 ± 0.003	0.22 ± 0.06
	0.081 ± 0.006		
	0.081 ± 0.005		
	0.092 ± 0.002		
	0.104 ± 0.003		
	0.105 ± 0.004		
	0.106 ± 0.003		
	0.117 ± 0.024		
	0.118 ± 0.024		
Cu^{61}	0.042 ± 0.008	0.061 ± 0.013	0.14 ± 0.05
	0.057 ± 0.011		
	0.085 ± 0.010		
Ni^{66}	0.0015 ± 0.0001	0.0016 ± 0.0002	0.0037 ± 0.0011
	0.0018 ± 0.0002		
	0.0027 ± 0.0003		
Ni^{65}	0.0076 ± 0.0004	0.0083 ± 0.0009	0.019 ± 0.005
	0.0081 ± 0.0012		
	0.0105 ± 0.0007		

Nuclide	$\sigma/\sigma_{Cu^{64}}$	$(\sigma/\sigma_{Cu^{64}})_{Av}$	σ_{Av} in millibarns
Co^{61}	0.021 ± 0.003 0.027 ± 0.002 0.034 ± 0.002 0.042 ± 0.013 0.047 ± 0.003	0.032 ± 0.004	0.074 ± 0.020
	$\sigma/\sigma_{Ga^{68}}$		
Ga^{73}	0.0128 ± 0.0006		0.22 ± 0.06
Ga^{72}	0.0470 ± 0.0021		0.80 ± 0.25
Ga^{66}	0.368 ± 0.012		6.3 ± 1.7
	$\sigma/\sigma_{Na^{24}(\text{from Al})}$	$(\sigma/\sigma_{Na^{24}})_{Av}$	
Cu^{64}	0.141 ± 0.015 0.142 ± 0.085 0.264 ± 0.012	0.215 ± 0.042	2.3 ± 0.6

4. IRRADIATION OF ARSENIC WITH 49 MEV PROTONS

The cross sections of the spallation products are given in Table 34. The nuclide Ga^{68} was used as an internal monitor.

Table 34

Cross sections for the spallation group *G* (As; *p*; 49 Mev)

Nuclide	$\sigma/\sigma_{Ga^{68}}$	$(\sigma/\sigma_{Ga^{68}})_{Av}$	σ_{Av} in millibarns
Se^{73}	12.1 ± 1.8 12.2 ± 0.8 13.0 ± 1.6 13.7 ± 1.8	12.5 ± 0.7	93 ± 22
Se^{72}	22 ± 3 24 ± 2	23 ± 2	170 ± 70
As^{74}	30 ± 3 38 ± 3 40 ± 3 43 ± 3 44 ± 3 45 ± 3	40 ± 3	300 ± 80

Nuclide	$\sigma/\sigma_{Ga^{68}}$	$(\sigma/\sigma_{Ga^{68}})_{Av}$	σ_{Av} in millibarns
As^{71}	25 ± 3 25 ± 3	25 ± 2	190 ± 70
Ge^{71}	8.6 ± 1.3 14.0 ± 1.1	12 ± 3	90 ± 50
Ge^{69}	5.1 ± 0.6 6.3 ± 0.5 8.4 ± 0.6 9.5 ± 2.5	6.6 ± 0.8	49 ± 18
Ge^{68}	0.74 ± 0.12 0.76 ± 0.07	0.75 ± 0.06	5.6 ± 1.0
Ga^{78}	0.0189 ± 0.0008		0.14 ± 0.02
Ga^{72}	0.134 ± 0.008		0.99 ± 0.17
Ga^{70}	2.5 ± 0.5 3.0 ± 1.1 4.3 ± 1.7	2.7 ± 0.4	20 ± 4
Ga^{67}	0.095 ± 0.016 0.115 ± 0.009	0.110 ± 0.009	0.82 ± 0.20
Zn^{69m}	0.039 ± 0.003 0.043 ± 0.004 0.047 ± 0.005	0.042 ± 0.002	0.31 ± 0.05
Zn^{69}	0.0136 ± 0.0019 0.0145 ± 0.0014 0.0155 ± 0.0028	0.0144 ± 0.0010	0.11 ± 0.02
Cu^{67}	0.0100 ± 0.0007 0.0105 ± 0.0008 0.0143 ± 0.0018	0.0106 ± 0.0008	0.079 ± 0.014
Cu^{64}	0.003 ± 0.001		0.022 ± 0.008
Ni^{66}	$(7 \pm 2).10^{-5}$		$(5.2 \pm 1.7).10^{-4}$
Ni^{65}	$(20 \pm 2).10^{-6}$ $(42 \pm 3).10^{-6}$	$(3 \pm 1).10^{-5}$	$(2.2 \pm 0.8).10^{-4}$
	$\sigma/\sigma_{Na^{24}\,(from\ Mg)}$	$(\sigma/\sigma_{Na^{24}})_{Av}$	
As^{72}	49 ± 3 51 ± 3	50 ± 2	370 ± 90
Ga^{68}	0.99 ± 0.06		7.4 ± 1.2

The cross sections are collected in Table 35. The nuclide Fe^{52} was used as an internal monitor.

Table 35

Cross sections for the spallation group *G* (Co; *p*; 170 Mev)

Nuclide	$\sigma/\sigma_{Fe^{52}}$	$(\sigma/\sigma_{Fe^{52}})_{Av}$	σ_{Av} in millibarns
Ni^{57}	2.1 ± 0.2 2.2 ± 0.2 2.6 ± 0.2	2.3 ± 0.2	1.1 ± 0.2
Fe^{55}	530 ± 40 610 ± 30	580 ± 40	270 ± 110
Mn^{56}	24 ± 2 27 ± 2	26 ± 2	12 ± 2
Mn^{52m}	25 ± 4		12 ± 3
Mn^{52}	61 ± 4 68 ± 6 70 ± 8 74 ± 8 75 ± 8	67 ± 3	31 ± 6
Mn^{51}	23 ± 3 27 ± 3	25 ± 2	12 ± 2
Cr^{49}	7.4 ± 0.7 9.6 ± 0.4 12.4 ± 0.5	10.1 ± 1.2	4.7 ± 1.0
Cr^{48}	0.77 ± 0.07		0.35 ± 0.08
V^{48}	12 ± 3 19 ± 1 23 ± 1	21 ± 2	10 ± 2
V^{47}	3.1 ± 0.2 4.1 ± 0.7	3.2 ± 0.3	1.5 ± 0.3
Ti^{45}	3.6 ± 0.4 4.5 ± 1.6 5.2 ± 0.9	3.9 ± 0.4	1.8 ± 0.4
Sc^{48}	0.54 ± 0.25		0.25 ± 0.12

Nuclide	$\sigma/\sigma_{Fe^{52}}$	$(\sigma/\sigma_{Fe^{52}})_{Av}$	σ_{Av} in millibarns
Sc^{47}	1.6 ± 0.7	2.5 ± 0.3	1.2 ± 0.2
	2.2 ± 0.4		
	2.6 ± 0.3		
	3.5 ± 0.7		
Sc^{46}	5.3 ± 0.3	5.5 ± 0.3	2.5 ± 0.5
	5.8 ± 0.5		
	6.4 ± 3.5		
Sc^{44m}	2.5 ± 0.3	2.6 ± 0.2	1.2 ± 0.2
	2.7 ± 0.4		
	2.9 ± 0.6		
$Sc^{43} + Sc^{44}$	2.7 ± 0.8	3.8 ± 0.4	1.8 ± 0.4
	3.4 ± 0.6		
	3.9 ± 0.4		
	4.9 ± 0.6		
K^{43}	0.24 ± 0.02	0.24 ± 0.02	0.11 ± 0.03
	0.26 ± 0.07		
K^{42}	0.71 ± 0.10	1.0 ± 0.2	0.46 ± 0.12
	1.28 ± 0.10		
	1.65 ± 0.40		
P^{32}	0.25 ± 0.06		0.12 ± 0.03
Si^{31}	0.10 ± 0.03		0.05 ± 0.02
	$\sigma/\sigma_{Na^{24}}$ (from Al)	$(\sigma/\sigma_{Na^{24}})_{Av}$	
Fe^{52}	0.039 ± 0.004	0.052 ± 0.003	0.46 ± 0.08
	0.051 ± 0.002		
	0.056 ± 0.002		

6. IRRADIATION OF MANGANESE WITH 170 MEV PROTONS

Table 36 contains the cross sections from the manganese experiments. The nuclides Cr^{49} and Mn^{52} were used as internal monitors.

Table 36

Cross sections for the spallation group *G* (Mn; *p*; 170 Mev)

Nuclide	$\sigma/\sigma_{Cr^{49}}$	$(\sigma/\sigma_{Cr^{49}})_{Av}$	σ_{Av} in millibarns
Cr^{48}	0.11 ± 0.01		0.70 ± 0.14
V^{48}	2.0 ± 0.3		13 ± 3
V^{47}	0.42 ± 0.06		2.7 ± 0.6
Sc^{48}	0.09 ± 0.03 0.19 ± 0.06	0.11 ± 0.04	0.70 ± 0.26
Sc^{47}	0.32 ± 0.08 0.33 ± 0.04 0.47 ± 0.04	0.39 ± 0.05	2.5 ± 0.5
Sc^{46}	0.63 ± 0.16 0.84 ± 0.07 0.96 ± 0.06	0.89 ± 0.07	5.7 ± 1.0
Sc^{44m}	0.34 ± 0.05 0.40 ± 0.05	0.37 ± 0.04	2.4 ± 0.5
$Sc^{43} + Sc^{44}$	0.48 ± 0.06 0.49 ± 0.09 0.71 ± 0.10	0.53 ± 0.07	3.4 ± 0.8
Ca^{47}	0.0039 ± 0.0011 0.0067 ± 0.0015	0.0049 ± 0.0013	0.031 ± 0.009
Ca^{45}	0.14 ± 0.06 0.22 ± 0.08	0.17 ± 0.05	1.1 ± 0.3
K^{43}	0.074 ± 0.007 0.120 ± 0.024	0.078 ± 0.013	0.50 ± 0.11
K^{42}	0.22 ± 0.01 0.23 ± 0.05 0.29 ± 0.05	0.22 ± 0.01	1.4 ± 0.2
Cl^{39}	0.0051 ± 0.0010		0.033 ± 0.009
$Cl^{34} + Cl^{38}$	0.009 ± 0.002		0.060 ± 0.015
P^{32}	0.016 ± 0.002 0.023 ± 0.006	0.017 ± 0.002	0.11 ± 0.04
Si^{31}	0.013 ± 0.003		0.083 ± 0.023

Nuclide	$\sigma/\sigma_{Mn^{52}}$	$(\sigma/\sigma_{Mn^{52}})_{Av}$	σ_{Av} in millibarns
Fe^{52}	0.013 ± 0.001 0.013 ± 0.001 0.019 ± 0.001	0.015 ± 0.003	0.24 ± 0.07
Mn^{52m}	0.47 ± 0.05 0.57 ± 0.07 0.83 ± 0.06	0.61 ± 0.23	10 ± 4
Mn^{51}	0.32 ± 0.02 0.47 ± 0.05 0.61 ± 0.05	0.37 ± 0.07	5.9 ± 1.5
	$\sigma/\sigma_{Na^{24}}$ (from Al)		
Mn^{52}	1.76 ± 0.12		16 ± 3
Cr^{49}	0.72 ± 0.03		6.4 ± 1.0
Ti^{45}	0.56 ± 0.09		5.0 ± 1.1

7. IRRADIATION OF VANADIUM WITH 170 MEV PROTONS

The cross sections of the spallation products from vanadium bombarded with 170 Mev protons are tabulated in Table 37. These cross sections as well as some of the cross sections from the cobalt and manganese experiments have been published earlier (234), but they have now been recalculated using the value 8.9 millibarns for the monitoring reaction $Al^{27}(p; 3\,pn)Na^{24}$ instead of 10.8 millibarns. The standard deviation of the determinations has also been estimated. The nuclide V^{48} was used as an internal monitor.

Table 37

Cross sections for the spallation group G (V; p; 170 Mev)

Nuclide	$\sigma/\sigma_{V^{48}}$	$(\sigma/\sigma_{V^{48}})_{Av}$	σ_{Av} in millibarns
Cr^{49}	0.051 ± 0.012 0.065 ± 0.009 0.083 ± 0.008 0.083 ± 0.017	0.072 ± 0.007	1.7 ± 0.4
Cr^{48}	0.0092 ± 0.0018 0.0094 ± 0.0008	0.0094 ± 0.0007	0.22 ± 0.07
V^{47}	0.18 ± 0.03 0.18 ± 0.03 0.20 ± 0.02 0.23 ± 0.03 0.28 ± 0.05	0.20 ± 0.01	4.6 ± 0.9
Ti^{45}	0.16 ± 0.06 0.18 ± 0.05 0.28 ± 0.05	0.21 ± 0.04	4.8 ± 1.2
Sc^{48}	0.15 ± 0.05 0.23 ± 0.07	0.18 ± 0.04	4.1 ± 1.1
Sc^{47}	0.24 ± 0.07 0.32 ± 0.05 0.34 ± 0.11 0.36 ± 0.09 0.37 ± 0.05	0.33 ± 0.03	7.6 ± 1.5
Sc^{46}	0.38 ± 0.07 0.43 ± 0.12 0.66 ± 0.18 0.70 ± 0.07	0.53 ± 0.13	12 ± 4
Sc^{44m}	0.18 ± 0.03 0.27 ± 0.03 0.35 ± 0.03	0.27 ± 0.05	6.2 ± 1.7
$Sc^{43} + Sc^{44}$	0.34 ± 0.05 0.35 ± 0.09 0.51 ± 0.05	0.41 ± 0.06	9.4 ± 2.2
Ca^{47}	0.0024 ± 0.0016 0.0025 ± 0.0007 0.0040 ± 0.0007 0.0043 ± 0.0004	0.0038 ± 0.0004	0.087 ± 0.019

Nuclide	$\sigma/\sigma_{V^{48}}$	$(\sigma/\sigma_{V^{48}})_{Av}$	σ_{Av} in millibarns
Ca^{45}	0.07 ± 0.02 0.12 ± 0.01 0.13 ± 0.03	0.11 ± 0.01	2.5 ± 0.6
K^{43}	0.073 ± 0.016 0.097 ± 0.023 0.108 ± 0.023	0.088 ± 0.019	2.0 ± 0.6
K^{42}	0.14 ± 0.03 0.14 ± 0.03	0.14 ± 0.02	3.2 ± 0.8
Cl^{39}	0.011 ± 0.001		0.25 ± 0.06
Cl^{38}	0.026 ± 0.003		0.60 ± 0.13
Cl^{34}	0.0011 ± 0.0001		0.025 ± 0.006
S^{35}	0.015 ± 0.003 0.021 ± 0.006 0.029 ± 0.004	0.020 ± 0.004	0.46 ± 0.13
P^{33}	0.009 ± 0.002 0.012 ± 0.002 0.014 ± 0.003 0.019 ± 0.003	0.012 ± 0.002	0.28 ± 0.08
P^{32}	0.010 ± 0.002 0.013 ± 0.002 0.021 ± 0.002	0.015 ± 0.003	0.35 ± 0.09
Si^{31}	0.0055 ± 0.0009 0.0073 ± 0.0004	0.0070 ± 0.0007	0.16 ± 0.04
Mg^{27}	0.0010 ± 0.0002		0.023 ± 0.007
Na^{24}	0.00102 ± 0.00029 0.00105 ± 0.00006 0.00105 ± 0.00007	0.00105 ± 0.00004	0.024 ± 0.005
	$\sigma/\sigma_{Na^{24}}$ (from Al)	$(\sigma/\sigma_{Na^{24}})_{Av}$	
V^{48}	2.5 ± 0.2 2.6 ± 0.3 2.6 ± 0.2 2.7 ± 0.3	2.6 ± 0.2	23 ± 4

CHAPTER III

Cross Section Distributions[1)]

A. *The Cross Section Formula*

Many spallation investigations have been carried out with medium weight targets (20–53). It is of interest to attempt to extract the general trends in the cross section distributions suggested by these various experiments. Such trends are very difficult to discern if the spallation yields are given merely as a set of tabulated cross sections. It has been shown by the author (234), however, that the cross section distributions can often be approximated by the following simple formula:

$$\sigma(A, Z) = \exp\,[PA - Q - R(Z - SA)^2], \qquad (47)$$

where $\sigma(A, Z)$ is the formation cross section of the nuclide with the mass number A and the atomic number Z, and P, Q, R, and S are parameters. This cross section formula can be applied to describe the cross sections of the spallation products of many spallation groups with a fair degree of accuracy. Thus the cross section distributions can be characterized by the four parameters P, Q, R, and S. It is then easy to compare different spallation groups just by studying the variation of these parameters with changes in targets, kind of bombarding particles, and irradiation energies.

B. *Evaluation of the Parameters of the Cross Section Formula*

The cross section formula (47) for a group of spallation reactions can be determined from the measured cross sections in the following way. The formula is written:

$$\ln \sigma(A, Z) = PA - Q - R(Z - SA)^2. \qquad (48)$$

[1] Part of the content of this chapter has been published earlier (235).

An arbitrary value is chosen for the parameter S, and the method of least squares is then applied to determine the best values of the parameters P, Q, and R from the known data of $\ln \sigma(A, Z)$, A, and $(Z - SA)^2$. The root-mean-square error ε of the logarithm of the cross sections is calculated, and different values of S are tried until the minimum of ε is found. The corresponding values of P, Q, R, and S give the best formula of the type (47) for the cross sections, and the value of $\varepsilon_{\min}$ shows how successful the formula is, because the average ratio between experimental and calculated cross sections is given by the factor $e^{\pm\varepsilon}$. The method of least squares used in this way also gives the standard deviation of P, Q, and R.

If the cross sections are given with their respective errors, the weight of each determination should be taken into account. In this case that value of S is chosen for which the weighted root-mean-square error has a minimum. Even in this case, however, the unweighted root-mean-square error ε can be used to show the applicability of the formula.

Instead of the method of determining P, Q, R, and S, just described, the method of differential corrections can be used. Approximate values of the four parameters (P_0, Q_0, R_0, and S_0) are chosen, and Eq. (48) is then written as follows:

$$\ln \sigma(A, Z) = \ln \sigma_0(A, Z) + A\,\Delta P - \Delta Q - (Z - S_0 A)^2\,\Delta R + \\ + 2 R_0 A (Z - S_0 A)\,\Delta S, \tag{49}$$

with

$$\ln \sigma_0(A, Z) = P_0 A - Q_0 - R_0 (Z - S_0 A)^2;$$

and

$$\Delta P = P - P_0;$$
$$\Delta Q = Q - Q_0;$$
$$\Delta R = R - R_0;$$
$$\Delta S = S - S_0.$$

Eq. (49) is in a linear form, and the method of least squares can be applied to determine the best values of ΔP, ΔQ, ΔR,

and ΔS. From these differences new approximate values of the parameters P, Q, R, and S are obtained, and the whole procedure is repeated until the values obtained for ΔP, ΔQ, ΔR, and ΔS are smaller than the corresponding standard deviations. This means that the best values of the four parameters have been found.

The method of differential corrections is much more time-consuming than the first method. It was therefore used only to determine the standard deviation of S in a few cases.

The experimental cross sections for the determination of the cross section formula should be the independent cross sections for primarily formed spallation products. However, the independent cross section of a nuclide is generally much lower than the independent cross section of its daughter for the actual spallation groups. For this reason the measured cross sections can be used.

In practice the cross section formula was used in a mass region limited to between 30 and 3 (in some cases 2) mass numbers below the lowest mass number of the target isotopes.

C. *Results of the Calculations*

1. GENERAL CONCLUSIONS ABOUT THE CROSS SECTION DISTRIBUTIONS

The cross section distributions were determined for the spallation reactions reported in this work and also for a number of spallation investigations which have appeared in the literature. The values of the parameters P, Q, R, and S and the factor e^{ε} are tabulated in Table 38 for twenty-one different groups of spallation reactions. The table also contains, for each spallation group, the number of experimental cross sections used in the calculation.

The cross section formula fits remarkably well as is seen from the values of e^{ε}. In most cases this factor is less than 2, which means that the cross section formula reproduces the experimental cross sections within a factor of two on the

average. This is satisfactory since the cross sections often vary by a factor of 10^3 or more, and moreover the experimental cross sections may sometimes be inaccurate by a factor of two.

Table 38

Cross section distributions[1]

Spallation group	Number of cross sections	P	Q	R	S	e^{ε}	References
G (V; p; 170 Mev)[2]	23	0.327 ± 0.012	11.82 ± 0.44	1.78 ± 0.10	0.465 ± 0.0005	1.42	This work
G (Mn; p; 170 Mev)	18	0.294 ± 0.023	11.23 ± 1.04	1.60 ± 0.13	0.469 ± 0.0009	1.65	This work
G (Co; p; 170 Mev)	17	0.353 ± 0.020	14.06 ± 0.95	1.97 ± 0.15	0.470 ± 0.0007	1.48	This work
G (As; p; 49 Mev)	15	1.109 ± 0.093	73.48 ± 6.40	1.34 ± 0.11	0.460 ± 0.0029	2.30	This work
G (As; p; 103 Mev)	20	0.461 ± 0.048	28.70 ± 3.21	1.35 ± 0.09	0.459 ± 0.0012	1.89	This work
G (As; p; 170 Mev)	22	0.388 ± 0.033	22.90 ± 2.13	1.13 ± 0.08	0.460 ± 0.0013	1.96	This work
G (V; p; 60 Mev)	11	0.780 ± 0.077	32.80 ± 3.36	1.85 ± 0.22	0.471 ± 0.0020	2.03	(35)
G (V; p; 100 Mev)	12	0.489 ± 0.032	19.39 ± 1.11	1.49 ± 0.12	0.469 ± 0.0012	1.45	(35)
G (V; p; 175 Mev)	14	0.343 ± 0.037	12.92 ± 1.48	1.63 ± 0.23	0.467 ± 0.0017	1.82	(35)
G (V; p; 240 Mev)	16	0.250 ± 0.040	8.50 ± 1.58	1.38 ± 0.27	0.467 ± 0.0022	2.36	(35)
G (Fe; p; 340 Mev)	21	0.253 ± 0.018	9.98 ± 0.77	1.37 ± 0.11	0.472	1.59	(44)

[1] The formula gives cross sections relative to $\sigma_{Cu^{61}}$ for G (Cu; p; 49 Mev), G (Cu; p; 340 Mev), G (Cu; d; 190 Mev), and G (Cu; α; 380 Mev), and relative to $\sigma_{As^{72}}$ for G (As; d; 190 Mev). In all other cases the cross section unit is millibarn.

[2] These values differ somewhat from those given in reference (235) (where the value of P should be 0.337 and not 0.377), because weighted cross sections were not used in that calculation.

Spallation group	Number of cross sections	P	Q	R	S	e^{ε}	References
G (Co; p; 370 Mev)	24	0.232 ± 0.024	8.96 ± 1.03	1.28 ± 0.17	0.468	2.06	(22)
G (Cu; p; 49 Mev)	10	0.956 ± 0.119	57.84 ± 6.80	1.41 ± 0.21	0.472	1.94	(26)
G (Cu; p; 340 Mev)	26	0.256 ± 0.016	14.44 ± 0.82	1.41 ± 0.13	0.468	1.81	(21)
G (Cu; p; 680 Mev)	32	0.209 ± 0.059	8.54 ± 1.25	1.40 ± 0.22	0.466	2.89	(51)
G (Cu; p; 2200 Mev)	33	0.072 ± 0.015	1.36 ± 0.71	1.22 ± 0.13	0.466	1.87	(29)
G (Cu; d; 190 Mev)	18	0.311 ± 0.026	18.55 ± 1.25	1.10 ± 0.25	0.465	2.09	(21)
G (Cu; α; 380 Mev)	10	0.236 ± 0.036	15.04 ± 1.88	0.81 ± 0.32	0.468	1.81	(21)
G (Cu; n; 400 Mev)	13	0.350 ± 0.067	17.11 ± 3.70	1.21 ± 0.37	0.466	2.62	(40)
G (Zn; p; 340 Mev)	22	0.239 ± 0.022	10.41 ± 1.07	1.45 ± 0.15	0.469	1.97	(53)
G (As; d; 190 Mev)	17	0.348 ± 0.054	24.86 ± 3.40	0.68 ± 0.17	0.463	3.13	(36)

To summarize we may say that for a given spallation group the cross section distribution can be roughly characterized in the following way:

1) The yields of the spallation products vary fairly regularly with the atomic number and the mass number of the product. This is indicated by the mere possibility of expressing all the cross sections by a simple formula.

2) The yield-mass curve, that is the total isobaric yield $\sigma(A)$ *versus* the mass number, increases exponentially with the mass number. This is seen by the following argument:

$$\sigma(A) = \sum_Z \sigma(A, Z) = \exp[PA - Q] \sum_Z \exp[-R(Z - SA)^2] \sim$$
$$\sim \exp[PA - Q] \int_{Z_1}^{Z_2} \exp[-R(Z - SA)^2]\, dZ. \qquad (50)$$

The limits of integration, Z_1 and Z_2, are the smallest and the largest obtainable value of Z. If R is not too small, this integral will not differ much from the integral with the limits $-\infty$ and $+\infty$. One then obtains

$$\sigma(A) \sim \exp[PA - Q] \int_{-\infty}^{\infty} \exp[-R(Z - SA)^2]\, dZ = \\ = (\pi/R)^{1/2} \exp[PA - Q]. \tag{51}$$

The parameter P is thus a measure of the steepness of this exponential increase in the yield-mass curve.

3) The charge distribution curve, that is the independent yield *versus* the atomic number for isobars, is a gaussian function of the atomic number with a precision index ($= R^{1/2}$) which is independent of the mass number. In this connection it is of interest to note that the assumption of a charge distribution curve independent of mass number is consistent with evidence from the study of yields of fragments in the fission of uranium with thermal neutrons (71).

4) The most probable primary charge, that is the "atomic number", generally non-integral, giving maximum yield in the charge distribution curve, can be approximated by a linear function of the mass number, passing through the origin and having a slope equal to S in a Z *versus* A plot.

2. COMPARISON BETWEEN EXPERIMENTAL AND CALCULATED CROSS SECTIONS

In Tables 39–44 the experimentally determined cross sections can be compared with cross sections calculated by means of Eq. (47) for the spallation investigations reported in this work. A few more comparisons of the same kind are found in the reference (235).

Table 39

Observed and calculated cross sections for the spallation group *G* (As; *p*; 170 Mev)

Nuclide	σ_{obs} mb	σ_{calc} mb	Nuclide	σ_{obs} mb	σ_{calc} mb
Se^{72}	10 ± 4	65	Ga^{66}	16 ± 3	10
As^{72}	58 ± 20	150	Zn^{69+69m}	2.4 ± 0.4	1.6
As^{70}	7.4 ± 1.9	35	Cu^{67}	0.55 ± 0.10	0.53
Ge^{71}	70 ± 40	63	Cu^{64}	7.2 ± 1.2	5.6
Ge^{69}	50 ± 20	44	Cu^{61}	1.5 ± 0.3	0.8
Ge^{68}	25 ± 5	18	Cu^{60}	0.34 ± 0.18	0.16
Ge^{67}	3.0 ± 0.9	4.6	Ni^{66}	0.024 ± 0.005	0.027
Ga^{72}	1.3 ± 0.3	1.0	Ni^{65}	0.13 ± 0.03	0.17
Ga^{70}	16 ± 3	14	Co^{61}	0.59 ± 0.10	0.60
Ga^{68}	29 ± 6	31	Fe^{59}	0.10 ± 0.02	0.06
Ga^{67}	52 ± 13	22	Mn^{56}	0.12 ± 0.04	0.16

Table 40

Observed and calculated cross sections for the spallation group *G* (As; *p*; 103 Mev)

Nuclide	σ_{obs} mb	σ_{calc} mb	Nuclide	σ_{obs} mb	σ_{calc} mb
Se^{72}	13 ± 5	26	Ga^{67}	25 ± 7	6.8
As^{73}	41 ± 10	89	Ga^{66}	6.3 ± 1.7	2.9
As^{71}	55 ± 25	45	Zn^{69+69m}	0.59 ± 0.13	0.52
Ge^{71}	12 ± 7	35	Zn^{65}	6.6 ± 2.5	3.5
Ge^{69}	11 ± 4	19	Cu^{67}	0.22 ± 0.06	0.14
Ge^{68}	4.1 ± 1.2	6.1	Cu^{64}	2.3 ± 0.6	1.8
Ge^{67}	0.58 ± 0.17	1.1	Cu^{61}	0.14 ± 0.05	0.15
Ga^{72}	0.80 ± 0.25	0.31	Ni^{66}	0.0037 ± 0.0011	0.0048
Ga^{70}	5.7 ± 1.5	6.3	Ni^{65}	0.019 ± 0.005	0.037
Ga^{68}	17 ± 4	13	Co^{61}	0.074 ± 0.020	0.15

Table 41

Observed and calculated cross sections for the spallation group *G* (As; *p*; 49 Mev)

Nuclide	σ_{obs} mb	σ_{calc} mb	Nuclide	σ_{obs} mb	σ_{calc} mb
Se^{72}	170 ± 70	210	Ga^{68}	7.4 ± 1.2	6.2
As^{72}	370 ± 90	590	Ga^{67}	0.82 ± 0.20	2.2
As^{71}	190 ± 70	160	Zn^{69+69m}	0.42 ± 0.05	0.36
Ge^{71}	90 ± 50	110	Cu^{67}	0.079 ± 0.014	0.030
Ge^{69}	49 ± 18	20	Cu^{64}	0.022 ± 0.008	0.062
Ge^{68}	5.6 ± 1.0	3.5	Ni^{66}	$(5.2 \pm 1.7).10^{-4}$	$4.4 \cdot 10^{-4}$
Ga^{72}	0.99 ± 0.17	1.4	Ni^{65}	$(2.2 \pm 0.8).10^{-4}$	$20 \cdot 10^{-4}$
Ga^{70}	20 ± 4	9			

Table 42

Observed and calculated cross sections for the spallation group *G* (Co; *p*; 170 Mev)

Nuclide	σ_{obs} mb	σ_{calc} mb	Nuclide	σ_{obs} mb	σ_{calc} mb
Fe^{55}	270 ± 110	210	Ti^{45}	1.8 ± 0.4	1.5
Fe^{52}	0.46 ± 0.08	0.62	Sc^{48}	0.25 ± 0.12	0.15
Mn^{56}	12 ± 2	10	Sc^{47}	1.2 ± 0.2	1.2
Mn^{52+52m}	43 ± 7	41	Sc^{46}	2.5 ± 0.5	4.2
Mn^{51}	12 ± 2	7	$Sc^{43+44+44m}$	3.0 ± 0.5	4.5
Cr^{49}	4.7 ± 1.0	4.1	K^{43}	0.11 ± 0.03	0.17
Cr^{48}	0.35 ± 0.08	0.31	K^{42}	0.46 ± 0.12	0.74
V^{48}	10 ± 2	12	P^{32}	0.12 ± 0.03	0.07
V^{47}	1.5 ± 0.3	2.5	Si^{31}	0.05 ± 0.02	0.03

Table 43

Observed and calculated cross sections for the spallation group *G* (Mn; *p*; 170 Mev)

Nuclide	σ_{obs} mb	σ_{calc} mb	Nuclide	σ_{obs} mb	σ_{calc} mb
Fe^{52}	0.24 ± 0.07	0.93	Sc^{46}	5.7 ± 1.0	6.0
Mn^{52+52m}	26 ± 5	32	$Sc^{43+44+44m}$	5.8 ± 1.0	5.3
Mn^{51}	5.9 ± 1.5	6.6	Ca^{47}	0.031 ± 0.009	0.017
Cr^{49}	6.4 ± 1.0	4.6	Ca^{45}	1.1 ± 0.3	1.0
Cr^{48}	0.70 ± 0.14	0.51	K^{43}	0.50 ± 0.11	0.46
V^{48}	13 ± 3	12	K^{42}	1.4 ± 0.2	1.4
V^{47}	2.7 ± 0.6	3.1	Cl^{39}	0.033 ± 0.009	0.090
Ti^{45}	5.0 ± 1.1	2.1	Cl^{34+38}	0.060 ± 0.015	0.37
Sc^{48}	0.70 ± 0.26	0.47	P^{32}	0.11 ± 0.04	0.16
Sc^{47}	2.5 ± 0.5	2.4	Si^{31}	0.083 ± 0.023	0.078

Table 44

Observed and calculated cross sections for the spallation group *G* (V; *p*; 170 Mev)

Nuclide	σ_{obs} mb	σ_{calc} mb	Nuclide	σ_{obs} mb	σ_{calc} mb
Cr^{48}	0.22 ± 0.07	0.33	K^{43}	2.0 ± 0.6	1.6
V^{48}	23 ± 4	22	K^{42}	3.2 ± 0.8	4.2
V^{47}	4.6 ± 0.9	3.4	Cl^{39}	0.25 ± 0.06	0.26
Ti^{45}	4.8 ± 1.2	2.4	Cl^{38}	0.60 ± 0.13	0.83
Sc^{48}	4.1 ± 1.1	2.2	Cl^{34}	0.025 ± 0.006	0.040
Sc^{47}	7.6 ± 1.5	3.4	S^{35}	0.46 ± 0.13	0.61
Sc^{46}	12 ± 4	19	P^{33}	0.28 ± 0.08	0.29
Sc^{44+44m}	12 ± 6	8	P^{32}	0.35 ± 0.09	0.26
Sc^{43}*	2.7 ± 0.6	1.6	Si^{31}	0.16 ± 0.04	0.13
Ca^{47}	0.087 ± 0.019	0.075	Mg^{27}	0.023 ± 0.007	0.029
Ca^{45}	2.5 ± 0.6	4.0	Na^{24}	0.024 ± 0.005	0.018
K^{44}*	0.19 ± 0.05	0.29			

* Obtained from the reference (147).

Eq. (48) can be rearranged in the following way:

$$\ln \sigma(A, Z) - PA + Q = -R\,(Z - SA)^2. \tag{52}$$

Thus the experimental values of

$$\ln \sigma(A, Z) - PA + Q$$

should lie on a parabola. These experimental values (with P and Q obtained from Table 38) are plotted *versus* $(Z - SA)$ in Fig. 15 for the spallation group $G(\mathrm{V}; p; 170\ \mathrm{Mev})$. The parabola

$$y = -R\,(Z - SA)^2$$

with R equal to 1.78 is also plotted in the figure (solid curve). The agreement between observed and calculated cross sections is clearly shown.

3. INDEPENDENT CROSS SECTIONS

With the cross section formula (47) at hand it is now possible to carry out a correction for the parent effect in such cases where the cross section of the parent nuclide has not been measured. This cross section is simply estimated by means of the formula (47), and the correction is carried out as described in Chapter I. If both the parent and the daughter nuclides are situated on the same side of the maximum of the charge distribution curve, the parent correction is small as will be seen from the following argument. For isobars denoted by the subscripts p and d the ratio between the cross sections will be

$$\frac{\sigma_p}{\sigma_d} = e^{-R(Z_p - Z_d)\,(Z_p + Z_d - 2SA)}. \tag{53}$$

With the assumption that

$$Z_p = Z_d + 1; \quad Z_d \geq SA,$$

one obtains

$$\frac{\sigma_p}{\sigma_d} = e^{-R} \times e^{-2R\,(Z_d - SA)} \leq e^{-R}. \tag{54}$$

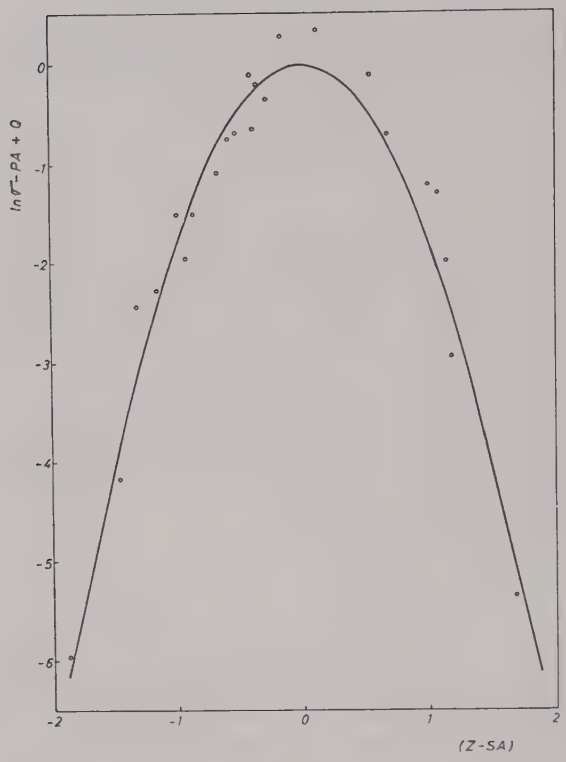

Fig. 15. $(\ln \sigma - PA + Q)$ *versus* $(Z - SA)$ for the spallation group $G(\mathrm{V}; p; 170\ \mathrm{Mev})$. The parameters have the following values: $P = 0.327$; $Q = 11.82$; $S = 0.465$. The parabola $y = -R(Z - SA)^2$ with $R = 1.78$ is also shown in the figure (solid curve).

This ratio is smaller than 0.15–0.30 for reasonable values of R. The correction is in most cases within the limits of error and might be neglected.

For $Z_p = Z_d - 1$ and $Z_d \leq SA$, the conclusion is analogous:

$$\frac{\sigma_p}{\sigma_d} = e^{-R} \times e^{-2R(SA - Z_d)} \leq e^{-R}. \tag{55}$$

D. *Comparison between Different Spallation Groups*

1. INTRODUCTORY REMARKS

The cross section distributions of different spallation groups can now be compared by studying the dependence of the parameters P, R, and S on the composition of the target and on the kind and energy of the bombarding particles. (The parameter Q is of minor interest here, since it merely fixes the absolute scale of the cross sections.) The goal of this comparison is just to establish empirical relationships for these parameters. A theoretical treatment of the spallation reactions will be postponed to Chapters IV–VI.

The parameters are regarded as variables not of the mass number and the atomic number of the target element, but of the mass number A_0 and the atomic number Z_0 of the hypothetical "compound nucleus". For poly-isotopic targets A_0 is put equal to the atomic weight increased by the mass number of the projectile.

The energy spectrum of the bombarding particles is seldom given in the published spallation investigations. Therefore, there is some ambiguity in the way of defining the irradiation energy. This is not serious, however, since the cross section distributions are not too strongly energy-dependent.

The kind of bombarding particle is denoted by the letters p, d, n, or α appearing above the corresponding point in the figures of this section.

2. THE PARAMETER P

The dependence of the parameter P on A_0 can be studied in Figs. 16 and 17 for the energies 170–190 Mev (Fig. 16) and 340–400 Mev (Fig. 17). It is evident from these figures that P is almost independent of A_0 in the mass region investigated ($A_0 = 52 - 77$). It is also apparent that P does not depend on the kind of the bombarding particles.

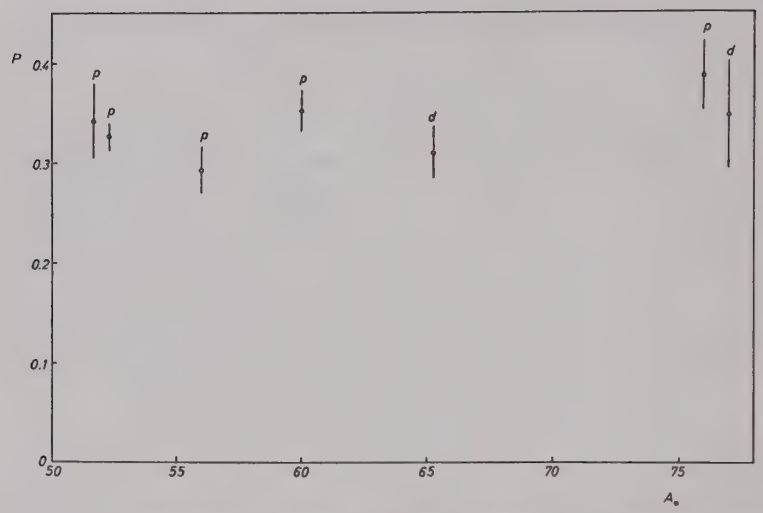

Fig. 16. The parameter P *versus* the mass number for irradiation energy 170-190 Mev. Two points at $A_0 = 52$ have been spread out in the figure.

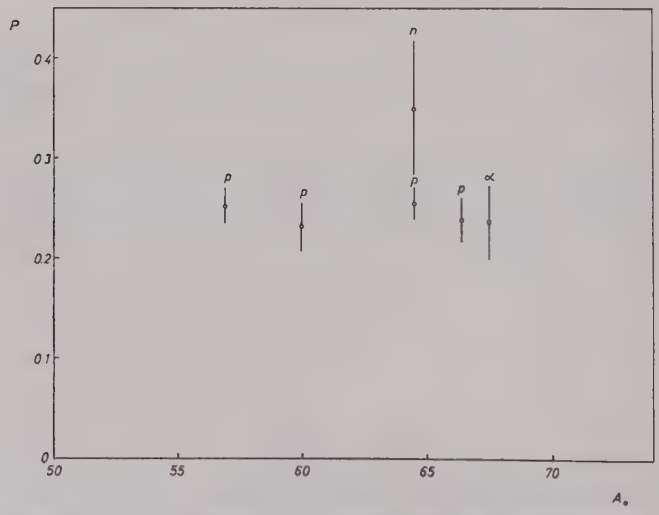

Fig. 17. The parameter P *versus* the mass number for irradiation energy 340-400 Mev.

The parameter P is plotted *versus* the irradiation energy in Fig. 18. Data from the spallation of vanadium, copper, and

arsenic with protons, deuterons, and α-particles have been included in the figure. The parameter P decreases with increasing energy. This is of course to be expected, since the steepness of the yield-mass curve should decrease with increasing irradiation energy. The experimental points in the figure can be combined into a curve which may be used to determine P for any spallation reaction in the mass region in question.

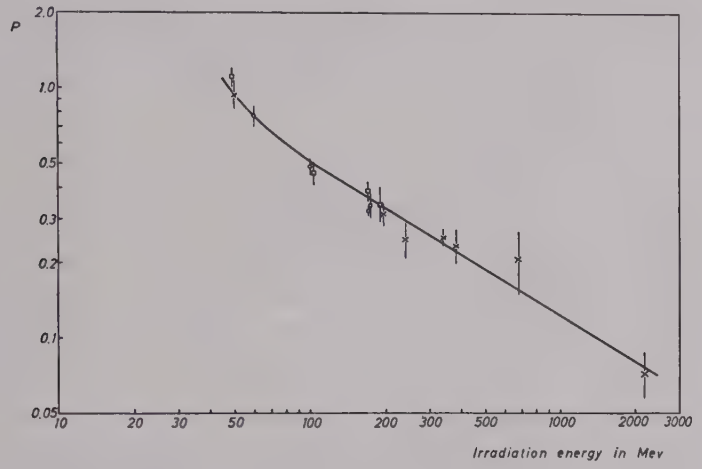

Fig. 18. The parameter P *versus* the irradiation energy. Target elements: vanadium (circles), copper (crosses), and arsenic (squares).

3. THE PARAMETER R

An examination of Table 38 reveals the striking fact that the parameter R seems to be nearly independent both of the irradiation energy and of A_0 (there might be a slight decrease with increasing A_0). The following values for proton experiments can be compared:

Target: Vanadium.

Energy:	60 Mev	100 Mev	170 Mev	175 Mev	240 Mev
R :	1.85	1.49	1.78	1.63	1.38

Target: Copper.

Energy:	49 Mev	340 Mev	680 Mev	2200 Mev
R :	1.41	1.41	1.40	1.22

Target: Arsenic.

Energy:	49 Mev	103 Mev	170 Mev
R :	1.34	1.35	1.13

The average of R for seventeen proton-induced spallation groups (Table 38) is 1.48, which corresponds to a standard deviation of 0.58 atomic number units. This figure may be taken as representative for the width of the cross section distributions in mass region investigated.

The parameter R seems to be somewhat smaller for irradiations with α-particles and deuterons indicating a wider distribution in these cases.

4. THE PARAMETER S

It is not very profitable to compare the values of the parameter S for different spallation groups. Instead, one may study the behaviour of the new parameter U defined by the relation

$$U = S - \frac{Z_0}{A_0}. \tag{56}$$

This parameter can be taken as a measure of the preference for neutron emission. It will be zero if the most probable ratio between emitted protons and neutrons (where both free and bound nucleons are considered) is the same as the ratio between protons and neutrons in the "compound" nucleus. If U is positive, neutron emission is more probable than proton emission.

For a given target element the parameter U should decrease with increasing irradiation energy reflecting the fact that the Coulomb barrier, which favours the emission of neutrons, is relatively more important when the energy of the bombarding particles is low. This tendency is clearly brought out in Fig. 19, where data from proton-induced spallation reactions in vanadium and copper are shown.

A correlation should exist between U and the atomic number Z_0. The parameter U can be expected to increase with increasing Z_0 since the potential barrier for charged particles rises

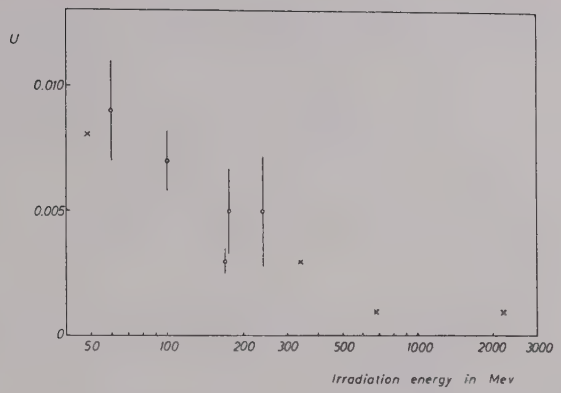

Fig. 19. The parameter *U versus* the irradiation energy. Target elements: vanadium (circles) and copper (crosses). The errors of the copper determinations are not given but should be of the same order as those of the vanadium determinations.

with the atomic number. It will probably also depend on the location of the target isotope(s) relative to the stability line, *i. e.* it should depend also on A_0. U is plotted *versus* Z_0 for some mono-isotopic targets (irradiation energy: 170 Mev) in Fig. 20. An increase with increasing Z_0 is indicated.

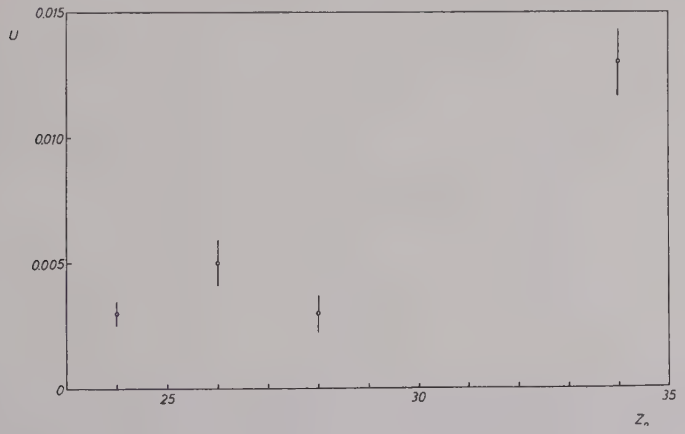

Fig. 20. The parameter *U versus* the atomic number for irradiation energy 170 Mev.

E. *Estimation of Relative Cross Sections*

One may attempt to estimate relative cross sections using the data of Table 38 and Figs. 18–20. Eq. (47) gives immediately as the ratio between the cross sections of the spallation products a and b:

$$\frac{\sigma_a}{\sigma_b} = e^{P(A_a - A_b) - R[(Z_a - SA_a)^2 - (Z_b - SA_b)^2]}. \qquad (57)$$

P is obtained from Fig. 18, R is put equal to 1.48, and S is estimated by means of Figs. 19 and 20 and the data in Table 38.

The spallation group G(Cu; p; 190 Mev) is chosen as an example. The following values of the parameters are found: $P = 0.32$; $S = 0.469$. The calculated data can be compared with experimental data, determined by Coleman and Tewes (27), in Table 45.

Table 45

Relative cross sections for
G (Cu; p; 190 Mev)

Nuclide	$(\sigma/\sigma_{Cu^{61}})_{obs}$	$(\sigma/\sigma_{Cu^{61}})_{calc}$
Cu^{60}	0.27	0.30
Ni^{57}	0.043	0.045
Co^{61}	0.07	0.72
Co^{55}	0.047	0.022
Fe^{53}	0.005	0.014
Fe^{52}	0.0033	0.0015
Mn^{56}	0.053	0.017
Mn^{51}	0.010	0.009
Cr^{49}	0.023	0.006

Next the spallation groups G(Co; p; 100 Mev) and G(Co; p; 240 Mev) will be investigated. For the former the parameters $P = 0.49$ and $S = 0.472$ and for the latter the parameters $P = 0.28$ and $S = 0.470$ are chosen The experimental determinations have

been carried out by Wagner and Wiig (49). The data are tabulated in Table 46.

Table 46

Relative cross sections for
G (Co; p; 100 Mev) and G (Co; p; 240 Mev)

Nuclide	G (Co; p; 100 Mev)		G (Co; p; 240 Mev)	
	$(\sigma/\sigma_{Mn^{56}})_{obs}$	$(\sigma/\sigma_{Mn^{56}})_{calc}$	$(\sigma/\sigma_{Mn^{56}})_{obs}$	$(\sigma/\sigma_{Mn^{56}})_{calc}$
Co^{55}	1.5	2.6	0.47	1.4
Fe^{52}	0.04	0.12	0.05	0.12
Mn^{51}	0.43	0.50	1.1	0.5
$Cl^{34} + Cl^{38}$	0.0021—0.0071	0.0008	0.014	0.028

Chapter IV

The Cascade Process

A. *Introduction*

As was mentioned before (compare p. 9) Serber (56) has proposed a model for nuclear reactions with high energy particles by which the incident particle develops a nucleon cascade in the nucleus. Goldberger (57) showed that it is possible to treat such a model quantitatively using a Monte Carlo technique. The Serber-Goldberger theory has been used by several investigators with the object of comparing calculated angular and energy distributions of the cascade particles with experimental data. Such comparisons have been carried out by Bernardini, Both, and Lindenbaum (8, 236), Combe (237), Cüer and Combe (238), Meadows (239), Morrison, Muirhead, and Rosser (16), and Muirhead and Rosser (17). The agreement between calculated and experimental data is satisfactory.

In the present work a calculation of the cross sections of the spallation products formed by the irradiation of arsenic with high energy protons will be carried out on the generally adopted assumption that a spallation reaction can be divided into two well-defined steps: first, a cascade process giving a few prompt particles and a product nucleus (from now on called the residual nucleus) in an excited state and, second, the de-excitation of this residual nucleus by the evaporation of different particles. The first step, the nucleon cascade, will be treated in this chapter.

The "pick-up" process (11, 240, 241), which is important at least when the energy is low, is neglected in the present work.

Since the irradiation energy is not too high, nonrelativistic calculations will be used throughout the work.

B. *The Cascade Model*

1. THE CASCADE MODEL *VERSUS* THE COMPOUND NUCLEUS MODEL

The cascade calculation has in most cases been carried out in such a manner that the cascade particles are traced until they have insufficient energy to escape from the nucleus. This extreme cascade model will be used in the present work (Assumption I). The success of the compound nucleus model (55) in explaining low energy reactions, however, suggests a combination between the cascade model and the compound nucleus model. Such a combination will also be tried (Assumption II). Cascade particles with an energy lower than 20 Mev *outside* the nucleus are then assumed to be absorbed to form a compound nucleus, and their energy is distributed among all the nucleons[1]. The low energy limit (20 Mev) is somewhat arbitrarily chosen. Analyses show, however, that the cascade process must be taken into account above this limit (242).

2. THE MOMENTUM DISTRIBUTION IN THE NUCLEUS

The momentum distribution of the neutrons and the protons in the nucleus is approximated by the momentum distribution of a Fermi gas in a "square well" potential. The Fermi gas is assumed to be in its lowest state (zero temperature) and to remain there during the whole cascade.

The maximum energy E_F of the protons or neutrons is given by the formula:

$$E_F = \frac{\hbar^2}{2M}\left(\frac{3\pi^2 N}{V}\right)^{2/3}. \tag{58}$$

N is the number of protons or neutrons, V is the nuclear volume, and M is the nucleon mass.

[1] It is possible, of course, to combine the cascade model and the compound model in a less drastic way, for instance by assuming a certain probability $P(E)$ for a cascade particle of the energy E to be absorbed by the nucleus. Such a probability function can easily be included in the cascade calculation.

The generally adopted formula for the nuclear radius

$$R = r_0 A^{1/3} \times 10^{-13} \text{ cm} \tag{59}$$

was used. For r_0 the value 1.2 was chosen for both protons and neutrons. This value (or 1.216) is given by Green (243) and is obtained from a "least squares" adjustment of nuclear masses to the semiempirical mass formula.

The following values are then obtained for the nucleus As^{75} (33 protons and 42 neutrons):

$R = 5.06 \times 10^{-13}$ cm $\sim 5.1 \times 10^{-13}$ cm;
$E_F = 30.8$ Mev ~ 31 Mev for protons;
$E_F = 36.2$ Mev ~ 36 Mev for neutrons.

The Pauli principle was taken into account in the usual way. If a nucleon after the collision has an energy less than the Fermi energy E_F the collision is assumed not to take place, since it would lead to a state already filled.

Certain investigations indicate that the momentum distribution in a nucleus, at least for light nuclei, would be better represented by a gaussian distribution (244, 245) or by an excited Fermi distribution (241) than by a Fermi distribution at zero temperature. Such a distribution could have been used in the calculation (see reference (237)).

3. THE DEPTH OF THE POTENTIAL WELL

The depth B of the potential well is

$$B = E_F + S, \tag{60}$$

where S is the separation energy of the last proton or neutron. The nuclides which will occur most often in the cascade calculation (carried out on As^{75}) are expected to be: Se^{76}, Se^{75},

As^{75}, Se^{74}, As^{74}, and Ge^{74}. The average separation energy[1] for these nuclides is

$$\text{for protons: } S_p = 8.5 \text{ Mev;}$$
$$\text{for neutrons: } S_n = 9.9 \text{ Mev.}$$

The average Coulomb barrier V_C (for protons without angular momentum) of the same nuclides is 9.2 Mev. It should be corrected for barrier penetration. Le Couteur (59) estimates the effective barrier V_C' to be 0.7 V_C, *i. e.* in the present case 6.4 Mev.

The energy which a cascade particle must have within the nucleus in order to be able to penetrate the nuclear surface is now immediately obtained as

$$\text{for protons: } E_F + S_p + V_C' = 30.8 + 8.5 + 6.4 = 45.7 \sim 46 \text{ Mev;}$$
$$\text{for neutrons: } E_F + S_n = 36.2 + 9.9 = 46.1 \sim 46 \text{ Mev.}$$

In the present work the incident proton was assumed to increase its energy by 39 Mev when entering the nucleus. A nucleon, leaving the nucleus, was assumed to decrease its energy by 39 Mev (proton) or 46 Mev (neutron).

From scattering experiments the potential depth seems to depend on the energy of the particle and actually to decrease with increasing particle energy (247). Low energy particles feel a potential depth of about 40 Mev, but for high energy particles the depth seems to decrease to 10–15 Mev. This effect was not introduced into the present calculation.

4. THE TWO-DIMENSIONAL GEOMETRY

A cascade inside the nucleus will in general take place in three dimensions. The use of a three-dimensional model to follow such a cascade has been attempted by Combe (237), who represented the nucleon paths by means of threads. Such a procedure is very time-consuming, and it is customary to simplify the treatment by studying instead a cascade assumed to lie entirely in a single plane (57, 236). The three-dimensional

[1] The separation energies were calculated from Wapstra's compilation of nuclear masses (246).

problem is then reduced to a two-dimensional one with the spherical nuclear surface replaced by a circle. In previous calculations of this type the radius R' of the circle has been taken equal to the nuclear radius R. It would appear, however, that a choice of R' somewhat smaller than R would be preferable, since the intersection of a typical collision plane with the sphere representing the nucleus is not, as a rule, a great circle.

In the present work the radius of the circle was chosen in such a way that the average distance from a representative point inside the circle to its periphery is equal to the average distance from a representative point inside the sphere to its surface. (By "representative" we shall understand taking an average of the position of the collision point over the volume of the sphere—see Eq. (63).)

Consider first a collision point P' at the distance r' from the centre of a circle of the radius R' (Fig. 21). The average distance from P' to the periphery is

$$\bar{a}' = \frac{\int_0^{2\pi} a' \, d\Theta}{\int_0^{2\pi} d\Theta} = \frac{2R'}{\pi} E(k'), \tag{61}$$

where $k' = r'/R'$. $E(k')$ is the complete elliptic integral of the second kind of the argument k'.

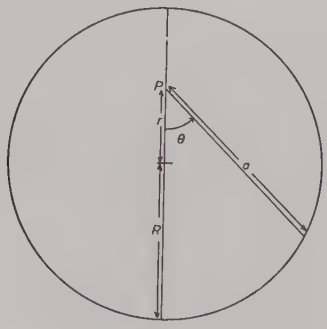

Fig. 21.

For a sphere of the radius R the average distance from a collision point P to the surface (Fig. 21) is

$$\bar{a} = \frac{\int_0^{\pi}\int_0^{2\pi} a \sin\Theta \, d\Theta \, d\varphi}{\int_0^{\pi}\int_0^{2\pi} \sin\Theta \, d\Theta \, d\varphi} = \frac{R}{4}\left[2 + \frac{1-k^2}{k} \ln\left(\frac{1+k}{1-k}\right)\right], \tag{62}$$

with $k = r/R$.

In order to get the average distance from a representative point in the circle or the sphere, an average over the volume of a sphere must be taken. The result is

$$\text{for the circle: } \bar{\bar{a}}' = \frac{\int_0^1 \bar{a}' (k')^2 \, dk'}{\int_0^1 (k')^2 \, dk'} \cong 0.83 \, R';$$

$$\text{for the sphere: } \bar{\bar{a}} = \frac{\int_0^1 \bar{a} \, k^2 \, dk}{\int_0^1 k^2 \, dk} = 0.75 \, R. \tag{63}$$

The radius of the circle is now to be adjusted so that these two distances are equal. This gives

$$R' = 0.90 \, R.$$

Thus the radius of the circle should be ninety per cent of the nuclear radius. For arsenic with the nuclear radius equal to 5.1×10^{-13} cm, the radius of the corresponding two-dimensional model should be 4.6×10^{-13} cm. This value was chosen for the cascade calculation.

5. THE MEAN FREE PATH IN THE NUCLEUS

The mean free path λ can be written

$$\lambda = \frac{1}{\varrho \, \sigma}, \tag{64}$$

where σ is total scattering cross section, and ϱ is the nucleon

density in the nucleus. The value of σ corresponding to free nucleon-nucleon scattering is chosen.

For a nucleus with Z protons and N neutrons the mean free path will be

$$\begin{aligned} &\text{for a proton: } \lambda_p = \frac{1}{\varrho\, \sigma_p}; \\ &\text{for a neutron } \lambda_n = \frac{1}{\varrho\, \sigma_n}; \end{aligned} \tag{65}$$

with

$$\begin{aligned} \sigma_p &= \frac{Z\,\sigma_{p-p} + N\,\sigma_{p-n}}{A}; \\ \sigma_n &= \frac{Z\,\sigma_{n-p} + N\,\sigma_{n-n}}{A}; \end{aligned} \tag{66}$$

and

$$\varrho = \frac{N+Z}{V}.$$

λ_p and λ_n were calculated as functions of the energy from the experimental determinations of total scattering cross sections given in the references (248–254) (approximate neutron-neutron cross sections were deduced from scattering experiments with neutrons on hydrogen and deuterium by subtraction of the neutron-proton cross sections from the neutron-deuteron cross sections). Fig. 22 shows the values obtained for λ_p and λ_n *versus* the square root of the energy.

As a matter of fact the mean free path given by Eq. (65) and in Fig. 22 does not correspond to the actual mean free path λ_e in nuclear matter. This is because some of the collisions will be forbidden by the exclusion principle. This will raise the mean free path by a factor $1/\alpha$, where α is defined as the ratio between the number of allowed collisions and the number of attempted collisions. Thus

$$\lambda_e = \frac{\lambda}{\alpha}. \tag{67}$$

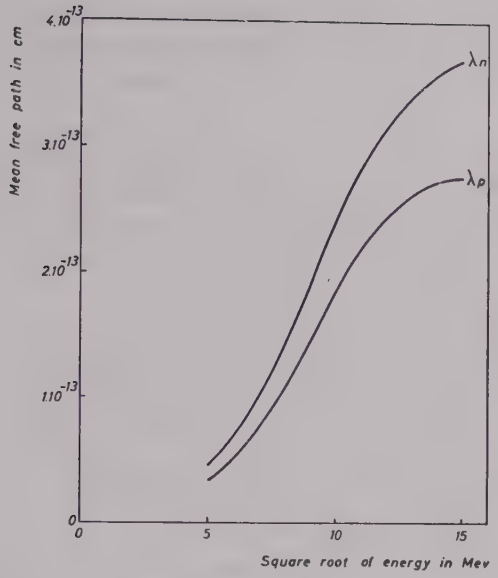

Fig. 22. The mean free path for protons (λ_p) and neutrons (λ_n) *versus* the square root of energy.

6. THE CASCADE CALCULATION

The cascade calculation consists of the following steps:

a) Determination of the energy of the incident proton.
b) Determination of the point where the proton enters the nucleus.
c) Determination of the place for the first collision.
d) Determination of the collision partner (proton or neutron).
e) Determination of the momentum of the collision partner.
f) Determination of the scattering angle.
g) Graphical evaluation of angles and energies after the collision.
h) Construction of the new particle paths, if the collision is not forbidden by the exclusion principle.

Six numbers chosen at random were used to determine the steps (a)–(f). After this, the remaining two steps were carried out graphically. The calculation was repeated with the collision partners until the particles either left the nucleus, *i. e.* passed

the periphery of the circle with an energy larger than 46 Mev, or were absorbed in the nucleus, *i. e.* were left with an energy between 31 (36) and 46 Mev for protons (neutrons) after the collision.

The random numbers were chosen by means of the roulette shown in Fig. 23. The roulette consisted of four wheels of lucite attached to a vertical axis with ball bearings. The wheels

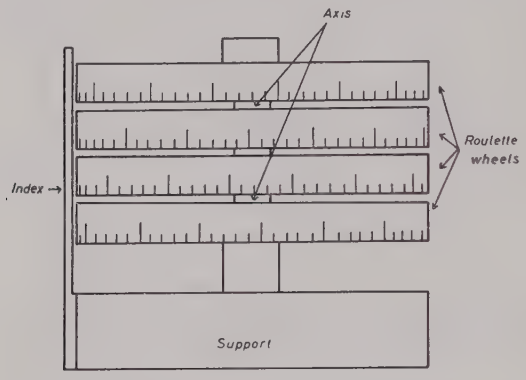

Fig. 23. Roulette for choosing random numbers.

could move very easily and completely independently of each other. Their circumference was divided into one hundred parts of equal size by means of numbered divisions. The wheels were set into rapid movement by hand, the second and fourth wheels in the opposite direction to the first and third ones. When the wheels had stopped, four numbers to be used in collision determinations were read off at an index.

The randomness of the roulette was tested by means of the χ^2-method and was found satisfactory.

The different steps of the cascade calculation will now be described in more detail.

a. *The Energy of the Incident Proton*

The energy spectrum of the protons (shown in Fig. 1) was divided into ten energy intervals, each containing the same number of protons. One interval was chosen at random, and

the incident proton was assumed to have the energy of the middle point of the interval chosen.

b. *The Penetration Point*

The circle representing the nucleus was divided into one hundred numbered parts by segments parallel to the beam in such a way that if the circle were rotated around a diameter in the beam direction, the segments would generate annular rings presenting equal areas to the incoming particles. One of the parts was chosen at random to define the point where the incident proton penetrated the surface of the nucleus.

c. *The Collision Point*

The probability for the particle not to collide within the distance x is $e^{-x/\lambda}$. The distance between zero and infinity was divided into one hundred parts by means of division points x_n ($x_{100} = \infty$) in such a way that the probability was the same for collision in any part. It is easily seen that x_n can be obtained from the formula

$$x_n = \lambda \ln\left(\frac{100}{100 - n}\right). \tag{68}$$

A number k between one and one hundred was chosen at random, and the collision was assumed to take place when the particle had travelled the distance

$$\frac{x_{k-1} + x_k}{2}.$$

d. *The Collision Partner*

The probability that a proton collides with another proton is

$$F_p = \frac{Z\sigma_{p-p}}{Z\sigma_{p-p} + N\sigma_{p-n}}. \tag{69}$$

The probability of a collision with a neutron is $(1 - F_p)$.

For a neutron the probability of a collision with a proton is

$$G_p = \frac{Z\,\sigma_{n-p}}{Z\,\sigma_{n-p} + N\,\sigma_{n-n}}. \tag{70}$$

The probability of a collision with a neutron is $(1 - G_p)$.

The probability factors F_p and G_p are plotted for different energies in Fig. 24. A number k between one and one hundred was chosen at random. If k was smaller than 100 F_p (or 100 G_p), the collision was assumed to take place with a proton. If it was larger, the collision was assumed to take place with a neutron.

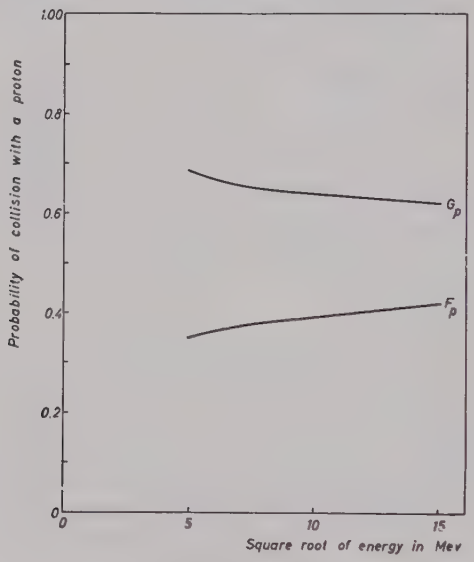

Fig. 24. Probability of a proton-proton collision (F_p) and a neutron-proton collision (G_p) *versus* the square root of energy.

e. *The Momentum of the Collision Partner*

The probability of a collision with a particle in a given volume element of the Fermi momentum sphere can be assumed to be proportional to the size of this volume element (236). Thus the momentum sphere should be divided into a

number of elements of equal volume. The probability of hitting a particle in any of these volume elements is then constant. The division can be made by a number of concentric circles and radii as shown in Fig. 25, where the momentum sphere is represented by a circle of the same diameter. The area elements of the circle must all give the same volume on rotation around the axis PQ. In the actual case the circle was divided into one thousand parts by ten concentric circles and one hundred radii.

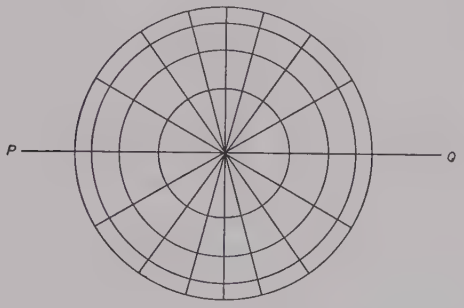

Fig. 25. The division of the Fermi momentum sphere. Only 16 radii and 4 circles are shown in the figure. In the actual case 100 radii and 10 circles were used.

The momentum of the collision partner was determined by choosing two numbers at random. The first number (between one and ten) determined the absolute momentum of the struck nucleon, and the second number (between one and one hundred) determined the angle between the momenta of the collision partners.

f. *The Scattering Angle*

The differential scattering cross section in the center of mass system is assumed to be given by $\sigma\ (E, \Theta)$, where E is the relative energy of the particles and Θ is the scattering angle. The probability for a scattering angle between Θ_n and Θ_{n+1} is then equal to

$$\frac{2\pi \int_{\Theta_n}^{\Theta_{n+1}} \sigma(E, \Theta) \sin \Theta \, d\Theta}{\sigma_{tot}(E)}, \tag{71}$$

where $\sigma_{tot}(E)$ is the total cross section.

The angular interval between 0° and 360° was divided into one hundred intervals such that the probability of scattering into any of these intervals was constant. The division is very simple to carry out for the isotropic proton-proton and neutron-neutron scattering. The angles Θ_n were then determined from

$$\cos \Theta_n = \frac{25 - n}{25}; \quad n = 0, 1, 2, \ldots 50;$$

$$\Theta_{100-n} = 360° - \Theta_n.$$

The neutron-proton scattering is anisotropic. For the energy 90 Mev the angular dependence can be expressed as follows:

$$4\pi\sigma(\Theta) = \sigma\ (1 - 0.14P_1 + 0.68P_2 + 0.02P_3 + 0.11P_4), \tag{72}$$

where P_i are Legendre polynomials (255). The angular dependence is different for different energies. For the sake of simplicity the angular dependence expressed by Eq. (72) was taken to be representative for all energies, however. This will give too large anisotropy for lower energies and too small anisotropy for higher energies, but the approximation is certainly good enough for the cascade calculation. The division of the angular interval was then carried out graphically using the angular dependence given by Eq. (72).

A number k between one and one hundred was chosen at random. The scattering angle was then assumed to be

$$\frac{\Theta_{k-1} + \Theta_k}{2}.$$

g. *Construction of Angles and Energies*

The angles and energies after the collision are readily obtained graphically as is shown in Fig. 26.

E_1 and E_2 are the energies of the particles before the collision, and v is the angle between their momenta. If the scattering angle is Θ (C.M.-system), the energies and angles after the

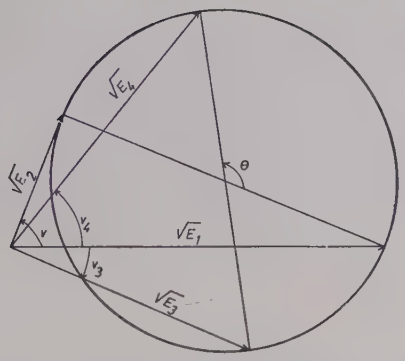

Fig. 26. Graphical determination of collision angles and energies.

collision, E_3 and E_4, v_3 and v_4, are obtained graphically from the figure.

h. *Example of a Nucleon Cascade*

An example of the cascade calculation is shown in Fig. 27. Here the incident proton gives rise to a cascade which results

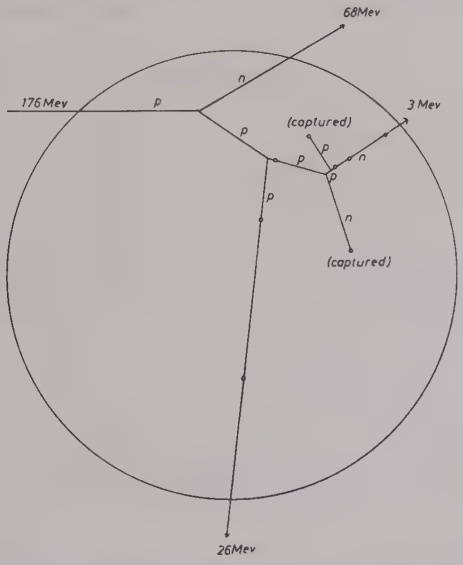

Fig. 27. Example of a cascade diagram. Collisions, forbidden by the exclusion principle, are indicated by circles.

in three cascade particles, one proton and two neutrons. In this case the residual nucleus is As^{73} with an excitation energy of 59 Mev and an angular momentum (compare p. 155) of about 4 $\hbar$. If Assumption II is used the slow cascade neutron (3 Mev) would be considered as captured by the nucleus. The residual nucleus would then be As^{74} with an excitation energy of 72 Mev.

C. *Results of the Cascade Calculation*

1. THE INELASTIC CROSS SECTION

A total number of 570 cascades were followed, 470 with 170 Mev protons and 100 with 103 Mev protons.

The number N of cases in which the proton passes through the nucleus without any collision at all can be used to determine the inelastic cross section. The ratio between the inelastic cross section σ_i and the geometrical cross section σ_0 is simply given by the ratio between the number of colliding protons and the total number N_0 of incident protons. Thus

$$\frac{\sigma_i}{\sigma_0} = \frac{N_0 - N}{N_0}. \tag{73}$$

The value σ_i obtained in this way depends on the radius of the circle representing the nucleus. For the actual problem the plane model gives exactly the same result as a spherical model of the same radius would do. The inelastic cross section should therefore be increased since a reduced radius was used for the circle.

The inelastic cross section is related to the mean free path (in nuclear matter) by the following formula (238):

$$\frac{\sigma_i(R)}{\sigma_0} = 1 - \frac{2}{y^2}[1 - e^{-y}(1+y)], \tag{74}$$

with $y = 2R/\lambda_e$.

This equation is used to determine $2R'/\lambda_e$ and thus λ_e ($R' = 4.6 \times 10^{-13}$ cm) from the value of $\sigma_i(R')/\sigma_0$ obtained from

Eq. (73). The values of the mean free path and the nuclear radius ($R = 5.1 \times 10^{-13}$ cm) can then be inserted into Eq. (74) to determine $\sigma_i(R)/\sigma_0$. The inelastic cross section is finally obtained using the geometrical cross section $\sigma_0 = \pi R^2 = 816$ mb.

The results concerning mean free paths and inelastic cross sections are tabulated in Table 47. The error given for λ_e and for σ_i is the standard deviation estimated from the statistics of the calculation.

Table 47

The inelastic cross section and the mean free path

	170 Mev	103 Mev
N_0	470	100
N	155	41
λ_e	$(5.2 \pm 0.6)\ 10^{-13}$ cm	$(6.5 \pm 1.1)\ 10^{-13}$ cm
σ_i/σ_0	0.70 ± 0.04	0.63 ± 0.06
σ_i	570 ± 30 mb	510 ± 50 mb

The values of λ_e obtained in this work are in good agreement with other determinations (16, 237, 256).

The inelastic cross section can be obtained from measurements of the total cross section and the ratio between the inelastic cross section and the total cross section. Several investigators, for instance Fox, Leith, Wouters, and Mac Kenzie (257), have observed that $(\sigma_{tot})^{1/2}$ is proportional to $A^{1/3}$. Using this, the total cross section of arsenic can be deduced from the measured values for copper. Neutron cross sections of copper can be used, since the total cross section for protons is the same as for neutrons (258). De Juren (259) has shown that the ratio σ_i/σ_{tot} is almost independent of the atomic number and only depends on the energy. At 270 Mev (neutrons) he gets for copper $\sigma_i/\sigma_{tot} = 0.50 \pm 0.02$ and at 95 Mev $\sigma_i/\sigma_{tot} = 0.39 \pm \pm 0.005$.

The inelastic cross sections of arsenic at 170 Mev and 103 Mev were calculated using total cross sections from the in-

vestigation by Taylor and Wood (260), and with σ_i/σ_{tot} estimated to be 0.44 at 170 Mev and 0.39 at 103 Mev. They are tabulated in Table 48. In the last column of the table, the inclastic cross sections obtained from the cascade calculation are included for comparison.

Table 48

Inelastic cross sections of arsenic

Irradiation energy	$(\sigma_{tot})_{Cu}$	$(\sigma_{tot})_{As}$	$(\sigma_i)_{As}$	$(\sigma_i)_{As}$ from cascade calculation
170 Mev	1.3 barns	1.5 barns	0.66 barns	0.57 ± 0.03 barns
103 »	1.9 »	2.1 »	0.82 »	0.51 ± 0.05 »

2. THE EXCITATION ENERGY OF THE RESIDUAL NUCLEUS

The result of the cascade calculation to be used in the cross section computation is the distribution of residual nuclides and their excitation energies. Two cases will now be distinguished, namely one corresponding to Assumption I and the other corresponding to Assumption II (see p. 109).

The excitation energy of the residual nucleus is the difference between the energy of the incident proton increased by the binding energy of this proton and the sum of the energies and separation energies of the cascade particles.

The distribution of residual nuclides and their average energies ($\bar{U}$) are tabulated in Table 49.

The excitation energy distributions are shown in Figs. 28–30. The residual nuclides obtained for 170 Mev protons using Assumption I have been divided into two groups, *A* and *B*. Group *A* consists of the nuclides Se^{75}, As^{75}, As^{74}, and Ge^{74}, and Group *B* contains all the rest. These two groups have different energy distributions. This depends probably on the fact that the nuclides belonging to Group *A* are often (about sixty per cent) formed through one single collision in the nucleus (average number of collisions: 1.6), which is not possible for the

Table 49

Residual nuclides from the cascade calculation

Nuclide	170 Mev				103 Mev			
	Assumption I		Assumption II		Assumption I		Assumption II	
	Number	$\bar{U}$ Mev	Number	$\bar{U}$ Mev	Number	$\bar{U}$ Mev	Number	$\bar{U}$ Mev
Se^{76}			2	183			1	107
Se^{75}	10	36	33	60	6	50	12	52
Se^{74}	9	60	12	70	1	36	1	36
Se^{73}	4	67						
As^{75}	34	27	96	53	15	28	22	36
As^{74}	95	28	94	39	22	22	16	18
As^{73}	30	50	9	44				
As^{72}	2	45						
As^{71}	1	53						
Ge^{74}	56	25	53	42	10	23	7	27
Ge^{73}	36	44	11	40	3	29		
Ge^{72}	13	54						
Ge^{71}	1	41						
Ga^{73}	14	44	4	39	2	25		
Ga^{72}	6	33	1	14				
Ga^{71}	2	39						
Zn^{72}	1	44						
Zn^{71}	1	71						
All nuclides	315	35	315	48	59	27	59	34

other nuclides (average number of collisions: 3.4). The excitation energy, therefore, will generally be less for Group *A* nuclides, which can be seen from the average energies in Table 49.

A similar division does not seem to be necessary in the other cases. Of course, the nuclide Se^{76} has to be separated from the other nuclides, since it has evidently a quite different energy distribution (compound nucleus).

The relative frequency of different residual nuclides is assumed to be constant over the whole excitation energy interval. This means that the differential cross section of any residual nuclide can be obtained from Table 49 and Figs. 28–30.

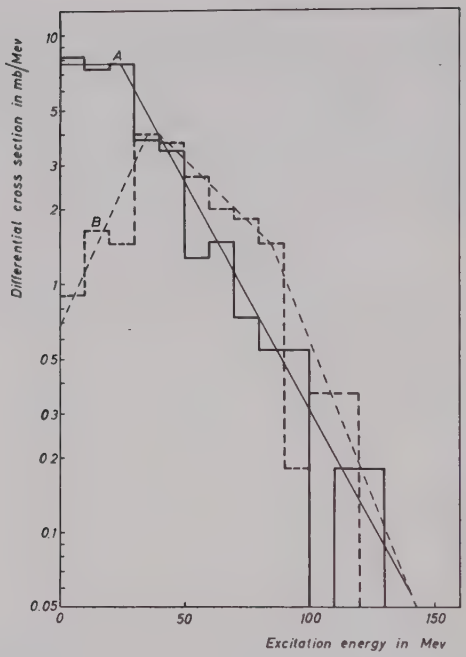

Fig. 28. Excitation energy distributions obtained for irradiation energy 170 Mev using Assumption I. The solid line refers to Group *A* nuclides and the broken line to Group *B* nuclides.

3. DISTRIBUTION IN ENERGY AND ANGLE OF THE CASCADE PARTICLES

From the cascade calculation the energy and angular distributions of the cascade particles can be obtained. The cascade particles have not been studied experimentally in the present work, but they have been the subject of many other investigations (8–19). It seems, therefore, appropriate to quote the results obtained from the present cascade calculation (using Assumption I).

For the irradiation energy 170 Mev the average number of cascade nucleons per reacting nucleus was found to be 2.3 (1.4 protons and 0.9 neutrons). The distributions in energy

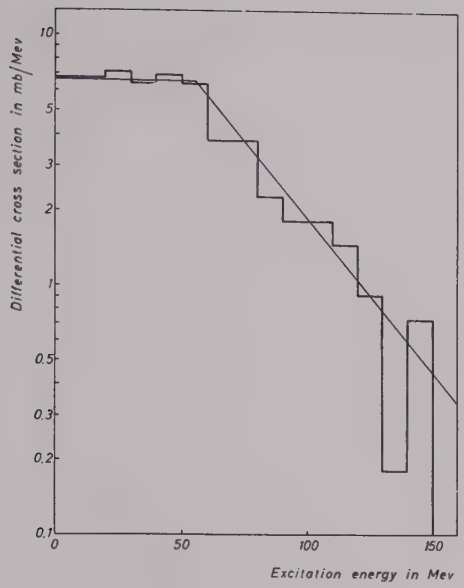

Fig. 29. Excitation energy distribution obtained for irradiation energy 170 Mev using Assumption II.

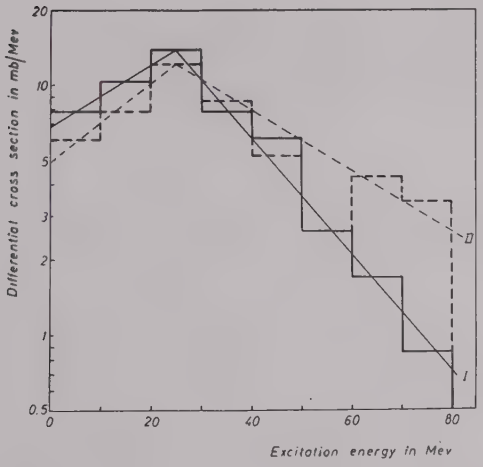

Fig. 30. Excitation energy distributions obtained for irradiation energy 103 Mev using Assumption I (solid line) and Assumption II (broken line).

Fig. 31. Energy distributions of the cascade particles obtained for irradiation energy 170 Mev.
Solid line: protons + neutrons.
Broken line: protons.
Dotted line: neutrons.

and angle[1] (laboratory system) are shown in Figs. 31 and 32. As is seen the distributions are very similar for protons and neutrons.

Figs. 33 and 34 show the corresponding distributions for the irradiation energy 103 Mev. In these figures protons and neutrons are taken together, because the total number of nucleons was small. The average number of cascade nucleons per reacting nucleus was 1.8 (1.2 protons and 0.6 neutrons).

[1] The angular distributions are not quite comparable with experimental results, since a plane model was used in the cascade calculation instead of a spherical one.

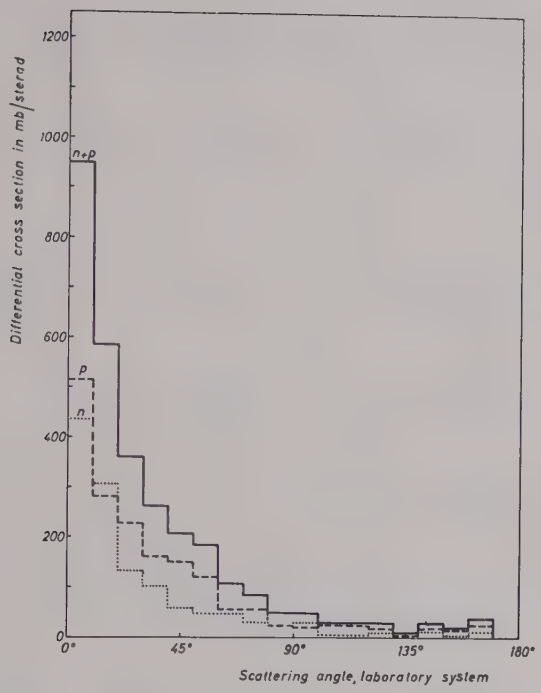

Fig. 32. Angular distributions of the cascade particles obtained for irradiation energy 170 Mev using Assumption I.

Solid line: protons + neutrons.
Broken line: protons.
Dotted line: neutrons.

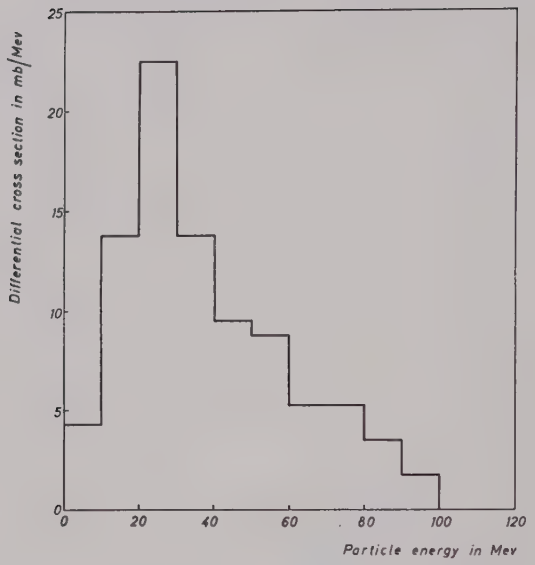

Fig. 33. Energy distribution of the cascade particles for irradiation energy 103 Mev.

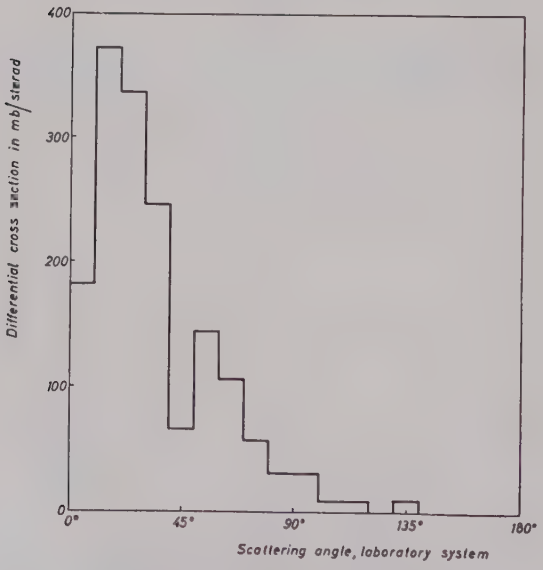

Fig. 34. Angular distribution of the cascade particles obtained for irradiation energy 103 Mev using Assumption I.

CHAPTER V

The Evaporation Process

A. *Introduction*

When the nucleon cascade is finished, a residual nucleus with a certain excitation energy is left. It now remains to investigate the evaporation process by which this nucleus is de-excited.

For low excitation energies the evaporation process can be easily calculated (261). For higher excitation energies, when many particles of different kind such as protons, neutrons, α-particles, and deuterons are emitted, the treatment is more complicated. Several authors (59, 262–264), however, have calculated analytically the average behaviour in the de-excitation of a highly excited nucleus and also the statistical fluctuations in the evaporation process. Another approach will be attempted here, which allows individual properties of the nuclides, such as anomalies in their binding energies, to be retained. The idea is to follow the evaporation of successive particles by a Monte Carlo method. For excitation energies below 20 Mev, however, the evaporation will be calculated using the method given by Blatt and Weisskopf (261).

B. *Monte Carlo Calculation for High Excitation Energies*

1. THE EMISSION PROBABILITIES

As a starting point Weisskopf's evaporation formula (265) will be used:

$$W_j(E)\,dE = \sigma(E)\frac{g\,m\,E}{\pi^2\,\hbar^3}\,\frac{w_f(U_f)}{w_i(U_i)}\,dE. \tag{75}$$

The formula describes the reaction $Z_i = Z_f + j$, and the significance of the symbols is the following:

$W_j(E)\,dE$ = probability per unit time for emission of the particle j with energy between E and $E + dE$;

$\sigma(E)$ = cross section for capture of the particle j by the nucleus Z_f;
g = number of spin states of the particle j;
m = mass of the particle j;
$w(U)$ = level density of a nucleus at the excitation energy U;
U_i = excitation energy of the nucleus Z_i;
U_f = excitation energy of the nucleus Z_f after the particle emission.

The following connection exists between U_i and U_f:

$$U_i = U_f + E + S_j, \tag{76}$$

where S_j is the separation energy of the particle j.

The total probability for the emission of the particle j is

$$P = \int_{V_j'}^{U_i - S_j} W_j(E)\, dE, \tag{77}$$

with V_j' equal to the potential barrier, corrected for penetration, of the particle j.

The following notation is introduced:

$$\gamma = \frac{g\, m}{\pi^2\, \hbar^3}.$$

Evidently:

$$\gamma_n : \gamma_p : \gamma_d : \gamma_t : \gamma_T : \gamma_\alpha = 1 : 1 : 3 : 3 : 3 : 2. \tag{78}$$

t here stands for triton and T for helium-3.

The following simplifying assumptions are made for the capture cross section (265):

$$\begin{cases} \sigma(E) = \sigma_0 \left(1 - \dfrac{V'}{E}\right) \text{ for } E > V'; \\ \sigma(E) = 0 \text{ for } E < V'; \\ \sigma_0 = \pi R^2. \end{cases} \tag{79}$$

The emission probability can now be written:

$$P_j(U_i) = \frac{\gamma_j \sigma_{0j}}{w_i(U_i)} \int_{V_j'}^{U_i - S_j} (E - V_j') w_f(U_f) \, dE. \tag{80}$$

For the calculation of the emission probabilities using Eq. (80) the level density $w_f(U_f)$ must be known. Lang and Le Couteur (266) give as the best equation of state for nuclides:

$$U = \frac{A}{11} t^2 - t + \frac{1}{8} A^{2/3} t^{7/3}, \tag{81}$$

where A is the mass number and t the nuclear temperature.

Using thermodynamical analogies Lang and Le Couteur arrive at the following formula for the level density of a Fermi gas:

$$w(U)\, dU = \text{const} \times A^{-1/4} (U+t)^{-5/4} \exp\left[2 (A\,U/11)^{1/2} + \right. \\ \left. + \frac{3}{32} (11\,U)^{2/3}\right] dU. \tag{82}$$

If t is neglected compared to U, P_j can be written:

$$P_j(U_i) = \text{const} \times \frac{\gamma_j \sigma_{0j}}{w_i(U_i)} A^{-1/4} I, \tag{83}$$

with

$$I = \int_{V_j'}^{U_i - S_j} (E - V_j') U_f^{-5/4} \exp(b\,U_f^{1/2} + c\,U_f^{2/3})\, dE. \tag{84}$$

For simplicity the following notations have been introduced:

$$b = 2\,(A/11)^{1/2}; \quad c = \frac{3 \times 11^{2/3}}{32}.$$

The mass number A refers to the product nucleus.

The transformations

$$U_f = y^2; \quad U_i - S_j - V_j' = y_0^2,$$

give:

$$I = 2 \int_0^{y_0} (y_0^2 - y^2)\, y^{-3/2} \exp(b\,y + c\,y^{4/3})\, dy. \tag{85}$$

The exchange of variable

$$y = y_0 - x$$

and the expansion of $y^{4/3}$:

$$y^{4/3} = y_0^{4/3} - \frac{4}{3} y_0^{1/3}\, x + \frac{2}{9} y_0^{-2/3}\, x^2 \pm \ldots .$$

transform (85) into

$$I = 2 y_0^{-3/2} \exp(b\, y_0 + c\, y_0^{4/3})\, I', \tag{86}$$

with

$$I' = \int_0^{y_0} x\,(2y_0 - x)\,(1 - x/y_0)^{-3/2} \exp(-b'\, x + c'\, x^2 \pm)\, d\, x; \tag{87}$$

$$b' = b + \frac{4c}{3} y_0^{1/3}; \quad c' = \frac{2c}{9} y_0^{-2/3}.$$

If $c'\, x^2 \pm \ldots$ in the exponent is approximated by $c' \frac{y_0}{2}\, x$, and the term $(1 - x/y_0)^{-3/2}$ is expanded, the integral (87) can be carried out. Keeping the first two terms the result is:

$$I' = \frac{2 y_0}{(b'')^2} \left(1 + \frac{2}{b''\, y_0}\right), \tag{88}$$

with

$$b'' = b' - c' \frac{y_0}{2}.$$

The formula for the level density is applicable only to nuclides of the same kind. Odd-odd nuclides have a larger level density and even-even nuclides a smaller density than odd-even nuclides. In order to correct for this, a factor C_j was introduced, which was chosen so that

$$\frac{1}{2}\, C_{o-o} = C_{o-e} = 2\, C_{e-e}. \tag{89}$$

This choice, which is rather arbitrary, was proposed by Weisskopf and Ewing (267).

The final formula for the ratio between the probability of emission of the particle j and the probability of emission of a neutron is the following:

$$\frac{P_j}{P_n} = \frac{C_j \gamma_j}{C_n \gamma_n} \left(\frac{A_j}{A_n}\right)^{5/12} \left(\frac{y_{0n}}{y_{0j}}\right)^{1/2} \left(\frac{b_n''}{b_j''}\right)^2 \times$$

$$\times \frac{1 + \dfrac{2}{b_j'' y_{0j}}}{1 + \dfrac{2}{b_n'' y_{0n}}} \exp\left[b_j y_{0j} - b_n y_{0n} + c\left(y_{0j}^{4/3} - y_{0n}^{4/3}\right)\right]. \tag{90}$$

The significance of the different symbols will be repeated here:

γ_j is defined in Eq. (78) and C_j in Eq. (89);

A_j = mass number of the nucleus remaining after the emission of the particle j;

U_i = excitation energy of the emitting nucleus;

S_j = separation energy of the particle j;

V_j' = potential barrier (corrected for penetration) of the particle j;

$$y_{0j} = (U_i - S_j - V_j')^{1/2};$$

$$b_j = 2\,(A_j/11)^{1/2}$$

$$b_j'' = 2\,(A_j/11)^{1/2} + \frac{11^{5/3}}{96} y_{0j}^{1/3};$$

$$c = \frac{3 \times 11^{2/3}}{32}$$

It must be pointed out that most of the factors of the formula (90) are close to unity. It is only the first factor, $C_j \gamma_j / C_n \gamma_n$, and the last exponential factor that are important.

2. SEPARATION ENERGY AND COULOMB BARRIER

The separation energies were usually obtained from the reference (246). In many cases, however, the total binding energies of nuclides of interest are not given in that reference. In such cases the separation energies were calculated from

binding energies obtained from the semiempirical mass formula (243).

The potential barrier is expected to decrease for higher excitation energies owing to surface oscillations (268, 269). Such a behaviour gives better agreement with experimental data (59, 270). Besides, the potential barrier should be corrected for penetration. In the present work the potential barrier was calculated from the following formula, given by Le Couteur (59):

$$V_j' = \frac{k_j V}{1 + U_i/200}. \tag{91}$$

V is the uncorrected proton barrier, U_i is the excitation energy in Mev, and the factors k_j have the following values:

$$k_p = 0.7;\ k_d = 0.77;\ k_t = 0.8;\ k_T = 1.6;\ k_\alpha = 1.66.$$

3. THE ENERGY DISTRIBUTION OF THE EVAPORATED PARTICLES

Weisskopf (265) gives the following formula for the energy distribution of the evaporated particles:

$$W_j(E)\,dE = \text{const} \times (E - V_j')\, e^{-(E - V_j')/\tau}(U_i - S_j - V_j')\,dE. \tag{92}$$

The parameter τ, which is usually called the nuclear temperature (compare Eq. (81)), was calculated using Lang's and Le Couteur's empirical formula (266):

$$\tau(U) = \sqrt{\frac{10.5 \times U}{A}}. \tag{93}$$

The change of variable

$$y = \frac{E - V'}{\tau},$$

transforms Eq. (92) into

$$W_j(y)\,dy = \text{const} \times \tau^2\ y\, e^{-y}\, dy. \tag{94}$$

The distribution (94) was divided into one hundred intervals with the same probability by means of division points y_n. If

the last division point y_{100} is put equal to infinity (properly $y_{100} = (U_i - S_j - V_j')/\tau$), the condition of equal probability gives:

$$\frac{\int_{y_n}^{Y_n+1} W_j(y)\,dy}{\int_0^{\infty} W_j(y)\,dy} = \frac{1}{100}. \tag{95}$$

Eq. (95) leads to the following system:

$$y_0 = 0;\ (1+y_1)\,e^{-y_1} = \frac{99}{100};\ \ldots;\ (1+y_n)\,e^{-y_n} = \frac{100-n}{100}. \tag{96}$$

The y_n's were obtained graphically from a plot of $(1+y)\ e^{-y}$ *versus* y. The y_n-system is independent of the nuclide, its excitation energy, and the kind of evaporated particle.

4. THE EVAPORATION CALCULATION

By means of Eq. (90) the relative probabilities for the emission of neutrons, protons, deuterons, tritons, helium-3, and α-particles were calculated for the different nuclides as functions of the excitation energy. The evaporation probabilities were then plotted in a diagram in the way shown in Figs. 35 and 36. For a given excitation energy, U_i say, the region 0–a (= neutron emission probability) corresponds to neutron emission, the region a–b (= proton emission probability) corresponds to proton emission, and so on. The vertical line at the left in the figures represents the separation energy of a neutron or the separation energy + the potential barrier of a proton, whichever is the lowest. Fig. 35 (Ge^{73}) is a typical example of an evaporation diagram with the neutron separation energy lowest, but for very proton-rich nuclides the proton separation energy + the potential barrier may be lower. Then the diagram looks like the one in Fig. 36 (Ge^{66}). Diagrams such as those in Figs. 35 and 36 had to be constructed for each nuclide which might be formed somewhere in the evaporation process, in the actual

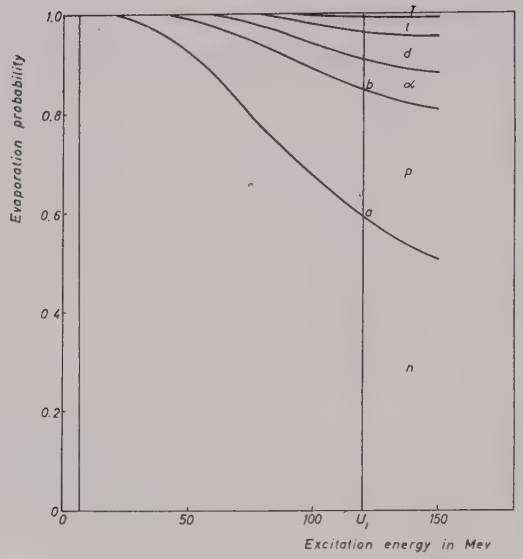

Fig. 35. Evaporation diagram for Ge^{73}.

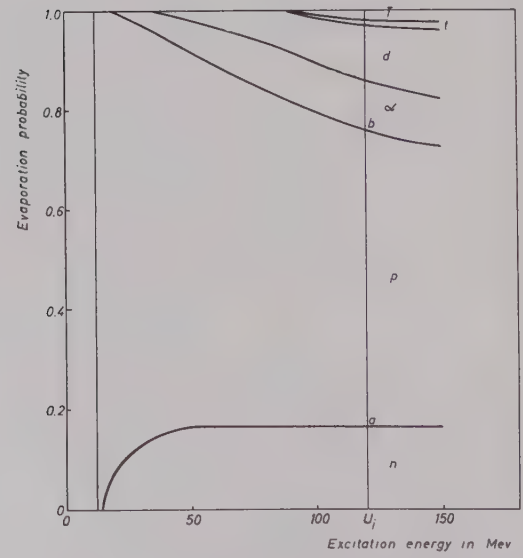

Fig. 36. Evaporation diagram for Ge^{66}.

case for the nuclides Se^{69-76}, As^{67-75}, Ge^{65-74}, Ga^{63-73}, Zn^{62-72}, Cu^{60-71}, Ni^{58-67}, and Co^{57-62}.

The evaporation calculation was carried out in the following way. An initial nuclide Z_i with a certain excitation energy U_i was chosen as a starting point. A random number between one and one hundred, obtained with the roulette shown in Fig. 23, determined the kind of evaporated particle. For instance, the number 75 would mean the evaporation of a proton in Fig. 35. A second random number between one and one hundred determined y_n (see Eq. (96)) and thus the energy of the evaporated particle j by the formula:

$$E_j = V_j' + y_n \tau, \tag{97}$$

where τ was calculated using Eq. (93).

The product Z_f of the evaporation and the excitation energy U_f of this nuclide are now defined.

$$\begin{cases} Z_f = Z_i - \text{evaporated particle}; \\ U_f = U_i - S_j - E_j. \end{cases} \tag{98}$$

The calculation was then repeated in the same way using Z_f and U_f as new initial values, until a value of U_f was obtained for which the nuclide Z_f could not evaporate more particles, *i.e.* U_f was situated to the left of the vertical line in Figs. 35 and 36. If this value of U_f was larger than the separation energy of a proton by at least 2 Mev, a slow proton was assumed to evaporate. It can be shown (59, 239) that under these circumstances the evaporation of a proton by barrier penetration is a faster and therefore more probable process than γ-emission. After this evaporation of a slow proton the evaporation process is finished, and the last Z_f was taken to be the final product. Thus the evaporation calculation yields both the final product and the kind and energy of the evaporated particles.

The excitation energies 25 Mev, 35 Mev, 45 Mev, . . . , 165 Mev were chosen as initial excitation energies of the residual nuclides. For each energy about one hundred cases were followed using different initial nuclides. The number of the different

Table 50

Distribution of initial nuclides

Nuclide	Se^{75}	Se^{74}	Se^{73}	As^{75}	As^{74}	As^{73}	As^{72}	As^{71}	Ge^{74}
Number	2	4	2	7	20	15	1	1	10
Nuclide	Ge^{73}	Ge^{72}	Ge^{71}	Ga^{73}	Ga^{72}	Ga^{71}	Zn^{72}	Zn^{71}	
Number	18	6	1	6	4	1	1	1	

initial nuclides was chosen according to the results of the cascade calculation. Table 50 gives the distribution usually used.

In addition the evaporation from Se^{76} was followed. This case is not included in Table 50 because Se^{76} results when no cascade particles at all are emitted, and its excitation energy is uniquely defined as the sum of the bombarding energy and the binding energy of the incident proton.

5. SOME RESULTS OF THE EVAPORATION CALCULATION

It is not possible to present all the results of the calculations here, since this would take far too much space. Only some data will be given. The product nuclides and the evaporation particles obtained from the initial nuclide As^{74} excited to 105 Mev are tabulated in Table 51 as an example.

Fig. 37 shows the average number of neutrons, protons, deuterons, α-particles, tritons, and helium-3 evaporated at different excitation energies. These results were obtained using the distribution of residual nuclides given in Table 50. They can be compared with the analytical treatments of the evaporation process carried out by Le Couteur (59), Yamaguchi (262), and Fujimoto and Yamaguchi (263) in Table 52. These analytical treatments are valid for the mass number 100.

Table 51

Evaporation calculation for As^{74} excited to 105 Mev

Products:												
Nuclide	Ge^{68}	Ge^{67}	Ge^{66}	Ga^{68}	Ga^{67}	Ga^{66}	Zn^{67}	Zn^{66}	Zn^{65}	Zn^{64}	Zn^{62}	Cu^{62}
Number	1	3	1	1	3	1	2	2	2	2	1	1

Evaporated particles:												
Energy (Mev)	0–1	1–2	2–3	3–4	4–5	5–6	6–7	7–8	8–9	9–10	10–11	11–12
Neutrons	11	13	13	9	11	6	8	9	2	4	2	3
Protons			2	1			4	2	1	3	4	
Deuterons							1	1				
α-Particles												1

Energy (Mev)	12–13	13–14	14–15	15–16	16–17	17–18	19–20
Neutrons	2	1	1		1		
Protons	3	2	1		1	1	
Deuterons	1						
Tritons	1						
α-Particles			1	1			3

The average decrease in energy per evaporated nucleon rises slowly from 12.8 Mev at an initial excitation energy of 25 Mev to 14.3 Mev at an initial excitation energy of 145 Mev.

The average decrease in energy per evaporated charged particle is 70 Mev at the initial excitation energy 105 Mev and 60 Mev at the initial excitation energy 145 Mev.

From the average energy $\overline{E}$ of the evaporated neutrons one can deduce the mean nuclear "temperature" from the relation (obtained from Eq. (92))

$$\overline{E} = 2\tau. \tag{99}$$

The average energy increases from 2.6 Mev at the initial excitation energy 25 Mev to 6.1 Mev at the initial excitation energy

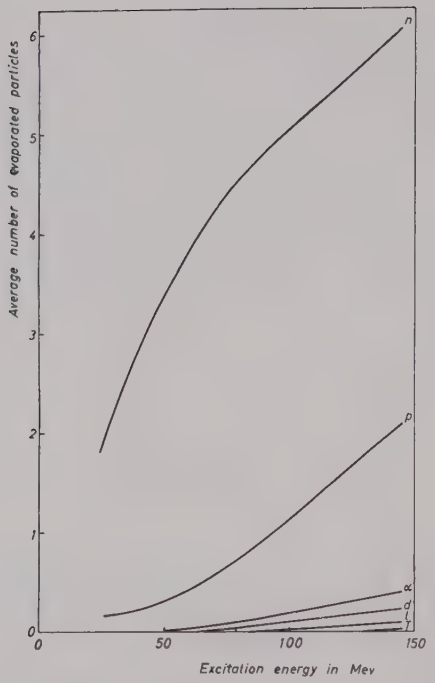

Fig. 37. Average number of evaporated particles *versus* the excitation energy. The mass number of the evaporating nucleus is about 75.

Table 52

Mean number of evaporated particles obtained in different evaporation treatments

Particle	Excitation energy Mev	Mean number of evaporated particles			
		This work	Fujimoto and Yamaguchi	Yamaguchi	Le Couteur
Proton	50	0.30	0.27		0.6
»	100	1.1	1.2	1.1	0.9
»	150	2.2	2.2		1.9
Neutron	50	3.4	2.7		
»	100	5.0	4.8	5.7	
»	150	6.1	6.5		
Deuteron	150	0.2			0.2
α-Particle	100	0.2		0.2	0.4
»	150	0.4			0.7

145 Mev corresponding to a mean nuclear temperature of 1.3 Mev and 3.1 Mev, respectively.

If the results of the evaporation calculation are combined with the results of the cascade calculation the cross sections of different spallation products and emitted particles can be obtained, as will be shown in the next Chapter.

C. *Low Excitation Energy*

In the excitation energy region 0–20 Mev the only evaporation particle which need be taken into account is the neutron. The energy region is for simplicity divided into two intervals, 0–10 Mev and 10–20 Mev, and the differential cross section is assumed to be constant in each interval, σ_1 and σ_2 millibarns per Mev, respectively.

Let Z^A be a residual nuclide from the cascade, and S_1 be the separation energy of a neutron. S_2 is assumed to be the separation energy of a neutron from the nucleus Z^{A-1}. The assumption is also made that a neutron is always evaporated when this is energetically possible. Then the cross section of the final nuclide Z^A, formed by γ-emission from the excited nuclide Z^A, will be

$$\sigma_{Z^A} = \int_0^{S_1} \sigma(U)\, dU = \begin{cases} S_1 \sigma_1; & S_1 < 10 \text{ Mev}; \\ 10\,\sigma_1 + (S_1 - 10)\,\sigma_2; & S_1 > 10 \text{ Mev}. \end{cases} \tag{100}$$

The cross section of the final nuclide Z^{A-1} will be

$$\sigma_{Z^{A-1}} = \int_{S_1}^{S_1+S_2} \sigma(U)\, dU + \int_{S_1+S_2}^{20} \sigma(U)\, F(U)\, dU, \tag{101}$$

where $F(U)$ is the probability that only one neutron is evaporated at an excitation energy which is larger than $S_1 + S_2$. From the reference (261) $F(U)$ is seen to be:

$$F(U) = \left[1 + \frac{U - S_1 - S_2}{\tau(U - S_1)}\right] e^{-(U - S_1 - S_2)/\tau(U - S_1)}. \tag{102}$$

Finally, the cross section of Z^{A-2} is

$$\sigma_{Z^{A-2}} = \int_{S_1+S_2}^{20} \sigma(U)\,[1 - F(U)]\,dU. \tag{103}$$

The integral

$$\int_{S_1+S_2}^{20} F(U)\,dU$$

is estimated, and the different cross sections are then easily obtained, if σ_1 and σ_2 are known.

Chapter VI

Comparison between Experimental and Calculated Cross Sections

A. *The Spallation Products*

1. CROSS SECTIONS OF THE SPALLATION PRODUCTS

The results of the cascade and the evaporation calculations can now be combined to give the formation cross sections of the spallation products. Such a combined cascade-evaporation calculation has been carried out for some simple reactions by Meadows (239) and by Nakasima and Kikuchi (242). In the present calculation the cross section of any nuclide was obtained by adding together contributions from different residual nuclides and excitation energies. The nuclide Ge^{68}, formed at the irradiation of arsenic with 170 Mev protons (using Assumption I), will be chosen as an example. From Table 51 Ge^{68} is seen to be the spallation product from the residual nuclide As^{74} excited to 105 Mev in one case out of twenty. The differential cross section of As^{74} is obtained from Table 49 and Fig. 28 and comes out to be

$$\frac{95}{195} \times 0.25 \text{ mb/Mev.}$$

Thus the formation cross section of Ge^{68} gets a contribution of

$$\frac{95}{195} \times 0.25 \times 10 \times \frac{1}{20} = 0.061 \text{ mb}$$

from the residual nuclide As^{74} in the excitation energy interval 100–110 Mev. The total cross section is in this case composed of forty such contributions, which add up to 29 millibarns. In this way the cross sections were obtained for sixty-seven nuclides at 170 Mev and for thirty-eight nuclides at 103 Mev.

The standard deviations of the calculated cross sections were roughly estimated from the statistics of the calculation

Table 53

Calculated and experimental cross sections for the spallation group *G* (As; *p*; 170 Mev)

Nuclide	σ_{obs} mb	σ_{calc} mb	
		Assumption I	Assumption II
Se^{73}	8.4 ± 1.9	4.4 ± 1.6	9.5 ± 3.0
Se^{72}	10 ± 4	5.0 ± 2.0	12 ± 5
As^{74}	90 ± 30	43 ± 10	36 ± 8
As^{72}	58 ± 20	45 ± 15	57 ± 20
As^{70}	7.4 ± 1.9	26 ± 7	31 ± 9
Ge^{71}	70 ± 40	40 ± 10	39 ± 10
Ge^{69}	50 ± 20	20 ± 5	23 ± 5
Ge^{68}	25 ± 5	29 ± 4	30 ± 4
Ge^{67}	3.0 ± 0.9	9.5 ± 2.0	6.5 ± 1.2
Ga^{73}	0.43 ± 0.09	1.8 ± 0.7	1.6 ± 0.6
Ga^{72}	1.3 ± 0.3	1.7 ± 0.7	0.91 ± 0.50
Ga^{70}	16 ± 3	8.5 ± 3.5	2.4 ± 1.0
Ga^{68}	29 ± 6	13 ± 3	14 ± 3
Ga^{67}	52 ± 13	11 ± 2	8.2 ± 1.4
Ga^{66}	16 ± 3	5.2 ± 0.9	5.6 ± 0.9
Zn^{69+69m}	2.4 ± 0.4	0.62 ± 0.35	0.85 ± 0.50
Cu^{64}	7.2 ± 1.2	0.52 ± 0.15	1.5 ± 0.4
Cu^{61}	1.5 ± 0.3	0.28 ± 0.09	0.83 ± 0.20
Cu^{60}	0.34 ± 0.18	0	0.10 ± 0.07

and are included in Tables 53 and 54, where calculated and experimental cross sections can be compared.

The general features of the comparison are more easily discerned in Figs. 38–40 where the calculated cross sections, using both Assumption I and Assumption II, are plotted for the different elements. In these figures the experimental cross sections and those (up to mass number 72) obtained from the cross section formula (47) are also plotted (the cross section formula represents the average trend of the experimental data). At the irradiation energy 170 Mev the calculated cross sections of selenium, arsenic, germanium, gallium, and zinc follow the experimental values fairly closely. Only

Table 54

Calculated and experimental cross sections for the spallation group *G* (As; *p*; 103 Mev)

Nuclide	σ_{obs} mb	σ_{calc} mb	
		Assumption I	Assumption II
Se^{78}	11 ± 3	12 ± 5	18 ± 8
Se^{72}	13 ± 5	8.5 ± 4.0	18 ± 8
As^{74}	70 ± 25	51 ± 10	42 ± 8
As^{72}	41 ± 10	74 ± 30	87 ± 35
As^{71}	55 ± 25	26 ± 9	29 ± 10
Ge^{71}	12 ± 7	40 ± 11	37 ± 10
Ge^{69}	11 ± 4	7.8 ± 2.0	18 ± 4
Ge^{68}	4.1 ± 1.2	4.6 ± 0.9	9.2 ± 2.0
Ge^{67}	0.58 ± 0.17	0.18 ± 0.07	0
Ga^{73}	0.22 ± 0.06	3.4 ± 1.4	0.68 ± 0.25
Ga^{72}	0.80 ± 0.25	3.1 ± 2.2	0
Ga^{70}	5.7 ± 1.5	3.3 ± 1.3	0.50 ± 0.20
Ga^{68}	17 ± 4	2.7 ± 0.7	5.5 ± 1.3
Ga^{67}	25 ± 7	1.0 ± 0.3	1.5 ± 0.4
Ga^{66}	6.3 ± 1.7	0.22 ± 0.08	0.36 ± 0.13
Zn^{69+69m}	0.59 ± 0.13	0.19 ± 0.13	0.41 ± 0.30
Zn^{65}	6.6 ± 2.5	0.23 ± 0.13	0.47 ± 0.14

for elements farther from the target (copper and nickel) the agreement is less good. The calculated cross sections are too low here. At 103 Mev the agreement is good for selenium, arsenic, and germanium, but for the gallium isotopes the calculated cross sections are too low. Thus the overall agreement between calculated and measured cross sections is satisfactory for elements not too far from the target element. This means that a cascade process followed by an evaporation process is a useful model for nuclear reactions at high energies.

For elements far from the target the cascade-evaporation calculation seems to give too low cross sections. The reason might be that other processes here play a part, for instance fission (5, 6, 7, 33, 271) or fragmentation (272). These processes

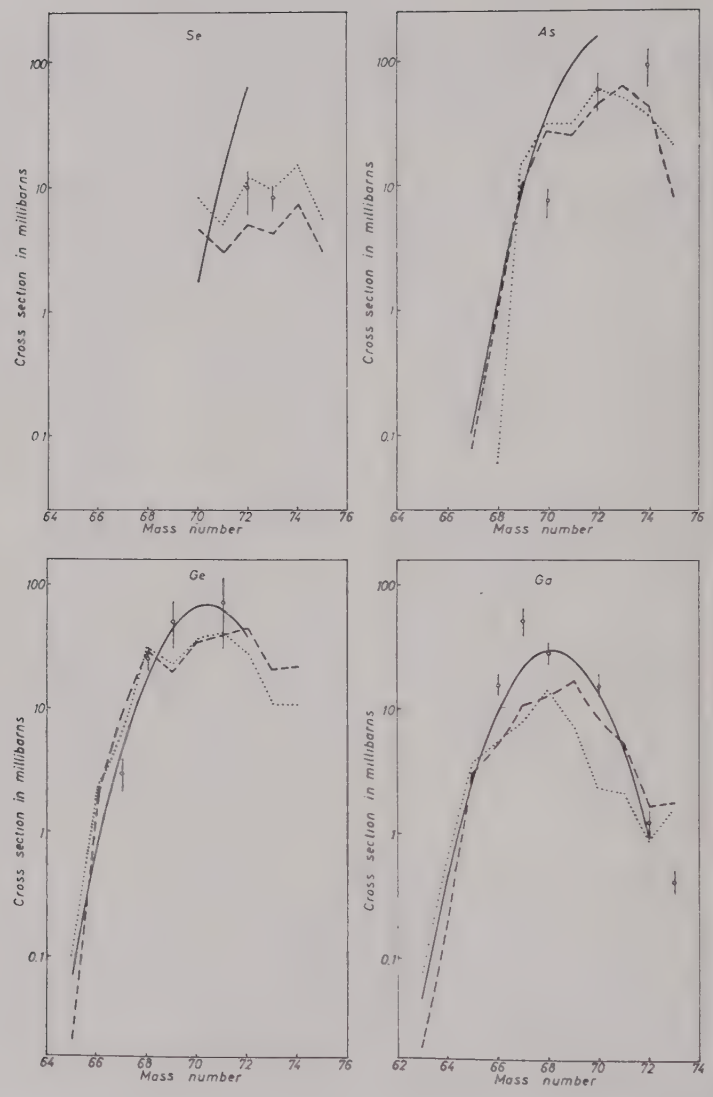

Fig. 38. Comparison between observed and calculated cross sections for the spallation group G(As; p; 170 Mev).

Circles: observed cross sections.
Solid curve: empirical cross section formula.
Broken curve: calculated cross sections using Assumption I.
Dotted curve: calculated cross section using Assumption II.

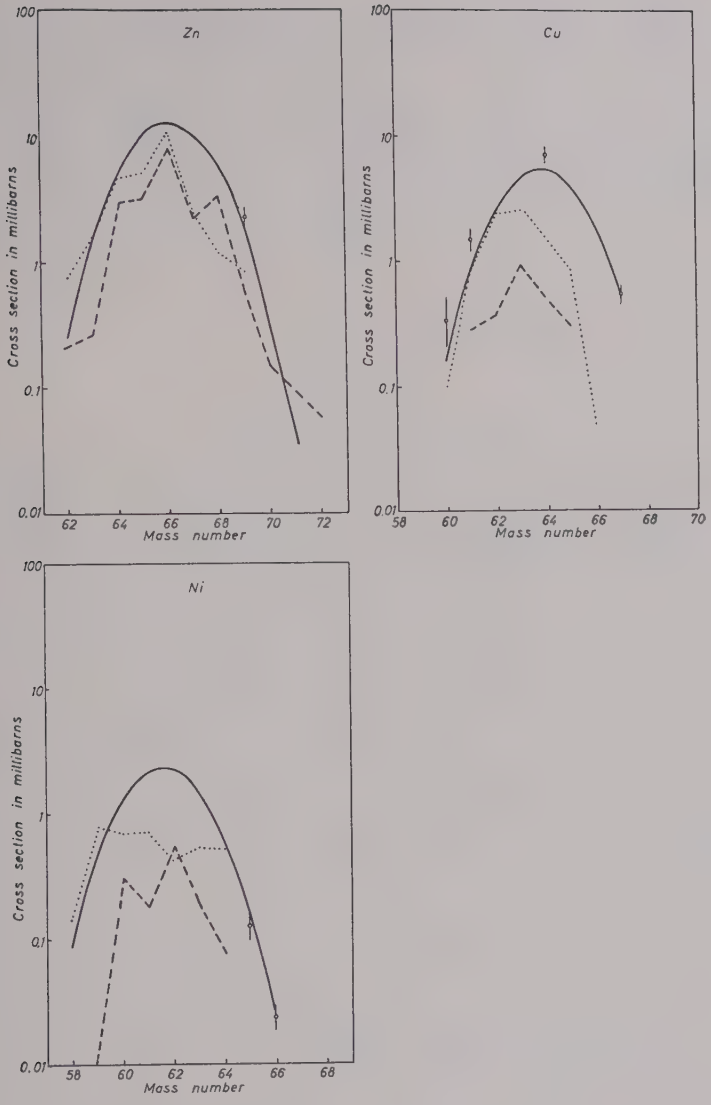

Fig. 39. Comparison between observed and calculated cross sections for the spallation group G(As; p; 170 Mev).

Circles: observed cross sections.
Solid curve: empirical cross section formula.
Broken curve: calculated cross sections using Assumption I.
Dotted curve: calculated cross sections using Assumption II.

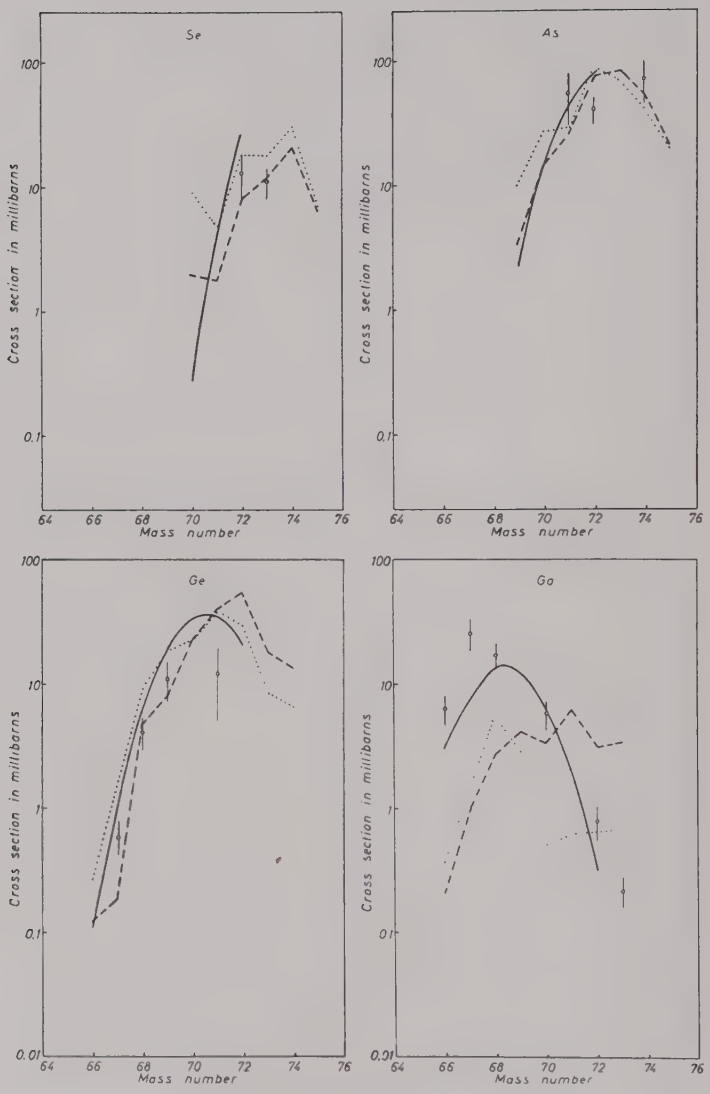

Fig. 40. Comparison between observed and calculated cross sections for the spallation group G(As; p; 103 Mev).

Circles: observed cross sections.
Solid curve: empirical cross section formula.
Broken curve: calculated cross sections using Assumption I.
Dotted curve: calculated cross sections using Assumption II.

might contribute substantially to the cross sections of the nuclides far from the target.

Both the extreme cascade model (Assumption I) and the combined cascade-compound nucleus model (Assumption II) give about the same results for the cross sections, and it is not possible to discriminate between them on the basis of a comparison with experimental values.

2. FINE STRUCTURE OF THE YIELDS

Pappas (273) has advanced the idea that there might be fine structure in the yields owing to differences in the separation energies, something which would affect the evaporation. For example, if it is assumed that all excitation energies of the final product (less than say 15 Mev) are equally probable, the yield should be proportional to the separation energy of a neutron (or separation energy of a proton increased by 2 Mev—compare p. 139), all other factors being equal. This means that even-even nuclides, as a rule, should have larger cross sections than odd-even nuclides, and these larger cross sections than odd-odd nuclides. There is another factor, which works in the opposite direction, however, namely the level density. The larger the level density of a spallation product, the larger should the cross section be, if all other factors are equal. This tends to increase the cross sections of the odd-odd nuclides which have a large level density (compare p. 134). Figs. 38–40 show a tendency for alternation in the calculated yields: even-even isotopes have generally larger cross sections than even-odd ones, and even-odd isotopes have larger cross sections than odd-odd ones, if a smoothed curve is used as a reference. Thus the effect of the separation energies outweighs the effect of the differences in the level densities. The experimental cross sections show no clear fine structure. This may be taken as an indication that the variation in level density represented by the expression (89) is too small.

B. *The Evaporated Particles*

The cross sections of the evaporated particles can be obtained in the same way as the cross sections of the spallation products. The data given here refer to the irradiation of arsenic with 170 Mev protons using the extreme cascade model. For the excitation energy region 0–20 Mev the evaporated neutrons were assumed to have a distribution corresponding to the excitation energy 15 Mev.

The total cross sections are tabulated in Table 55.

Table 55

Total cross sections of evaporation particles and cascade particles

Particle	Evaporation mb	Cascade mb
Proton	150	800
Neutron	1330	510
Deuteron	6.9	
α-Particle	12	
Triton	1.0	
Helium-3	0.03	

Martin, Thomson, Wardle, and Mayne (3) bombarded iron with 340 Mev protons and measured the amounts of helium-4, helium-3, and tritium formed. They found the following ratios: He^4: He^3: H^3 = 1.00:0.048:0.078. The corresponding ratios from the present calculation are: He^4: He^3: H^3 = 1.00:0.0025:0.083. The calculated amount of helium-3 seems to be much smaller than found experimentally. The fact that the irradiation energy is different might be responsible for this difference.

The differential cross sections of the evaporated protons, neutrons, deuterons, and α-particles are shown in Fig. 41.

The reason for the peculiar appearance of the energy distribution of the evaporated protons is the evaporation of slow protons (see p. 139). Provided that the separation energy of a

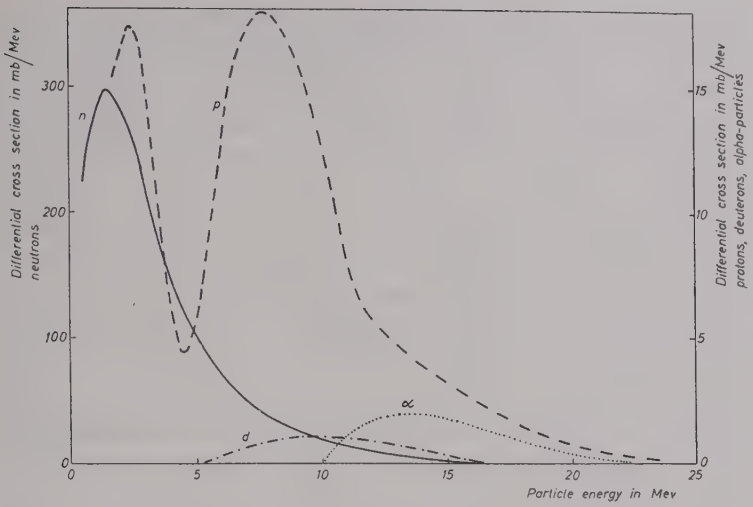

Fig. 41. Energy distributions of the evaporated particles obtained for irradiation energy 170 Mev using Assumption I.

Solid curve: neutrons.
Broken curve: protons.
Dotted curve: α-particles.
Dot- and dash-curve: deuterons.

proton is lower than that of a neutron by at least 2 Mev, an excitation energy interval exists in which the evaporation of a slow proton is the most probable process. As soon as the excitation energy exceeds the separation energy of a neutron, a competition with neutron evaporation starts, and the cross section for proton emission decreases.

The curves in Fig. 41 can be compared with experimental determinations. Skyrme and Williams (4) irradiated tungsten and carbon with 157 Mev protons and measured the energy distribution of the neutrons emitted at 180°. Their distributions are very similar to the neutron distribution in Fig. 41. For both tungsten and carbon they found a maximum of the distributions at about one Mev. The calculated maximum is found at about one and a half Mev. The half-width of the experimental distributions is 2–2½ Mev, which is slightly less than the value obtained from the distribution in Fig. 41.

Deutsch (2) measured the charged particles emitted at 0° from nickel and silver irradiated with 187 Mev deuterons. His distributions for protons and α-particles are similar to the corresponding curves in Fig. 41 except that no low energy proton peak was observed (sufficiently low energies were not examined).

The cascade protons and neutrons should also be taken into account in the comparisons. The cascade neutrons emitted at 180° are very few and can be neglected in the comparison with Skyrme's and Williams's measurements. On the other hand, the cascade protons emitted at 0° can not be neglected. It is seen from Table 55 that the number of cascade protons is much larger than the number of evaporated protons. Figs. 31 and 32 indicate that many low energy protons must be expected in the forward direction. These protons would almost mask the contribution from the evaporated protons. The agreement between the measured energy distribution and the calculated distribution for evaporated protons might be taken as an indication that low energy cascade protons are considerably rarer than one would expect from the cascade calculation using Assumption I. In other words, a combined cascade-compound nucleus model, which excludes most of the low energy cascade particles, seems to be more consistent with experimental results.

C. *Cross Sections of Isomers*

The nuclide Zn^{69} has two isomers whose cross sections were measured in the arsenic bombardments. The ratio between the cross section of the high spin (9/2) isomeric state and the low spin (1/2) ground state is as follows:

Irradiation energy:	49 Mev	103 Mev	170 Mev
$\frac{\sigma_{Zn^{69m}}}{\sigma_{Zn^{69}}}$:	2.8 ± 0.2	1.30 ± 0.05	0.76 ± 0.03

Thus the ratio decreases with increasing energy. The cascade calculation will now be used to make this trend plausible.

It is possible to get a rough measure of the total angular momentum, or spin, of the residual nucleus in a cascade (Fig. 27) simply as the difference between the angular momentum introduced by the incident proton and the sum of the angular momenta carried away by the cascade particles. The spin is correlated with the excitation energy of the nucleus: larger excitation energy generally corresponds to larger spin. This tendency is brought out in Fig. 42, where the frequency of different spins is plotted for residual nuclides with the excitation energy 0–30 Mev, 30–60 Mev, and $>$ 60 Mev. The diagrams are normalized to the same total number of cases, and they refer to the spallation of arsenic with 170 Mev protons using the extreme cascade model. The spin of the target nucleus (3/2) should widen the spin distributions somewhat, but this effect is neglected here. In order to use the results of Fig. 42 for an estimate of the cross sections of isomers, the following assumptions are made:

1) The evaporation process does not change the spin of the nucleus appreciably. This is of course very questionable, but the evaporated particles have generally a low energy and will not carry away much angular momentum each. Besides, the spin of the remaining nucleus can either increase or decrease in the evaporation process, so that the net effect of the evaporation might be small as regards the angular momentum. Thus there is some reason to believe that the spin of the residual nucleus is largely retained in the final spallation product, but the spin distribution, of course, will be widened by the evaporation process.

2) When the excited spallation product is formed in a certain spin state, the γ-cascade will in general lead to the isomer with its spin closest to this spin state. Katz, Pease, and Moody (274) have shown this to be a very reasonable assumption by means of which they are able to explain the ratio between the yields of the isomers of Br^{80} from different reactions.

Using the two assumptions stated above Fig. 42 leads to the following conclusion. Of isomers close to the target, which can be formed at low excitation energies (0–30 Mev), the low spin state should have the largest yield, whereas of isomers far from

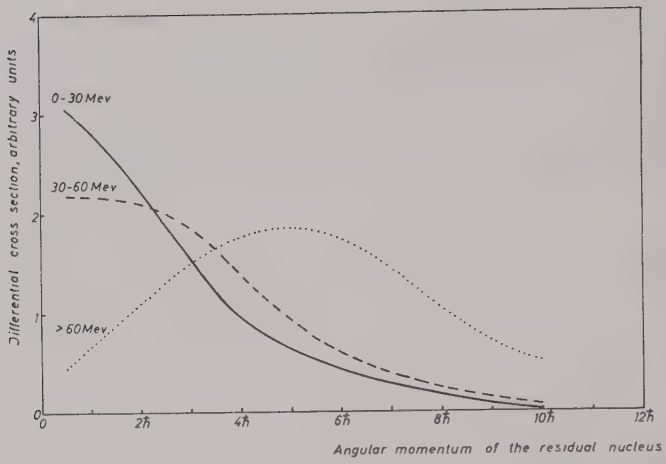

Fig. 42. Angular momentum distributions of the residual nuclides.
Solid curve: excitation energy 0-30 Mev.
Broken curve: excitation energy 30-60 Mev.
Dotted curve: excitation energy $>$ 60 Mev.

the target (properly: the residual nuclides), which require high excitation energy ($>$ 60 Mev) for their formation, the isomer with the high spin should be preferentially formed. Intermediate isomers (excitation energy 30–60 Mev) may be formed in about equal yields.

In order to apply these considerations to the zinc isomers it must be noted that these isomers can be formed from residual nuclides of both high and low excitation energy. Zinc isotopes, Zn^{71} and Zn^{72}, are namely found among the residual nuclides, and they do not need a high excitation energy to produce Zn^{69} or Zn^{69m}. Therefore the spin distribution of the excited Zn^{69}-nuclei might be approximated by the spin distribution of the residual nuclides regardless of initial excitation energy. This distribution is shown in Fig. 43. The average spin is 3.1 $\hbar$. Both isomers might thus be formed in roughly the same yield. In the irradiation with 49 Mev protons, however, Zn^{69} will probably be produced only in such cases when a compound nucleus is formed. Meadows, Diamond, and Sharp (275) have shown that the compound nucleus will have a high spin. The

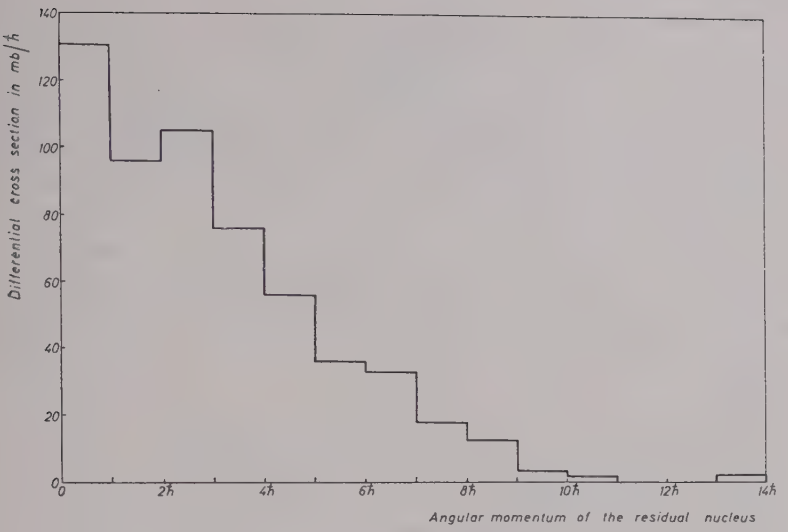

Fig. 43. Angular momentum distribution of the residual nuclides at the irradiation of arsenic with 170 Mev protons.

average spin in the actual case should be higher than about 6 $\hbar$ which they calculate for Br^{81} (spin 3/2) bombarded with 30 Mev protons. This might explain the experimental result that the production of the high spin isomer is favoured in the irradiation with 49 Mev protons.

Summary

The present investigation deals with the spallation of medium weight elements (mass number between 51 and 75) and may be summarized as follows.

The cross sections of the spallation products have been measured for the following spallation reactions: vanadium, manganese, cobalt, and arsenic irradiated with 170 Mev protons; arsenic as well irradiated with 103 Mev and 49 Mev protons.

A new technique using small amounts of carriers (0.1–0.2 mg) has been used in the cross section determinations.

The correction factors, used in converting the counting rate in a GM-counter to disintegration rate, have been studied.

A mixture of the powdered target element and aluminium (or magnesium) powder has been used in the determination of absolute cross sections (by comparison with the known formation cross section of sodium-24 from aluminium or magnesium).

Many half-life determinations have been carried out using the method of least squares.

An empirical formula with four parameters has been found, which describes the cross sections of the spallation products, within a factor of about two on the average, for most spallation groups in the mass region in question.

A theoretical study of the nucleon cascades developed in the target nucleus by high energy protons has been carried out using a Monte Carlo technique in essentially the same way as was done by Goldberger.

The Monte Carlo technique has been used also for a study of the de-excitation of excited nuclei by evaporation of different particles.

A combination of the cascade calculation and the evaporation calculation yields the absolute cross sections of the spallation products. These calculated cross sections have been compared with the experimentally determined ones. The agreement is

good, which supports the model chosen for the spallation reactions.

The cascade-evaporation calculation also gives information about the particles emitted in the reaction, namely their distributions in angle and energy.

References

1. Barkas, W. H., and Tyrén, H., Phys. Rev. **89**, 1 (1953).
2. Deutsch, R. W., Phys. Rev. **97**, 1110 (1955).
3. Martin, G. R., Thomson, S. J., Wardle, G., and Mayne, K. I., Phil. Mag. **45**, 410 (1954).
4. Skyrme, D. M., and Williams, W. S. C., Phil. Mag. **42**, 1187 (1951).
5. Batzel, R. E., and Seaborg, G. T., Phys. Rev. **82**, 607 (1951).
6. Marquez, L., and Perlman, I., Phys. Rev. **81**, 953 (1951).
7. Wright, S. C., Phys. Rev. **79**, 838 (1950).
8. Bernardini, G., Booth, E. T., and Lindenbaum, S. J., Phys. Rev. **85**. 826 (1952).
9. Combe, J., J. phys. et radium **16**, 445 (1955).
10. Fishman, H., and Perry, A. M., Phys. Rev. **86**, 167 (1952).
11. Hadley, J., and York, H., Phys. Rev. **80**, 345 (1950).
12. Hodgson, P. E., Phil. Mag. **44**, 1113 (1953).
13. Hofmann, J. A., and Strauch, K., Phys. Rev. **90**, 449 (1953).
14. Lees, C. F., Morrison, G. C., Muirhead, H., and Rosser, W. G. V., Phil. Mag. **44**, 304 (1953).
15. Miller, R. D., Sewell, D. C., and Wright, R. W., Phys. Rev. **81**, 374 (1951).
16. Morrison, G. C., Muirhead, H., and Rosser, W. G. V., Phil. Mag. **44**. 1326 (1953).
17. Muirhead, H., and Rosser, W. G. V., Phil. Mag. **46**, 652 (1955).
18. Randle, T. C., Cassels, J. M., Pickavance, T. G., and Taylor, A. E., Phil. Mag. **44**, 425 (1953).
19. Willoughby, D. S., Phys. Rev. **101,** 324 (1956).
20. Bartell, F. O., Helmholz, A. C., Softky, S. D., and Stewart, D. B., Phys. Rev., **80**, 1006 (1950).
21. Batzel, R. E., Miller, D. R., and Seaborg, G. T., Phys. Rev. **84**, 671 (1951).
22. Belmont, E., and Miller, J. M., Phys. Rev. **95**, 1554 (1954).
23. Bonner, N. A., and Orr, W. C., Phys. Rev. **76**, 140 (1949).
24. Chackett, G. A., Chackett, K. F., and Fremlin, J. H., Phil. Mag. **46**. 1 (1955).
25. Caretto, A. A., and Wiig, E. O., Phys. Rev. **103**, 236 (1956).
26. Carleson, G., Acta Chem. Scand. **8**, 1697 (1954).
27. Coleman, G. H., and Tewes, H. A., Phys. Rev. **99**, 288 (1955).
28. Debs, R. J., Eisinger, J. T., Fairhall, A. W., Halpern, I., and Richter, H. G., Phys. Rev. **97**, 1325 (1955).
29. Friedlander, G., Miller, J. M., Wolfgang, R., Hudis, J., and Baker, E., Phys. Rev. **94**, 727 (1954).
30. Friedlander, G., Hudis, J., and Wolfgang, R. L., Phys. Rev. **99**, 263 (1955).

31. Fink, R. W., and Wiig, E. O., Phys. Rev. **94**, 1357 (1954).
32. Fink, R. W., and Wiig, E. O., Phys. Rev. **96**, 185 (1954).
33. Greenberg, D. H., and Miller, J. M., Phys. Rev. **84**, 845 (1951).
34. Greenlees, G. W., and Souch, A. E., Phil. Mag. **46**, 682 (1955).
35. Heininger, C. G., and Wiig, E. O., Phys. Rev. **101**, 1074 (1956).
36. Hopkins, H. H., and Cunningham, B. B., Phys. Rev. **73**, 1406 (1948).
37. Kundu, D. N., Donaven, T. W., Pool, M. L., and Long, J. K., Phys. Rev. **89**, 1200 (1953).
38. Kurchatov, B. V., Mekhedov, V. N., Borisova, N. I., Kuznetzova, M. Y., Kurchatova, L. N., and Chistyakov, L. V., Session of the Academy of Sciences of the U. S. S. R. on the Peaceful Use of Atomic Energy, July 1-5, 1955, p. 178 (Moskva, 1955).
39. Lindner, M., and Perlman, I., Phys. Rev. **78**, 499 (1950).
40. Marquez, L., Phys. Rev. **88**, 225 (1952).
41. Miller, D. R., Thompson, R. C., and Cunningham, B. B., Phys. Rev. **74**, 347 (1948).
42. Murin, A. N., Preobrazhensky, B. K., Yutlandov, I. A., and Yakimov, M. A., Session of the Academy of Sciences of the U. S. S. R. on the Peaceful Use of Atomic Energy, July 1-5, 1955, p. 160 (Moskva, 1955).
43. Reynolds, H. L., and Zucker, A., Phys. Rev. **96**, 1615 (1954).
44. Rudstam, G., Stevenson, P. C., and Folger, R. L., Phys. Rev. **87**, 358 (1952).
45. Sugihara, T. T., and Halpern, I., Phys. Rev. **101**, 1768 (1956).
46. Sharp, R. A., Diamond, R. M., and Wilkinson, G., Phys. Rev. **101**, 1493 (1956).
47. Turkevich, A., and Sugarman, N., Phys. Rev. **94**, 728 (1954).
48. Hopkins, H. H., Phys. Rev. **77**, 717 (1950).
49. Wagner, G. D., and Wiig, E. O., Phys. Rev. **96**, 1100 (1954).
50. Webb, W. H., Reynolds, H. L., and Zucker, A., Phys. Rev. **102**, 749 (1956).
51. Vinogradov, A. P., Alimarin, I. P., Baranov, V. I., Lavrukhina, A. K., Baranova, T. V., and Pavlotskaya, F. I., Session of the Academy of Sciences of the U. S. S. R. on the Peaceful Use of Atomic Energy, July 1-5, 1955, p. 132 (Moskva, 1955).
52. Wolke, R. L., and Bonner, N. A., Phys. Rev. **102**, 530 (1956).
53. Worthington, W. J., University of California Radiation Laboratory Report UCRL-1627 (1952).
54. Templeton, D. H., Annual Review of Nuclear Science, Volume **2**, p. 93 (Stanford, 1953).
55. Bohr, N., Nature **137**, 344 (1936).
56. Serber, R., Phys. Rev. **72**, 1114 (1947).
57. Goldberger, M. L., Phys. Rev. **74**, 1269 (1948).
58. Ulam, S., and von Neumann, J., Bull. Am. Math. Soc. **53**, 1120 (1947).
59. Le Couteur, K. J., Proc. Phys. Soc. (London) **63** A, 259 (1950); Ibid. **65** A, 718 (1952).

60. Svanheden, Å., personal communication (1956).
61. Bloembergen, N., and van Heerden, P. J., Phys. Rev. **83**, 561 (1951).
62. Fung, S., and Perlman, I., Phys. Rev. **87**, 623 (1952).
63. Hintz, N. M., and Ramsey, N. F., Phys. Rev. **88**, 19 (1952).
64. Chackett, G. A., Chackett, K. F., Reasbeck, P., Symonds, J. L., and Warren, J., Proc. Phys. Soc. (London) **69** A, 43 (1956).
65. Hicks, H. G., Stevenson, P. C., and Nervik, W. E., Phys. Rev. **102**, 1390 (1956).
66. Meadows, J. W., and Holt, R. B., Phys. Rev. **83**, 47 (1951).
67. Aamodt, R. L., Peterson, V., and Phillips, R., Phys. Rev. **88**, 739 (1952).
68. Crandall, W. E., Millburn, G. P., Pyle, R. V., and Birnbaum, W., Phys. Rev. **101**, 329 (1956).
69. Burcham, W. E., Symonds, J. L., and Young, J. D., Proc. Phys. Soc. (London) **68** A, 1001 (1955).
70. Zumwalt, L. R., U. S. Atomic Energy Commission Unclassified Report AECU-567 (1950).
71. Pappas, A. C., Technical Report No. 63, Laboratory for Nuclear Science, Massachusetts Institute of Technology (1953).
72. Curran, S. C., and Craggs, J. D., Counting Tubes, Chapter 6 (New York, 1949).
73. Rydberg, J., and Rydberg, B., Svensk Kem. Tidskr. **64**, 200 (1952).
74. Seagrave, J. D., Phys. Rev. **84**, 1219 (1951).
75. Lamb, W. E., Phys. Rev. **58**, 696 (1940).
76. Knipp, J., and Teller, E., Phys. Rev. **59**, 659 (1941).
77. Edwards, R. R., and Davies, T. H., Nucleonics **2**, No. 6, 44 (1948).
78. Wahl, A. C., and Bonner, N. A., editors, Radioactivity Applied to Chemistry, Chapter 8 (New York, 1951).
79. Chackett, G. A., and Chackett, K. F., Nature **174**, 232 (1954).
80. Long, F. A., and Olson, A. R., J. Am. Chem. Soc. **58**, 2214 (1936).
81. Halford, R. S., J. Am. Chem. Soc. **62**, 3233 (1940).
82. Langer, L. M., Rev. Sci. Instr. **20**, 216 (1949).
83. Cook, G. B., Duncan, J. F., and Hewitt, M. A., Nucleonics **8**, No. 1, 24 (1951).
84. Lundell, G. E. F., and Hoffman, J. I., Outlines of Methods of Chemical Analysis (New York, 1948).
85. Sandell, E. B., Colorimetric Determination of Traces of Metals (New York, 1950).
86. DeMeio, R., Anal. Chem. **20**, 488 (1948).
87. Furman, N. H., editor, Scott's Standard Methods of Chemical Analysis, p. 96 (New York, 1939).
88. Moeller, T., and Cohen, A. J., Anal. Chem. **22**, 686 (1950).
89. Von Endrédy, A., and Brugger, F., Z. anorg. u. allgem. Chem. **249**, 263 (1942).
90. Eberle, A. R., and Lerner, M. W., Anal. Chem. **27**, 1551 (1955).
91. Burtt, B. P., Nucleonics **5**, No. 2, 28 (1949).

92. Cook, G. B., and Duncan, J. F., J. Chem. Soc. **1949**, S 369 (1949).
93. Novey, T. B., Rev. Sci. Instr. **21**, 280 (1950).
94. Kalmon, B., Nucleonics **11**, No. 7, 56 (1953).
95. Gleason, G. I., Taylor, J. D., and Tabern, D. L., Nucleonics **8**, No. 5, 12 (1951).
96. Graf, W. L., Comar, C. L., and Whitney, I. B., Nucleonics **9**, No. 4, 22 (1951).
97. Coryell, C. D., and Sugarman, N., editors, Radiochemical Studies: The Fission Products, National Nuclear Energy Series, Div. IV, Volume 9, Introduction to Part I (New York, 1951).
98. Nervik, W. E., and Stevenson, P. C., Nucleonics **10**, No. 3, 18 (1952).
99. Baker, R. G., and Katz, L., Nucleonics **11**, No. 2, 14 (1953).
100. Lerch, P., Helv. Phys. Acta **26**, 663 (1953).
101. Broda, E., Grummitt, W. E., Guéron, J., Kowarski, L., and Wilkinson, G., Proc. Phys. Soc. (London) **60** A, 460 (1948).
102. Yaffe, L., and Justus, K. M., J. Chem. Soc. **1949**, S 341 (1949).
103. Glendenin, L. E., and Solomon, A. K., Science **112**, 623 (1950).
104. Müller, R. H., Phys. Rev. **93**, 891 (1954).
105. Seliger, H. H., Phys. Rev. **78**, 491 (1950).
106. Seliger, H. H., Phys. Rev. **88**, 408 (1952).
107. Glendenin, L. E., Nucleonics **2**, No. 1, 12 (1948).
108. Balfour, J. G., J. Sci. Instr. **31**, 395 (1954).
109. Studier, M., and James, R., unpublished work (1946).
110. Compton, A. C., and Allison, S. K., X-Rays in Theory and Experiment, Chapter VII (New York, 1935).
111. Bouchez, R., and Kayas, G., J. phys. et radium **10**, 110 (1949).
112. Bergström, I., Beta- and Gamma-Ray Spectroscopy, Chapter XX (I), ed. K. Siegbahn (Amsterdam, 1955).
113. Forro, M., Phys. Rev. **92**, 931 (1953).
114. Harley, J. H., and Hallden, N., Nucleonics **13**, No. 1, 32 (1955).
115. Katz, L., and Penfold, A. S., Revs. Modern Phys. **24**, 28 (1952).
116. Feather, N., Proc. Cambridge Phil. Soc. **34**, 599 (1938).
117. Cook, G. B., and Duncan, J. F., Modern Radiochemical Practice, p. 100 (Oxford, 1952).
118. Scott, F. R., Phys. Rev. **84**, 659 (1951).
119. Hooge, F. N., and Aten, A. H. W., Physica **19**, 1047 (1953).
120. Butement, F. D. S., and Prout, E. G., Phil. Mag. **46**, 357 (1955).
121. Verkerk, B., and Aten, A. H. W., Physica **18**, 974 (1952).
122. Souch, A. E., Proc. Phys. Soc. (London) **68** A, 760 (1955).
123. Graves, W. E., and Mitchell, A. C. G., Phys. Rev. **97**, 1033 (1955).
124. Thulin, S., Moreau, J., and Atterling, H., Arkiv Fysik **8**, 219 (1954).
125. Stoker, P. H., and Ong Ping Hok, Physica **19**, 279 (1953).
126. Watters, H. J., and Fagan, J. F., Phys. Rev. **92**, 1248 (1953).
127. Brun, E., Kraushaar, J. J., and Meyerhof, W. E., Phys. Rev. **102**, 808 (1956).

128. Johansson, S., Cauchois, Y., and Siegbahn, K., Phys. Rev. **82**, 275 (1951).
129. McCown, D. A., Woodward, L. L., and Pool, M., Phys. Rev. **74**, 1311 (1948).
130. Aten, A. H. W., De Vries-Hamerling, T., and Lindner, L., Physica **19**, 1046 (1953).
131. Crasemann, B., Rehfuss, D. E., and Easterday, H. T., Phys. Rev. **102**, 1344 (1956).
132. Huddleston, C. M., and Smith, A. B., Phys. Rev. **84**, 289 (1951).
133. Bisi, A., Germagnoli, E., Zappa, L., and Zimmer, E., Nuovo cimento **2**, 290 (1955).
134. Langer, L. M., and Moffat, R. D., Phys. Rev. **80**, 651 (1950).
135. Mukerji, A., and Preiswerk, P., Helv. Phys. Acta **25**, 387 (1952).
136. Mann, L. G., Meyerhof, W. E., and West, H. I., Phys. Rev. **92**, 1481 (1953).
137. Meyerhof, W. E., Mann, L. G., and West, H. I., Phys. Rev. **92**, 758 (1953).
138. Tobailem, J., J. phys. et radium **16**, 48 (1955).
139. Ridenour, L. N., and Henderson, W. J., Phys. Rev. **52**, 889 (1937).
140. Bunker, M. E., Starner, J. W., and Mize, J. P., Phys. Rev. **95**, 612 (1954).
141. Barker, E. C., Oak Ridge National Laboratory Report Mon P-269 (1947).
142. Haynes, S. K., Phys. Rev. **74**, 423 (1948).
143. Bishop, G. R., Wilson, R., and Halban, H., Phys. Rev. **77**, 416 (1950).
144. Siegel, J. M., and Glendenin, L. E., National Nuclear Energy Series, Div. IV, Volume 9, Paper 53 (1951).
145. Johansson, S., reported in M. Siegbahn Commemorative Volume, p. 183 (Uppsala, 1951).
146. Andersson, G., and Burgman, O., unpublished work (1956).
147. Andersson, G., Phil. Mag. **45**, 621 (1954).
148. Perkins, J. F., and Haynes, S. K., Phys. Rev. **92**, 687 (1953).
149. Tobailem, J., J. phys. et radium **14**, 553 (1953).
150. Duffield, R. B., and Langer, L. M., Phys. Rev. **89**, 854 (1953).
151. Livingood, J. J., and Seaborg, G. T., Phys. Rev. **55**, 457 (1939).
152. Van Lieshout, R., Nussbaum, R. H., Nijgh, G. J., and Wapstra, A. H., Phys. Rev. **93**, 255 (1954).
153. Leith, C. E., Bratenahl, A., and Moyer, B. J., Phys. Rev. **72**, 732 (1947).
154. Bouchez, R., De Groot, S. R., Nataf, R., and Tolhoek, H. A., J. phys. et radium **11**, 105 (1950).
155. Owen, G. E., Cook, C. S., and Owen, P. H., Phys. Rev. **78**, 686 (1950).
156. Cook, C. S., and Langer, L. M., Phys. Rev. **74**, 227 (1948).
157. Plassman, E., and Scott, F. R., Phys. Rev. **84**, 156 (1951).
158. Silver, L. M., Phys. Rev. **76**, 589 (1949).
159. Schuman, R. P., and Camilli, A., Phys. Rev. **84**, 158 (1951).

160. Friedlander, G., and Alburger, D. E., Phys. Rev. **84**, 231 (1951).
161. Bartholomew, R. M., Brown, F., Howell, W. D., Shorey, W. R. J., and Yaffe, L., Can. J. Phys. **31**, 714 (1953).
162. Easterday, H. T., Phys. Rev. **91**, 653 (1953).
163. Kundu, D. N., and Pool, M. L., Phys. Rev. **78**, 488 (1950).
164. Friedlander, G., Perlman, M. L., Alburger, D., and Sunyar, A. W., Phys. Rev. **80**, 30 (1950).
165. Siegbahn, K., and Ghosh, A., Phys. Rev. **76**, 307 (1949).
166. Johnson, N. R., Sheline, R. K., and Wolfgang, R., Phys. Rev. **102**, 831 (1956).
167. Kjelberg, A., and Pappas, A. C., Nuc. Phys. **1**, 322 (1956).
168. Nussbaum, R. H., Wapstra, A. H., Bruil, W. A., Sterk, M. J., Nijgh, G. J., and Grobben, N., Phys. Rev. **101**, 905 (1956).
169. Smith, L. A., Haslam, R. N. H., and Taylor, J. G. V., Phys. Rev. **84**, 842 (1951).
170. Friedlander, G., and Miller, J. M., Phys. Rev. **84**, 588 (1951).
171. Maeder, D., and Preiswerk, P., Phys. Rev. **84**, 595 (1951).
172. Brownell, G. L., and Maletskos, C. J., Phys. Rev. **80**, 1102 (1950).
173. Deutsch, M., Downing, J. R., Elliot, L. G., Irvine, J. W., and Roberts, A., Phys. Rev. **62**, 3 (1942).
174. Folger, R. L., Stevenson, P. C., and Seaborg, G. T., University of California Radiation Laboratory Report UCRL-1195 (1951).
175. Burgus, W. H., and Kennedy, J. W., J. Chem. Phys. **18**, 97 (1950).
176. Koester, L., Z. Naturforsch. **9** a, 104 (1954).
177. Hemmendinger, A., Phys. Rev. **58**, 929 (1940).
178. Livingood, J. J., and Seaborg, G. T., Phys. Rev. **54**, 391 (1938).
179. Sehr, R., Z. Physik 137, 523 (1954).
180. Backofen, E. W., and Herber, R. H., Phys. Rev. **97**, 743 (1955).
181. Elliott, L. G., and Deutsch, M., Phys. Rev. **64**, 321 (1943).
182. Bartholomew, R. M., Hawkings, R. C., Merritt, W. F., and Yaffe, L., Can. J. Chem. **31**, 204 (1953).
183. Lockett, E. E., and Thomas, R. H., Nucleonics **11**, No. 3, 14 (1953).
184. Van Lieshout, R., Greenberg, D. H., Koerts, L. A. C., and Wu, C.S., Phys. Rev. **100**, 223 (1955).
185. Sheline, R. K., and Wilkinson, J. R., Phys. Rev. **99**, 165 (1955).
186. Crasemann, B., and Easterday, H. T., Phys. Rev. **90**, 1124 (1953).
187. O'Connor, J. J., Pool, M. L., and Kurbatov, J. D., Phys. Rev. **62**, 413 (1942).
188. Daniel, H., Z. Naturforsch. **9** a, 974 (1954).
189. Casson, H., Goodman, L. S., and Krohn, V. E., Phys. Rev. **92**, 1517 (1953).
190. Burgus, W. H., Cowan, G. A., Hadley, J. W., Hess, W., Shull, T., Stevenson, M. L., and York, H. F., Phys. Rev. **95**, 750 (1954).
191. Meyer, P., and Schlieder, S., Z. Physik **135**, 119 (1953).
192. Wiedling, T., Phys. Rev. **91**, 767 (1953).
193. Sheline, R. K., and Wilkinson, J. R., Phys. Rev. **94**, 729 (1954).

194. Ter-Pogossian, M., Cook, C. S., Porter, F. T., Morganstern, K. H., and Hudis, J., Phys. Rev. **80**, 360 (1950).
195. Kubitschek, H. E., Phys. Rev. **79**, 23 (1950).
196. Lindqvist, T., and Mitchell, A. C. G., Phys. Rev. **95**, 1535 (1954).
197. Hibdon, C. T., Pool, M. L., and Kurbatov, J. D., Phys. Rev. **67**, 289 (1945).
198. Langevin, H., and Marty, N., J. phys. et radium **15**, 127 (1954).
199. Blue, J. W., and Bleuler, E., Phys. Rev. **100**, 1324 (1955).
200. Bruner, J. A., and Langer, L. M., Phys. Rev. **79**, 606 (1950).
201. Goldhaber, M., and Hill, R. D., Revs. Modern Phys. **24**, 179 (1952).
202. Porter, F. T., and Cook, C. S., Phys. Rev. **81**, 640 (1951).
203. Walke, H., Williams, E. J., and Evans, G. R., Proc. Roy. Soc. (London) **171** A, 360 (1939).
204. Nichols, R. T., and Jensen, E. N., Phys. Rev. **100**, 1407 (1955).
205. Marquez, L., Phys. Rev. **92**, 1511 (1953).
206. Cork, J. M., LeBlanc, J. M., Brice, M. K., and Nester, W. H., Phys. Rev. **92**, 367 (1953).
207. Walke, H., Phys. Rev. **57**, 163 (1940).
208. Ketelle, B. H., Phys. Rev. **80**, 758 (1950).
209. Delaney, C. F. G., and Poole, J. H. J., Phys. Rev. **89**, 529 (1953).
210. Lyon, W. S., and Handley, T. H., Phys. Rev. **100**, 1280 (1955).
211. Lidofsky, L. J., Benczer, N., and Fischer, V. K., Phys. Rev. **99**, 658 (1955).
212. Emery, E. W., and Veall, N., Proc. Phys. Soc. (London) **68** A, 346 (1955).
213. Burch, P. R. J., Nature **172**, 361 (1953).
214. Lindqvist, T., and Mitchell, A. C. G., Phys. Rev. **95**, 444 (1954).
215. Overstreet, R., Jacobson, L., and Stout, P. R., Phys. Rev. **75**, 231 (1949).
216. Green, D., and Richardson, J. R., Phys. Rev. **101**, 776 (1956).
217. Langer, L. M., Phys. Rev. **77**, 50 (1950).
218. Cobble, J. W., and Atteberry, R. W., Phys. Rev. **80**, 917 (1950).
219. Haslam, R. N. H., Katz, L., Moody, H. J., and Skarsgard, H. M., Phys. Rev. **80**, 318 (1950).
220. Haslam, R. N. H., Katz, L., Johns, H. E., and Moody, H. J., Phys. Rev. **76**, 704 (1949).
221. Arbman, E., personal communication (1953).
222. Langer, L. M., Motz, J. W., and Price, H. C., Phys. Rev. **77**, 798 (1950).
223. Hendricks, R. H., Bryner, L. C., Thomas, M. D., and Ivie, J. O., J. Phys. Chem. **47**, 469 (1943).
224. Hollander, J. M., Perlman, I., and Seaborg, G. T., Revs. Modern Phys. **25**, 469 (1953).
225. Klema, E. D., and Hanson, A. O., Phys. Rev. **73**, 106 (1948).
226. Bayly, J. G., Can. J. Research **28** A, 520 (1950).

227. Jensen, E. N., Nichols, R. T., Clement, J., and Pohm, A., Phys. Rev. **85**, 112 (1952).
228. Motz, H. T., Phys. Rev. **85**, 501 (1952).
229. Wennerblom, A., Zimen, K. E., and Ehn, E., Svensk Kem. Tidskr. **63**, 207 (1951).
230. Benĕs, J., Hedgran, A, and Hole, N., Arkiv Mat., Astron. Fysik **35** A, No. 12 (1948).
231. Sargent, B. W., Yaffe, L., and Gray, A. P., Can. J. Phys. **31**, 235 (1953).
232. Siegbahn, K., and Johansson, A., Arkiv. Mat., Astron. Fysik **34** A, No. 10 (1947).
233. Solomon, A. K., Phys. Rev. **79**, 403 (1950).
234. Rudstam, S. G., Phil. Mag. **44**, 1131 (1953).
235. Rudstam, S. G., Phil. Mag. **46**, 344 (1955).
236. Bernardini, G., Booth, E. T., and Lindenbaum, S. J., Phys. Rev. **83**, 669 (1951); Ibid. **88**, 1017 (1952).
237. Combe, J., Nuovo cimento **3**, S 182 (1956).
238. Cüer, P., and Combe, J., Compt. rend. **238**, 1799 (1954); Ibid. **239**, 351 (1954).
239. Meadows, J. W., Phys. Rev. **88**, 143 (1952); Ibid. **98**, 744 (1955).
240. Chew, G. F., and Goldberger, M. L., Phys. Rev. **77**, 470 (1950).
241. Heidmann, J., Phys. Rev. **80**, 171 (1950).
242. Nakasima, R., and Kikuchi, K., Progr. Theor. Phys. **14**, 126 (1955).
243. Green, A. E. S., Phys. Rev. **95**, 1006 (1954).
244. Cladis, J. B., Hess, W. N., and Moyer, B. J., Phys. Rev. **87**, 425 (1952).
245. Wilcox, J. M., and Moyer, B. J., Phys. Rev. **99**, 875 (1955).
246. Wapstra, A. H., Physica **21**, 385 (1955).
247. Mandl, F., and Skyrme, T. H. R., Phil. Mag. **44**, 1028 (1953).
248. Kruse, U. E., Teem, J. M., and Ramsey, N. F., Phys. Rev. **94**, 1795 (1954).
249. Sleator, W., Phys. Rev. **72**, 207 (1947).
250. Marshall, J., Marshall, L., and Nedzel, V. A., Phys. Rev. **92**, 834 (1953).
251. Hildebrand, R. H., and Leith, C. E., Phys. Rev. **80**, 842 (1950).
252. Cook, L. J., McMillan, E. M., Peterson, J. M., and Sewell, D. C., Phys. Rev. **75**, 7 (1949).
253. DeJuren, J., and Knable, N., Phys. Rev. **77**, 606 (1950).
254. Alphonce, R., Johansson, A., Taylor, A. E., and Tibell, G., Phil. Mag. **46**, 295 (1955).
255. Christian, R. S., Reports on Progress in Physics, Volume XV, p. 68, ed. A. C. Stickland (London, 1952).
256. Fernbach, S., Serber, R., and Taylor, T. B., Phys. Rev. **75**, 1352 (1949).
257. Fox, R., Leith, C., Wouters, L., and MacKenzie, K. R., Phys. Rev. **80**, 23 (1950).
258. De Carvalho, H. G., Phys. Rev. **96**, 398 (1954).

259. DeJuren, J., Phys. Rev. **80**, 27 (1950).
260. Taylor, A. E., and Wood, E., Phil. Mag. **44**, 95 (1953).
261. Blatt, J. M., and Weisskopf, V. F., Theoretical Nuclear Physics, Chapter VIII (New York, 1952).
262. Yamaguchi, Y., Progr. Theor. Phys. **5**, 142 (1950).
263. Fujimoto, Y., and Yamaguchi, Y., Progr. Theor. Phys. **4**, 468 (1949); Ibid. **5**, 787 (1950).
264. Takayanagi, K., and Yamaguchi, Y., Progr. Theor. Phys. **5**, 894 (1950).
265. Weisskopf, V., Phys. Rev. **52**, 295 (1937).
266. Lang, J. M. B., and Le Couteur, K. J., Proc. Phys. Soc. (London) **67** A, 586 (1954).
267. Weisskopf, V. F., and Ewing, D. H., Phys. Rev. **57**, 472 (1940).
268. Yamaguchi, Y., Progr. Theor. Phys. **5**, 501 (1950).
269. Bagge, E., Ann. Physik **33**, 389 (1938).
270. Hodgson, P. E., Phil. Mag. **43**, 934 (1952).
271. Marquez, L., Phys. Rev. **86**, 405 (1952).
272. Wolfgang, R., Baker, E. W., Caretto, A. A., Cumming, J. B., Friedlander, G., and Hudis, J., Phys. Rev. **103**, 394 (1956).
273. Pappas, A. C., Fra Fysikkens Verden **16**, 161 (1954).
274. Katz, L., Pease, L., and Moody, H., Can. J. Phys. **30**, 476 (1952).
275. Meadows, J. W., Diamond, R. M., and Sharp, R. A., Phys. Rev. **102**, 190 (1956).

UPPSALA 1956
APPELBERGS BOKTRYCKERI AB